ADDIS ABABA UNIVERSITY
ADDIS ABABA INSTITUTE OF TECHNOLOGY
SCHOOL OF ELECTRICAL AND COMPUTER ENGINEERING

DESIGN OF INTELLIGENT AND HYBRID BASED MPPT CONTROLLER FOR PHOTOVOLTAIC WATER PUMPING SYSTEM

A Thesis Submitted to the School of Electrical and Computer Engineering of Addis Ababa Institute of Technology in Partial Fulfillment of the Requirement for the Degree of Master of Science in Electrical Engineering (**Control Engineering**)

By

Abemelek Molla

Advisor: Dereje Shferaw (Ph.D.)

December 2018

Addis Ababa, Ethiopia

ADDIS ABABA UNIVERSITY
ADDIS ABABA INSTITUTE OF TECHNOLOGY
SCHOOL OF ELECTRICAL AND COMPUTER ENGINEERING

DESIGN OF INTELLIGENT AND HYBRID BASED MPPT CONTROLLER FOR PHOTOVOLTAIC WATER PUMPING SYSTEM

A Thesis Submitted to the School of Electrical and Computer Engineering of Addis Ababa Institute of Technology in Partial Fulfillment of the Requirement for the Degree of Master of Science in Electrical Engineering (**Control Engineering**)

By

Abemelek Molla

Approved By Board of Examiners

_____	_____
Chairman, Department of Graduate Committee	Signature
Dr.Dereje Shiferaw_____	_____
Advisor	Signature
_____	_____
Internal Examiner	Signature
_____	_____
External Examiner	Signature

DECLARATION

I, the undersigned declare that this thesis is my original work, and has not been presented for a degree in this or any other university, and all sources of materials used for the thesis have been fully acknowledged.

Name: Abemelek Molla
Signature: _____

Place: Addis Ababa University Institute of Technology, Addis Ababa, Ethiopia
Date of Submission: December, 2018

This thesis has been submitted with my approval as a university advisor

Dr.Dereje Shiferaw _____
Advisor's Name Signature

ACKNOWLEDGEMENT

I have a great many thanks to many people who helped me during this work. My deepest appreciation and gratitude goes to my advisor, Dr. Dereje Shferaw, for guiding and motivating me. As great advisor, He is trying to provide me with guidance and feedbacks about my performance. I'm truly honored by having him as teachers and advisors.

I would also like to express my sincere thanks to my family for their encouragement and patience, and for inspiring me to always strive towards high expectations and insist to achieve them. Their support gave me the faith to further my education and reach out new goals. Last, but not the least, I would like to express my deep gratitude to MizanTepi University for their continuous encouragement financial support and study environment that it provides.

ABSTRACT

Maximum power point tracking plays an important role for Photovoltaic power pumping systems because it optimize the power output from a Pholovoltaic system for a given set of conditions. This thesis presents a maximum power point tracker using artificial intelligence and hybrid methods for a standalone Photovoltaic water pumping system. This work focused on designing of different intelligence control methods to get maximum amount of power for Dolo Ado Woreda refugee camp appropriate power for the required amount of demand to pump water from the ground to 600 residential house hold needs. In this work scaling and sizing the whole components of the standalone photovoltaic water pumping system, such as, Photovoltaic panel, direct converter, inverter, and low pass filter is applied to generate a 29.04kW power by using a boost converter as a supporter for maximum power point traking algorithm by adjusting the duty cycle of the boost converter to maximize the output to the inverter which is feeding an alternative 17.5kW current load would achieved with three proposed intelligent controllers.

After sized and designed the proposed system components, each System elements are individually modelled in MATLAB/SIMULINK and then connected to assess performance under different environmental conditions. First, each technique is compared with the direct connection matched system. The results show that the direct connection PV system response oscillates far from the tracking point and the three proposed controller method dynamics responses are around the maximum power point under different level of temperature and irradiation. The performance of the three proposed controllers for photovoltaic water pumping system is evaluated through simulation studies and compared. The simulation results show that the efficiency of the photovoltaic water pumping system with the fuzzy logic, artificial neural network and artificial neuro fuzzy inference system controller is 97.68%, 99.32% and 99.88% respectively, whereas the same without any controller is found to be 88.06.

Keywords: Maximum Power Point Traking (MPPT), Artificial intelligent (AI) , Hybrid, neural network (NN), Fuzzy logic (FL), Photovoltaic (PV).

TABLE OF CONTENTS

LIST OF FIGURES

LIST OF TABLES

LIST OF SYMBOLS AND ABBREVIATIONS

AC	Alternating Current
μ	Dynamic viscosity
ANFIS	Artificial Neuro Fuzzy Inference System
ANFISC	Artificial neuro Fuzzy Inference System controller
ANN	Artificial Neural Network
ANNC	Artificial Neural Network Controller
Cb	Boost capacitor
C_f	Filter capacitance
COG	Centre of Gravity
D	Duty cycle ration
DC	Direct Current
E	The roughness of the pipe take PVC
f_h	A head due to friction loss
FIS	Fuzzy Interface System
FL	Fuzzy Logic
FLC	Fuzzy logic controller
F_o	Resonant frequency
G	Photovoltaic cell's operating irradiation
I_{mp}	Maximum power point voltage at reference condition
Ipv	Output current of the solar cell
Isc	Short Circuit current
LCL	Inductor capacitor inductor low pass filter
Lb	Boost inductor
MOM	Mean of maximum method
MPP	Maximum Power Point
MPPT	Maximum Power Point Tracking
MSE	Mean Square Error
η	Tracking efficiency
NP	Number of connected PV cells in parallel
NS	Number of connected PV cells in series
P_h	Pump level head

P_{inv}	Rated output power of inverter.
P_{max}	Maximum power point
P_{out}	Output power of the converter
P_{pv}	Output power of the solar cell
PV	Photovoltaic
PWM	Pulse Width Modulation
q	The charge of electron
R_d	damping resistance
RMS	Root mean square
R_S	Series resistance of the photovoltaic cell
R_{Sh}	Shunt resistance of the photovoltaic cell
S	Switch
T	Photovoltaic cell's operating temperature
T_C	Photovoltaic cell's operating temperature in kelvin
T_H	Total system dynamic head
t_{off}	Off period of converter switch
t_{on}	On period of converter switch
T_s	DC/DC converter switching period
V_{dc}	Output voltage of the boost converter
V_{inma}	The maximum input voltage of the DC/DC converter
V_{mp}	Voltage at maximum power of the PV array
V_{oc}	Open Circuit voltage
V_{pv}	Output voltage of the solar cell
VR_h	Vertical rise head
ρ	Dencity of water

CHAPTER ONE

INTRODUCTION

1.1 Back ground

Energy has the great importance for our life and economy. The energy demand has greatly increased due to the industrial revolution. Fossil fuels have been started to be gradually depleted. The sustainability of our civilization is seriously threatened. On the other hand the greenhouse gas emissions are still increasing due to the conventional generation of energy. It is a really global challenge to reduce carbon dioxide emissions and ensuring secure, clean and affordable energy, and to achieve more sustainable energy systems. Renewable energy sources are considered as a perfect option for generating clean and sustainable energy, among the renewable energy sources, solar energy is sustainable with less carbon emissions [1].

Solar power system finds extensive application in remote areas where access to the grid supply is impractical [1]. From livestock watering to remote home or village water supply needs are met from the solar based water pumps. Most of the PV water pumping systems are connected directly to the solar arrays and use DC motor driven pumps [2]. This system is easy to operate but is inefficient and requires frequent maintenance. Solar pump operated with AC drive uses an inverter with ac motor. Induction motor offer better choice in terms of size, ruggedness, efficiency and maintainability [2].

The DC power from solar array is boosted and fed to an inverter which gives AC to the inverter that drives the motor coupled to a water pump. The output power of a Photovoltaic (PV) array varies according to the sunlight conditions such as solar irradiation, shading and temperature. To obtain maximum power from photovoltaic array, photovoltaic power system usually requires maximum power point tracking (MPPT) controller [3]. Various approaches have been reported to implement MPPT such as perturb and observe (P&O) method, the incremental conductance method, constant voltage method and short-circuit current method [4]. Using this method the maximum power point can be found for specified solar irradiation and temperature condition but they display oscillatory behavior around the maximum power point under normal operating conditions. Moreover the system will not respond quickly to rapid changes in temperature or irradiance. On the other hand the conventional PI controllers are fixed gain feedback controllers. Therefore they cannot compensate the parameter variations in the process and cannot adapt changes in the environment. PI-controlled system is less responsive to real and relatively fast alterations in state and so the system will be

slower to reach the set point. Recently artificial intelligent based schemes have been introduced [5]. Among the intelligent based methods fuzzy logic controller has its own merits such that the MPPT algorithm can be easily formed. The shape of the membership function of the fuzzy logic controllers can be adjusted such that the gap between the operation point and maximum power point can be optimized. Therefore in this thesis an artificial intelligent control technique associated with MPPT controller are used to improve energy conversion efficiency of the photovoltaic system. The proposed intelligent process comprises of expert knowledge which extracts maximum power from a PV module under varying solar irradiation and temperature

1.2 Photovoltaic system

The photovoltaic system consists of interconnected components designed in a way to achieve the specific target of delivering the desired electricity from a small device to the load. Photovoltaic systems are categorized by the main categories of grid connected, standalone systems and hybrid system which comprises different sources of energy such as PV arrays, diesel generators and wind generators. In the grid connected and the stand-alone systems, storage elements such as batteries or super capacitors may be adopted to store the energy during the day time when there is enough sunshine. Hybrid and stand-alone systems are used increasingly in rural areas. Therefore, the PV water pumping system considered in this thesis is a stand-alone system to fulfil the urgent needs of people in the rural locations. The power from the photovoltaic array in the stand-alone system is directly fed to the load without connection to the utility system.

1.3 PV water pumping system energy storage

The system performs well during periods of intense sunlight; but the system output is susceptible to change during cloud cover highly, and gradually falls and rises at the beginning and end of the day. There is a total loss of output during night time when it is dark, unless a storage element is available such as a battery; or in the case of water pumping systems, a storage tank is filled and empties more slowly by the force of gravity. In a time of using the storage element, Lead-acid battery technology is considered to be the most cost effective for many PV systems due to its relatively low cost and wide availability, but the typical life-time of the battery in PV systems is around three to eight years, but in hot climate countries this goes down to typically two to six years since the internal corrosion dramatically increases with high ambient temperature. In addition, batteries are able to satisfy transient surges of

current that are much higher than the instantaneous current directly obtainable from a PV array. However, this process leads to extra power loss since approximately 15-25% of the energy is lost during charging and discharging processes and the PV array must be oversized to cover the energy losses[6]. Furthermore, the batteries require regular maintenance and will degrade very rapidly if the electrolyte is not topped up. Therefore, these factors add significantly to the system cost and maintenance burden. So that energy in a water pumping system can be alternatively stored using water tanks to store the water to be used at night and on days when the solar radiation is insufficient to operate the system by designed matched to the maximum load.

1.4 Problem statements

The PV system is basic in rural area to generate electric sources for the purpose of water pumping system, but many factors limit the implementation of photovoltaic systems . These are high installation cost, power loss and low efficiency of energy conversion. Out of the total installation cost of PV system the storage battery takes the highest one and this process leads to extra power loss since approximately 15-25% of the energy is lost during charging and discharging processes and the PV array must be oversized to cover the energy losses. On the other hand changing atmospheric conditions have an effect on the output characteristics of the PV array, this is a challenge to track the exact MPPT with varying source and load conditions due to non-linear voltage-current characteristics of PV array.

The PV water pumping system considered in this thesis is a stand-alone system to fulfil the urgent needs of people in the rural locations. This thesis focuses on the design of various types of intellent controlers for MPPT tracking system to improve the efficiency of the PV water pumping system.

1.5 Research Objectives

General Objectives: The main objective of this thesis is to design an intelligent and hybrid based MPPT controllers for water pumping system to increase the efficiency of PV standalone water pumping systems.

The Specific Objectives:

The specific objectives considered in thesis are as follows:

- To size and calculate the required amount of generated PV power, for Dolo ado woreda

- To study and analyze how to increase efficiency of PV water pumping system using its output characteristics.
- To investigate and analyses the effect of irradiation and temperature changes on the output characteristics of the PV array and to optimize their effects.
- To develop artificial intelligent and hybrid MPPT control techniques to increase the efficencey of the prposed system.
- Implement the the proposed controllers using MATLAB/SIMULINK to test the overall system efficiency in different weather conditions.
- To analyse the simulation results and make recommendation based on the finding of this research.

1.6 Scope and significance of the thesis

The scope of this thesis is to investigate how to improve the MPPT in a stand-alone PV water pumping system by implementing using MATLAB/SIMULINK to test the overall system efficiency and compared FLC, ANNC and ANFIS controller. In this thesis the application of artificial intelligence controller is signify in a time of hard non-linear systems occur to control a system like a linear one and the thesis up grades the detail knowledge of internal characteristics of maximum power point tracking (MPPT) in different techniques.

1.7 Methodology

The methodologies that we followed in this thesis are listed by the following chart.

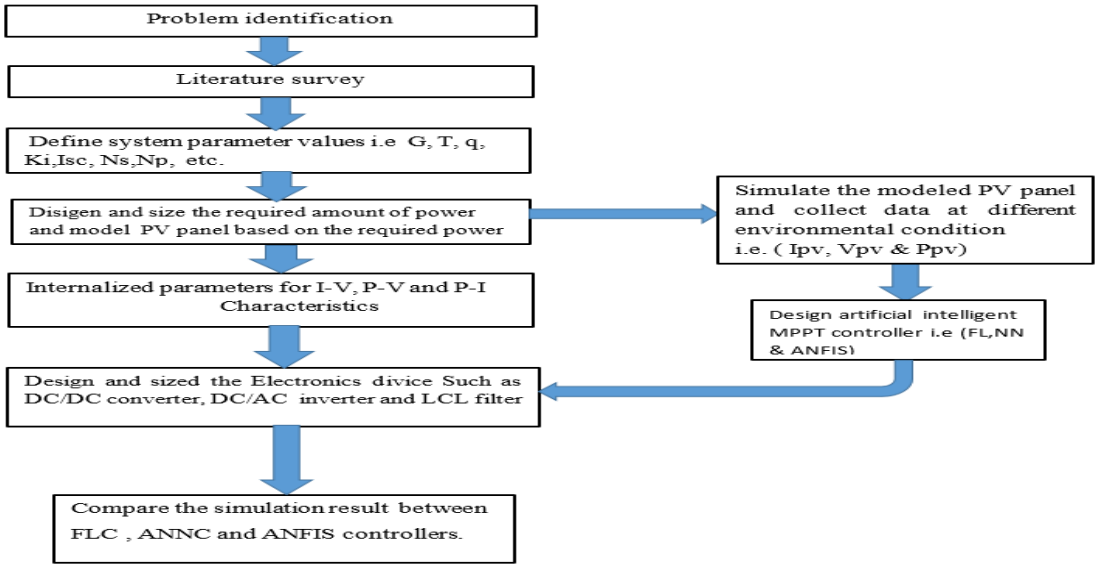

Fig. 1.1 General methodology flow chart

1.8 Thesis outlines

This thesis contains totally six chapters and the content of each chapters are disused below

Chapter one is an introductory chapter and presents an overview of the thesis background, objectives, scope and significance and a brief summary of the thesis. It presents a brief introduction to PV energy, and how increasing the efficiency of PV water pumping systems attractive and economically viable in remote locations.

Chapter two provides a review of the literature on some components of PV water pumping systems and the MPPT algorithms with controlling techniques and Performance specifications of MPPT control algorithm techniques are presented and briefly explained.

Chapter three contains the modeling and design the Standalone PV Water Pumping System. In this chapter the design of system for Delo adwo wareda is presented and the modelling of the whole components of the PV water pumping system and its operation is discussed detail and sized is done.

Chapter four introduces the design of controllers for PV standalone water pump system. In this chapter discussed detail in two artificial intelligent controller techniques and the hybrid of them. for Dolo-ado woreda PV water pumping system based on the sizing in chapter three. It provides a fuzzy logic control development and applications, and illustrates its basic structure and the working principles. This chapter also provides a brief explanation of the working principles including the learning and testing processes of the ANN. Then the construction of the proposed ANN controller is presented and the collection of training data sets which is used for training the proposed ANN controller is discussed in detail along with the training process. This chapter also discussed the hybridization of the NN and FL controllers starting from their weakness and strongest it gives brief explanation and working principles of ANFIS controller and finally discussion of each control based MPPT method for the PV water pumping system is presented.

Chapter Five presents the MATLAB/SIMULINK implementation results of the system and describes each of the subsystems in detail. This chapter also discusses and compares the MATLAB results for the proposed maximum power-point tracking algorithms applied to photovoltaic water pumping system. It also shows the behavior and performance of each method under similar conditions of temperature and irradiation and chapter six conclusions and contribution summary of the thesis are presented. Moreover, potential research ideas for future work in this field are proposed.

CHAPTER TWO

CONTROL OF MAXIMUM POWER POINT TRACKING FOR PHOTOVOLTAIC WATER PUMPING SYSTEM

2.1 Maximum Power point Tracking (MPPT) System

MPPT is basic for photovoltaic generation to operate the system at high power efficiency by ensuring that, the system is always working at the peak power point in a time of changes weather conditions. In other words transfer the maximum power to the load by matching the source impedance with the load impedance. To confirm that, an MPPT system has been implemented, which enables the maximum power to be delivered during the operation of the solar array and which tracks the variations in maximum power caused by the changes in the atmospheric conditions. The MPPT system is basically an electronic device inserted between the PV array and the load. A DC-DC switching power converter or DC-AC inverter along with an MPPT control algorithm to operate the PV system in such way it can transfer the maximum capable power to the load.

As the solar panel outputs power, maximum generated power changes with the atmospheric conditions and the electrical characteristic of the load may also vary. The main objective of the MPPT is to match these two parameters by adjusting the duty ratio of the power converter [7]. The matching of MPP illustrate as the following Fig.

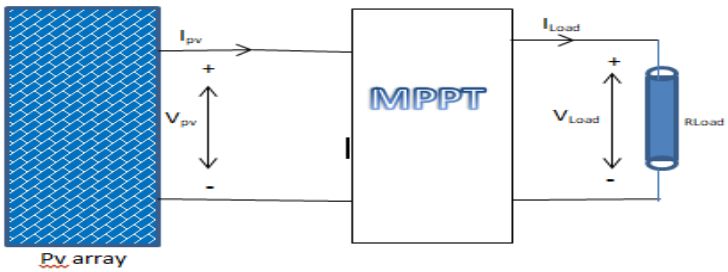

Fig. 2.1 Converter acting as a Maximum Power Point Tracker

2.2 Performance specifications of MPPT controller

The dynamic response, steady-state error and tracking efficiency would be considered for a successful design when evaluating the performance of a new or modified MPPT control algorithms [7].

The dynamic response

The Response of a MPPT control algorithm needs to be fast to track the MPP during the rapid changes in the atmospheric conditions. The higher the tracking speed of the MPPT algorithm, the lower the loss in solar energy in the system

Steady-state error

MPPT control algorithm should stop tracking, once the MPP is located and should force the system to maintain operation at this optimal operating point as long as possible. However, this is impossible to achieve practically in an actual MPPT system because of the active perturbation process in MPPT algorithms and the continuous variation in solar insolation and temperature. This phenomenon has a negative impact on the PV system efficiency.

Tracking efficiency

The tracking efficiency is a very important step, to quantify how successfully an MPPT control algorithm tracks the MPP and to what extent it contributes to increase the overall performance of the PV system compared to other methods. According to [8] the tracking efficiency is defined as the ratio between the actual power of the PV array and the theoretical power during the same time period. To calculate the tracking efficiency we have use the following equation

$$\eta_{MPPT} = \frac{1}{n}\sum_{i}^{n} \frac{P_{actual,i}}{P_{Max,i}} \tag{2.1}$$

2.3 DC-DC converter for photovoltaic system

The switch mode DC-DC converter is considered the main part of a MPPT system. These are widely used to convert unregulated DC inputs into a controlled DC output at a desired voltage and current levels in DC power supplies and DC motor drives or as input of the inverte [9]. The same converter is used for a MPPT to provide load matching for the maximum power transfer by regulating the input voltage at the PV array MPP by controlling the duty ratio (D). DC-DC converters are used to interface the photovoltaic module with an inverter, in order to ensure the photovoltaic module is always operating at the maximum power point to get the desired input voltage level to the inverter. This is done by controlling the converter duty ratio (D) with maximum power point tracking algorithms (MPPT).

Generally, converters are categorized into two types: isolated and non-isolated converters. In the isolated topologies a small high frequency electrical isolation transformer is used to provide the DC isolation between the input and output of the DC converter; and step up or down of the output voltage is achieved by changing the transformer turns ratio. These types of converter are used in switch mode power supply, (half bridge and full bridge are most common).

Non-isolated converters do not have an isolation transformer. They are very often used in DC motor drives [9]. Non-isolated converters are classified into three types: step up (boost), step down (buck), and step up & step down (buck-boost).

2.3.1 Step-down (buck) converter

In this type of DC-DC converter, the average output voltage Vo produced is always lower than the DC input voltage. The buck converter is used for voltage step-down in PV applications, such as for charging batteries and in water pumping systems.

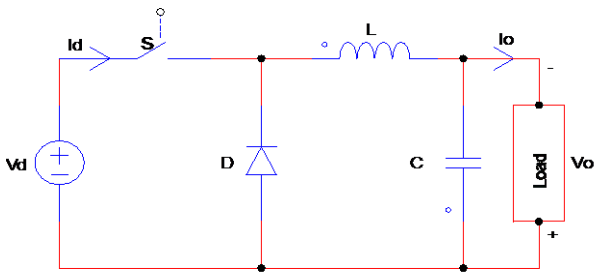

Fig. 2.2 step-down Buck converter

The diode (d) is used to enhance the output filtering effect and prevent the switch from absorbing or dissipating the inductive energy because this would lead to overheating the switch. In addition to that, there is an inductor and capacitor at the output of the converter which forms a low-pass filter to attenuate the output voltage fluctuation. Thus the diode enables the converter to convert stored energy in the inductor to the load. This is a reason why we have higher efficiency in a DC-DC Converters as compared to a linear regulator. When the switch closes, the current rises linearly. When the switch opens, the freewheeling diode causes a linear decrease in current.

The function of the inductor is to limit the current slew rate (current in rush) through the power switch when the circuit is ON. The current through the inductor cannot change suddenly. When the current through an inductor tends to fall, the inductor tends to maintain

the current by acting as a source. The key advantage is when the inductor is used to drop voltage, it stores energy. Also the inductor controls the percent of the ripple and determines whether or not the converter is operating in the continuous conduction mode. The smaller inductor value enables a faster transient response; it also results in larger current ripple, which causes higher conduction losses in the switches, inductor, and parasitic resistances. Also the smaller inductor value requires a larger filter capacitor to decrease the output voltage ripple.

The capacitor provides the filtering action by providing a path for the harmonic currents away from the load. Output capacitance (across the load) is required to minimize the voltage overshoot and ripple present at the output of a step-down converter.

The capacitor is large enough so that its voltage does not have any noticeable change during the time of switch is off [9].

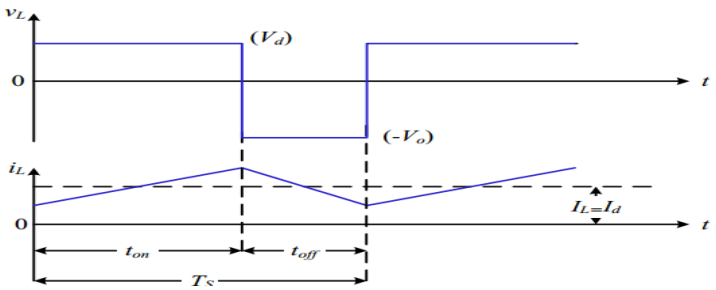

Fig. 2.3 Buck converter wave form

During the steady-state condition the relation between the output voltage Vo and the duty ratio of the converter can be defined by the following equation.

$$\frac{Vo}{Vd} = \frac{D}{1-D} \tag{2.2}$$

From the above equation the output voltage could be higher or lower than the input voltage according to the value of the duty ratio. For the duty ratio condition D > 0.5, the output is higher than the input as in a boost converter. If D < 0.5 the output is lower than the input as in a buck converter.

$$L = \frac{(1-D)^2 R}{2Fs} \tag{2.3}$$

$$C = \frac{D}{(Rfs(\Delta Vo/Vo)} \tag{2.4}$$

2.3.2 Step-up (boost) converter

The applications of boost converter operation are the regenerative braking circuit of DC motors and in regulated DC power supplies. In this type of converter the output voltage is always greater than the input voltage. Therefore the step up converter can be applied to MPPT systems where the output voltage needs to be greater than the input voltage. Such as in a grid-connected system where the boost converter maintains a high output voltage even if the PV array voltage falls to low values.

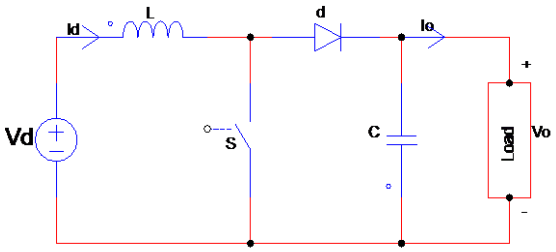

Fig. 2.4 Step-up boost converter

When the switch S is on the diode d is reverse based. Consequently, the current in the inductor L rises linearly due to the input voltage source, and in this case the output stage is isolated and the capacitor (C) is partially discharged supplying the current load. When the switch is off during the second interval the diode is conducting, and during this time the output stage receives energy from both the inductor and the input source. The wave form of the inductor current during continuous conduction mode is shown below, where the inductor current flows continuously, i.e. $I_L(t) > 0$ [9].

A dual stage power electronic system comprising a boost type dc-dc converter and an inverter is used to feed the power generated by the PV array to the load. To maintain the load voltage constant a DC-DC step up converter is introduced between the PV array and the inverter. The DC-DC converter is considered the main part of a MPPT system. These are widely used to convert unregulated DC inputs into a controlled DC output at a desired voltage and current levels in DC power supplies The voltage across the DC-DC converter is fed to a three-phase, sine wave six step inverter a three-phase fixed amplitude and fixed frequency supply is obtained to feed an inverter as input. When the converter is operating at steady-state condition, the duty ratio (D), can be expressed by Equation

$$D = 1 - \frac{\text{Vd\_min}}{\text{Vout}}\eta \tag{2.5}$$

Where D denotes the duty ratio, ($assume\ \eta \cong 1$) efficiency, Vd and Vout denotes the input and the output voltages of the converter, respectively. From the above equation it can be seen that, the increase in the duty ratio D will increase the value of the output voltage, Vout. In addition the change in the duty ratio results in change in the input and the output current of the converter.

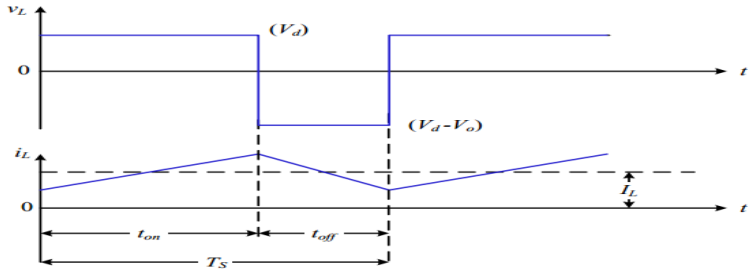

Fig. 2.5 Step-up converter wave form of the inductor current and voltage in continuous current

The filter inductor and capacitor to oprate the converter in the continuous conduction mode can be calculated by the following equations

$$L = \frac{\mathrm{Vd_{min}}}{\Delta \mathrm{IL} f_s} D \tag{2.6}$$

$$C = \frac{\mathrm{Io}}{\Delta \mathrm{Vo} f_s} D \tag{2.7}$$

where fs is switching frequency, Io and I_{in} is output and input current respectively.

2.3.3 Cuk (buck-boost) converter

The Cuk converter can be obtained by using the duality principle on the circuit of a Buck-Boost topology.. It is clear that the input circuit of Cuk converter is a Boost converter and the output circuit is seen to be a Buck converter. Hence the Cuk converter is similar to the Buck-Boost converter, it provides a negative polarity regulated output voltage with respect to its terminal of the input voltage [9, 10].

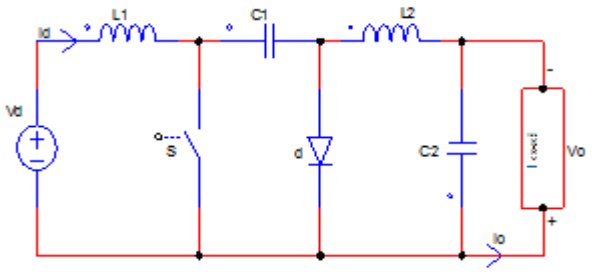

Fig. 2.6 Cuk converter

In steady-state operation, the average voltage of the inductor is zero, therefore by applying Kirchoff's voltage law to the circuit.

$$Vc1 = Vd + Vo \tag{2.8}$$

Cuk converter shows two different operating modes. The first mode obtained when the switch S is off. In this case the diode d is conducting. Therefore, the capacitor C1 is charged by the input Vd through the inductor L1. The energy stored in the inductor L2 feeds the load. Hence, the following relationship is obtained [9, 10].

$$Ic1 = Il1 \tag{2.9}$$

The second mode of operation exists when the switch S is on. The diode d is not conducting because it is reverse-based due to C1. The capacitor C1 discharges through the switch S, transferring its energy to the load and L2. Assume the inductor currents are ripple free, because the inductors are large enough. Therefore, the following relationship is obtained.

$$-Ic1 = Il2 \tag{2.10}$$

For one time period of operation, the average capacitor current is zero. Therefore, by rearranging the above two equation

$$[Ic1_{SON}]DTs + [Ic1_{SOFF}][1-D]T_s = 0 \tag{2.11}$$

$$I_{L2}.DT_s + I_{L1}[1-D]Ts = 0 \tag{2.12}$$

$$\frac{IL1}{IL2} = \frac{D}{D-1} \tag{2.13}$$

Where D is the duty ratio of the converter and it is the ratio of the conduction time ton to the switching period TS. The value of D changes between 0 and 1 [9]. Assuming the converter is ideal in other words there are no losses. Therefore, the input power of the converter P_{in} is equal to the output power P_{out}.

$$Pin = Pout \tag{2.14}$$

$$V_d I_{L1} = Vo I_{L2} \tag{2.15}$$

$$I_{L1}/I_{L2} = Vo/Vd \tag{2.16}$$

Then finally;

$$\frac{Vo}{Vd} = \frac{D}{D-1} \tag{2.17}$$

- If $0 < D < 0.5$ the output is smaller than the input.

- If D = 0.5 the output is the same as the input.
- If 0.5 < D < 1 the output is larger than the input.

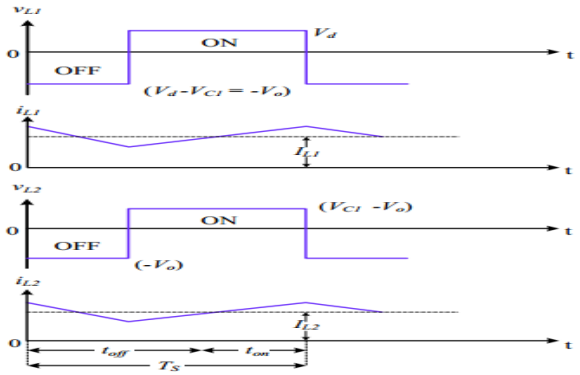

Fig. 2.7 cuk converter wave form

In the literature, many types of DC-DC converters have been studied to see which converter is suitable for the MPPT stage of the PV system. In the literature [9,11], a comparative analysis from different viewpoints has been made between some commonly used topologies to track the maximum power of the PV array. Reference [12] showed that, the Buck-Boost converter has the advantage over individual Buck and Boost converters of following the MPP at all times, under any conditions of solar global radiation, cell temperature and connected load. However, the individual Boost and Buck types are the most efficient converters for a given price. The author in [13] found that each topology has its pros and cons in comparison to the others. For example, some of them present low current ripple such as SEPIC and Cuk converter and may provide input-output isolation. For water pumping systems, the output voltage needs to be stepped down or step-up so that Buck and Boost converter is suitable. The Cuk and SEPIC converters have the advantage that their input current is continuous, and they can draw ripple free current from a PV array [14]. However, Cuk, SEPIC and Buck-Boost converters have a higher number of passive components and high current, voltage and switched power stresses in the switch or transistor compared to the Boost converter. This also affects the whole system efficiency [15], since the switched current and voltage are higher for the same output power as an individual buck or boost.And also it needs the higer Voltages to feed the inverter inorder to get the desired AC voltages which is supply to the Ac machins. Boost converters developed to maximize the energy harvest for photovoltaic systems. Transformers used for voltage conversion at mains frequencies of 50–60 Hz must be large and heavy for powers exceeding a few watts. This makes them expensive, and they are subject to energy losses in their windings and due to eddy currents in their cores. Boost techniques that use transformer's work at much higher frequencies, requiring only much

smaller, lighter, and cheaper wound components. Therefore, in this work it was decided to use a boost converter because the DC-DC boost converter is an important stage in the PV inverter system because it increases the overall efficiency of the system. In fact, the operating with higher input voltage leads to lower input current required for a given power and hence reduces the losses. It is responsible to regulate and boost the DC output voltage of the PV system. In this work, a boost converter operating in continuous conduction mode has been designed to step up the voltage of the PV system to a higher constant voltage of 680V to feed an inverter.

2.4 DC-AC converter for photovoltaic system

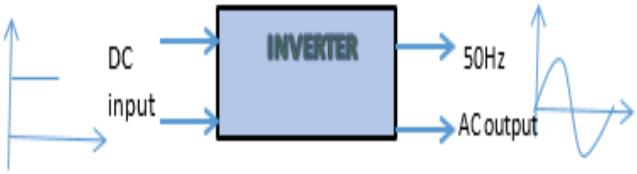

Fig. 2.8 Inverter block diagram

An inverter is a device that changes DC voltage into AC voltage. A direct current (DC) is a current that flows in only one direction, while an alternating current (AC) is that which flows in both positive and negative directions. There are two basic types of inverters based on type of sources input; Voltage source(VSI) and Current Source(CSI). Voltage/current source implies that the voltage/current level doesn't change instantly as the result of switching. Photovolatic source and Battries source can be used as voltage sources. It is difficult to get ideal voltage or current sources. In practice voltage sources are simulated by voltage stiff (power supply with shunt capacitor) and hence voltage stiff inverter. Similarly, current sources are simulated by current stiff (power supply with serious inductor). In the other way Inverter may be single-phase (hafe bridge, full bridge) or three phase(hafe bridge, full bridge) but single-phase half and full bridge voltage source inverter cover low-range power applications. The main purpose of these topologies is to provide a three-phase voltage source, where the amplitude, phase and frequency of the voltages can be controlled.in this worke I have to discused three phase inverters with the controling techniques and select the best one based on the performance parametres.

2.4.1 Three phase inverter topology

There are many three phase inverter types ,but for coparation I have desccused some of them. Three phase inverters are often used to supply three-phase loads, such as ac motors. The basic structure of a three-phase inverter is shown in Figure below. Each of the three legs produces an output which is displaced by 120◦ with respect to each other. The output of each leg depends on the status of the switch and the input voltage, Vdc. Since one of the two switches in each leg is always on, the output voltage is independent of the output load current

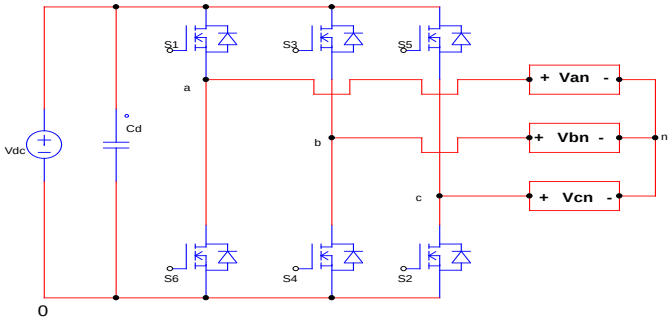

Fig. 2.9 Three-phase full –Bridge Inverter

The standard three-phase VSI topology is shown in Fig.2.9, And the eight valid switch states are given in Table 2.1. As in single-phase VSIs, the switches of any leg of the inverter (S1 and S4, S3 and S6, or S3 and S2) cannot be switched on simultaneously because this would result in a short circuit across the dc link voltage supply. Similarly, in order to avoid undefined states in the VSI, and thus undefined ac output line voltages, the switches of any leg of the inverter cannot be switched off simultaneously as this will result in voltages that will depend upon the respective line current polarity. As explained earlier in order that the circuit satisfies the KVL and the KCL,thus the nature of the two switches in the same leg is complementary [16].

$$S1 + S6 = 1 \tag{2.18}$$

$$S3 + S4 = 1 \tag{2.19}$$

$$S5 + S2 = 1 \tag{2.20}$$

Table 2.1 Eight state of three phase inverter

	S1	S3	S5	Vab	Vbc	Vca
1	0	0	0	0	0	0
2	0	0	1	0	-Vdc	Vdc
3	0	1	0	-Vdc	Vdc	0
4	0	1	1	-Vdc	0	-Vdc
5	1	0	0	Vdc	0	-Vdc
6	1	0	1	Vdc	-Vdc	0
7	1	1	0	0	Vdc	-Vdc
8	1	1	1	0	0	0

Among the eight valid states, two of them produce zero ac line voltages. In this case, the ac line currents freewheel through either the upper or lower components. The remaining states produce non-zero ac output voltages. In order to generate a given voltage wave form, the inverter moves from one state to another. Thus the resulting ac output line voltages consist of discrete values of voltages that are Vdc , 0, and -Vdc for the topology shown above. The selection of the states in order to generate the given waveform is done by the modulating technique that should ensure the use of only the valid states[16].

$$\frac{Vdc}{2}(S1 - S6) = Van + Vno \tag{2.21}$$

$$\frac{Vdc}{2}(S3 - S4) = Vbn + Vno \tag{2.22}$$

$$\frac{Vdc}{2}(S5 - S2) = Vcn + Vno \tag{2.23}$$

Expressing the Equations above in terms of modulation signals and making use of conditions

$$\frac{Vdc}{2}(M1) = Van + Vno \tag{2.24}$$

$$\frac{Vdc}{2}(M3) = Vbn + Vno \tag{2.25}$$

$$\frac{Vdc}{2}(M5) = Vcn + Vno \tag{2.26}$$

where M is called the modulation signal, which can be any sine or cos term(in accordance to Fourier series) depending on the control we want to implement. The more general fundamental component for M is given as

$$M = m_\alpha cos(\omega t - \alpha) \tag{2.27}$$

And m_α is called the modulation index which can vary from 0 to 1 and for values of m_α less than '1' a linear modulation range is supposed to exist and for values of m_α greater than '1' it is operated in the over modulation range.

Then adding the valide state equation above which is equal to;

$$\frac{Vdc}{2}\{(S1+S3+S5-(S6+S4+S2)\}=Van+Vbn+Vcn+3Vno \quad (2.28)$$

As we know the balanced voltages $Van+Vbn+Vcn=0$ and making use of the conditions from Equations above the Equation becomes

$$\frac{Vdc}{6}(2S1+2S3+2S5)=Vno \quad (2.29)$$

Substituting for Vno then each phase voltage becomes

$$\frac{Vdc}{3}(2S1-S3-S5)=Van \quad (2.30)$$

$$\frac{Vdc}{3}(2S3-2S1-S5)=Vbn \quad (2.31)$$

$$\frac{Vdc}{3}(2S5-S1-S3)=Vcn \quad (2.32)$$

Then the RMS value can be calculated as follws

$$VRMS=V_{ratio}V_{dc} \quad (2.33)$$

whre, V_{ratio} is different for the type of applying control techniques which is the basic parameter.

Sinusoidal pulse widith Modulation in Three-Phase Voltage Source Inverters

As in the single phase voltage source inverters PWM technique can be used in three-phase inverters, in which three sine waves phase shifted by 120°with the frequency of the desired output voltage is compared with a very high frequency carrier triangle, the two signals are mixed in a comparator whose output is high when the sine wave is greater than the triangle and the comparator output is low when the sine wave or typically called the modulation signal is smaller than the triangle.

The output voltage from the inverter is not smooth but It's a discrete waveform and so it is more likely than the output wave consists of harmonics, which are not usually desirable since they deteriorate the performance of the load, to which these voltages are applied[16].

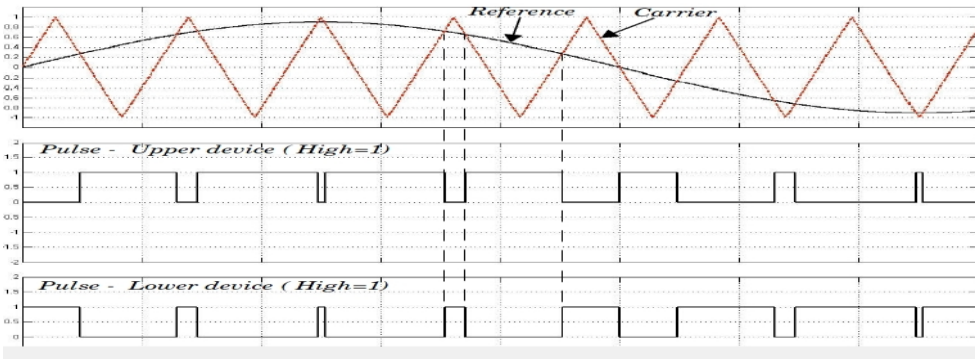

Fig. 2.10 PWM illustration by the sine-triangle comparison method

This signal is internally generated by phase-shifting the original reference signal by180 degrees. For a three-phase bridge, three reference signals are required to generate the six pulses. The reference signals can also be internally generated by the PWM generator. In this case, specify a modulation index, a voltage output frequency, and phase.

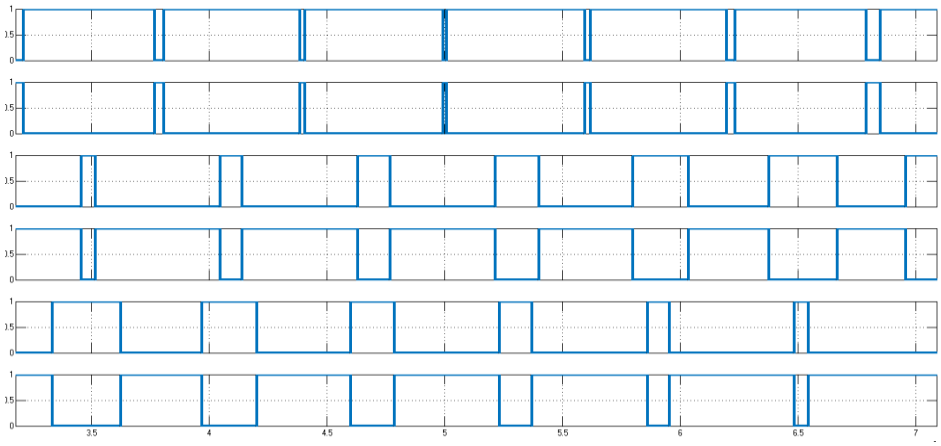

Fig. 2.11 pulse generated by 2-level PWM in Three-Phase VSI

Six Step Voltage Source Inverter

Three-phase bridge inverters are most commonly used in ac motor drives and general-purpose ac supplied. The circuit for the six-step VSI is as shown in Figure below, which consists of three half-bridges, which are mutually phase-shifted by $\frac{3}{2}\pi$ angle [17].

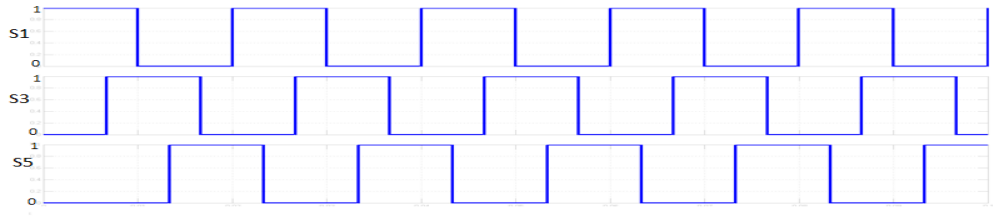

a)

b)

Fig 2.12 180^0 mode Generation of the switching signals for (a) top devices, (b) bottom devices

The square wave phase voltages with respect to the fictitious dc center tap can be expressed using Fourier series as,

$$Van = \frac{2Vdc}{\pi}\left[cos\omega t - \frac{1}{3}cos3\omega t - \frac{1}{5}cos5\omega t - \cdots\right] \quad (2.34)$$

Vbn is Shifted by 120 degree

$$Vbn = \frac{2Vdc}{\pi}\left[\cos(\omega t - \frac{2\pi}{3}) - \frac{1}{3}\cos 3(\omega t - \frac{2\pi}{3}) - \frac{1}{5}\cos 5(\omega t - \frac{2\pi}{3}) - \cdots\right) \quad (2.35)$$

$$Vcn = \frac{2Vdc}{\pi}\left[\cos(\omega t + \frac{2\pi}{3}) - \frac{1}{3}\cos 3(\omega t + \frac{2\pi}{3}) - \frac{1}{5}\cos 5(\omega t + \frac{2\pi}{3}) - \cdots\right) \quad (2.36)$$

The line voltages can thus be obtained from the phase voltages as

$$\text{Vab} = Van - Vbn$$

$$Vab = \frac{2\sqrt{3}Vdc}{\pi}\left[\cos(\omega t + \frac{\pi}{6}) - \frac{1}{5}\cos 5(\omega t + \frac{\pi}{6}) - \frac{1}{7}\cos 7(\omega t + \frac{\pi}{6}) - \cdots\right) \quad (2.37)$$

$$\text{Vbc} = Vbn - Vcn$$

$$Vbc = \frac{2\sqrt{3}Vdc}{\pi}\left[\cos(\omega t - \frac{\pi}{2}) - \frac{1}{5}\cos 5(\omega t - \frac{\pi}{2}) - \frac{1}{7}\cos 7(\omega t - \frac{\pi}{2}) - \cdots\right) \quad (2.38)$$

$$\text{Vca} = Vcn - Van$$

$$Vab = \frac{2\sqrt{3}Vdc}{\pi}\left[\cos(\omega t + \frac{5\pi}{6}) - \frac{1}{5}\cos 5(\omega t + \frac{5\pi}{6}) - \frac{1}{7}\cos 7(\omega t + \frac{5\pi}{6}) - \cdots\right) \quad (2.39)$$

The fundamental of the line voltages is $\sqrt{3}$ times that of the phase voltage, and there is a leading phase-shift of $\frac{\pi}{6}$.The line voltages waves as shown in below have a characteristic six-step wave shape and thus the name for this inverter. The characteristic harmonics in the wave form are 6n ±1, n is being an integer.

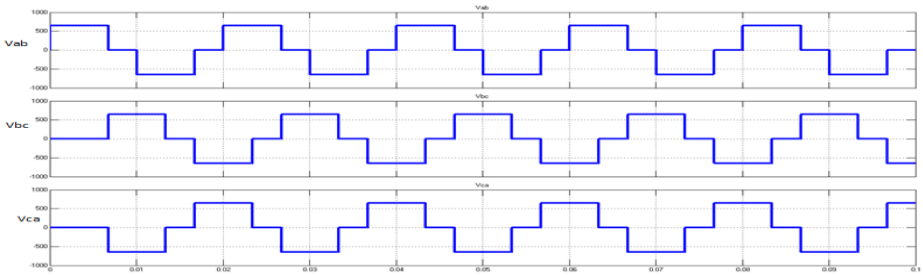

Fig. 2.13 180^0 conduction mode six step inverter line voltage (Vab, Vbc & Vca)

The three-phase fundamental as well as the harmonic components are balanced with a mutual phase-shift angle of $\frac{2\pi}{3}$.

Now from the above equation the Line-to-line peak voltage value is

$$Vp = \sqrt{3 \times}[\frac{2}{2\pi}\int_0^{\frac{2}{3}\pi}(Vdc)^2 d(\omega t)]^{\frac{1}{2}}$$

$$Vp = \frac{\sqrt{3}\,Vdc}{2}*\mathrm{m} \qquad (2.40)$$

where Vp is peak voltage and m is modulation indeix.

2.4 Output Filters for photo voltaic system

The output of the full bridge inverter is connected to a low pass filter to supply a pure sinusoidal output voltage to the load. The factors such as efficiency, voltage and current harmonics constraints, weight, volume and cost must be taken in to account when selecting the optimal filter design [14]. Also, the saturation of the inductor core should be avoided [18]. There are various filters topologies of sine wave inverter. These topologies include L filter, LC filter and LCL filter.

L-filter

L-filter filter has super performance in terms of voltage to current conversion but the damping of the high frequency (HF) noise is weak.

LC filter

The LC filter has good performance in terms of current to voltage conversion and noise damping but the filter capacitor may be insecure to line voltage harmonics, which result in large currents.

LCL filter

The LCL filter has the same good properties with the L and the LC filters. Moreover, the damping of high frequency noise is better due to the extra inductance, and the capacitor is no more exposed to line voltage distortion. On the other hand, LCL can sometimes cost more than other topologies and is inherently unstable due to resonance [14]. For reducing oscillations and unstable conditions of the LCL filter, a damping resistor (R_d) is placed in series with the filter capacitor. Damping resistor is reliable, but it increases the losses and decreases the efficiency of the system, but the benefits of LCL filter over other types of filter are the reasons that made this filter are used in the proposed inverter circuit.

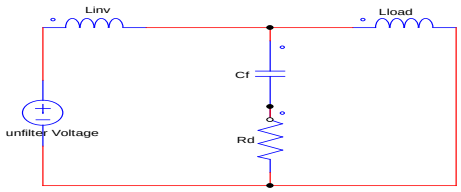

Fig. 2.14 LCL-filter

There are some important factors that should be considered when design LCL filter which comprise such as: Inverter output ripple current, Inverter to load inductor ratios and filter capacitance maximum power variations.

2.5 MPPT Controller algorithms

Several MPPT algorithms have been proposed for PV power systems in recent years, to locate the MPP and increase the system efficiency.

The MPPT algorithms may be divided into two types, which are indirect control or “quasi tracking techniques” and direct control or “true tracking techniques” [19]. In the indirect control techniques, the MPP is calculated either by measuring the voltage and current of the PV array, the solar insolation, or by the use of mathematical functions obtained from empirical data. Therefore, these techniques are incapable of tracking the MPP with varying irradiation and temperature.

The indirect control techniques are look-up table technique, constant voltage technique, fractional open-circuit voltage and fractional short-circuit current. However, the true tracking techniques have the ability to find the optimum operating point even under changing atmospheric conditions, because they do not rely on previous knowledge of or calculated data from the PV array V-I characteristics. The true tracking techniques are the perturbation and observation (P&O) technique, incremental conductance (INC) technique. In the tracking process one or two variables are used for calculating the MPP. The fractional open-circuit voltage and fractional short-circuit current use only one variable, either the PV array output voltage or current respectively, though the P&O and INC methods need both variables to determine the MPP.

2.5.1 Simple panel load matching

The simple panel load matching technique is one of the simplest techniques to operate a PV array close to its maximum power point. In this technique the optimum operating point of the PV array is determined either by a series of measurements under average operating conditions or theoretical calculation. The load is designed to produce the values of PV voltage and current corresponding to the MPP [20].

- This method has the advantages of simplicity and no additional circuit is used, therefore, the power loss between the panel and the battery is reduced and the risk of component failure is kept low for the whole system.
- However, the system does not take into consideration the changes of solar irradiation or temperature

2.5.2 Load switching technique

In this configuration different panels are connected in series and parallel in an appropriate manner to form a PV array. Then, the PV array is connected to a number of controllable battery cells connected in series to fulfill the load matching process as illustrated in Fig 2.15.

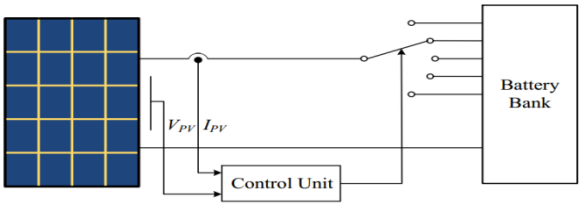

Fig. 2.15 Schematic block diagram of the load-switching method

The group of batteries is used to store the energy produced by the PV array. The control unit detects the output of the solar array in real time, finds out the optimum operating point, and maintains operation as close as possible to this by switching the battery connection.

This technique has the drawbacks that it requires extra switching circuits and wiring, and the stepwise, switched operating voltage cannot guarantee accurate tracking of MPP, Moreover; it is difficult to keep an equal charge level on all the battery cells, hence degrading battery life in the long term.

2.5.3 Constant voltage method (CV)

If the PV system is implemented without a battery to tie the bus voltage to an approximately constant level, a simple control scheme of the constant voltage method can be applied as presented in [9]. In this method the feedback of the PV voltage is compared with a fixed reference voltage and the resultant signal adjusts the duty ratio of the DC-DC converter to keep the operating point of the PV array at the MPP or close to it. The reference voltage is set to be equal to the V_{MPP} of the characteristic PV array or to another calculated best fixed voltage.

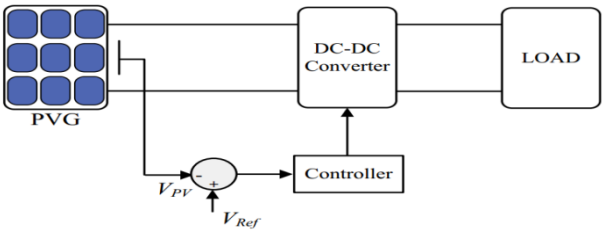

Fig. 2.16 Voltage feedback MPPT method with constant voltage reference

This technique has the drawback that it does not correct for environmental variation such as change in irradiation and temperature it fixes the reference voltage to a best fixed voltage value and holds it constant under any operating condition instead of following the MPP [15].

2.5.4 Perturb and observe (P&O) algorithm

The perturb and observe algorithm considered to be the most commonly used MPPT algorithm, among the other techniques because of its simple structure and ease of implementation. It is based on the concept that on the power-voltage curve, the change in the PV array output power is equal to zero (ΔPPV = 0) on the top of the curve. The P&O operates by periodically perturbing (incrementing or decrementing) the PV array terminal voltage or current and comparing the corresponding output power of PV array. If the

perturbation in terminal voltage leads to increase in the PV power (ΔPpv > 0) the perturbation should be kept in the same direction, otherwise the perturbation is moved to the opposite direction. The perturbation cycle is repeated until reaching the maximum power at(ΔPpv = 0).

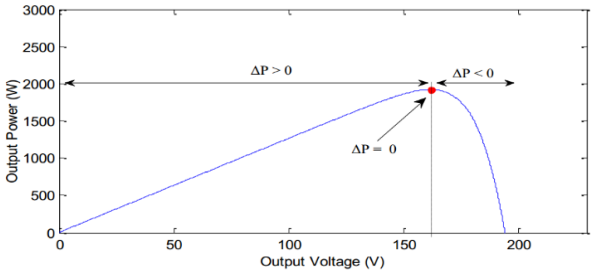

Fig. 2.17 perturbs and observes technique

The advantages of this technique are simplicity, ease of implementation and it does not require a previous knowledge of the PV array. On the other hand P&O will not stop perturbing when the MPP is reached and will oscillate around it resulting in some unnecessary power loss.

2.5.5 Intelligent control techniques

Fuzzy logic Control

Fuzzy logic is implemented in a control system to emulate human-like decisions in control. FL techniques have been widely used in a wide range of engineering applications due to their heuristic nature associated with simplicity and effectiveness for both linear and nonlinear systems [21]. It can be implemented in software, hardware or a combination of both. Fuzzy sets are considered as the brain of the fuzzy control system which in turn is responsible for converting analog input values into a scale of 0 to 1. Fuzzy logic control uses human expert knowledge to make control decisions. Fuzzy logic can be used in the treatment of unknown systems to model imprecise data and experience knowledge. The fuzzification block is responsible for converting the numerical input variables to linguistic variables in accordance with the membership functions. The Fuzzy inference is the process of formulating the mapping from a given input to an output using fuzzy logic. The defuzzification block converts the linguistic output from the inference engine to numerical output values using the membership function. Fuzzy rule base refer to a set of pre-defined instructions which link the different values of crisp values with different subsets of fuzzy output space [22].

The inputs to the fuzzy control are the error in the power and the change of error the output is the duty cycle variable that controls the pulse width generation block. The error is given by the following equation. [23]

$$E(K) = P(K) - P(K-1) \; or \; E(K) = V(K) - V(K-1) \tag{2.41}$$

The change in error is given by

$$CE(K) = E(K) - E(K-1) \tag{2.42}$$

The output of the fuzzy controller is the duty cycle

$$(K) = D(K-1) - dD \tag{2.43}$$

- Fuzzy systems are suitable for uncertain or approximate reasoning, especially for a system with a mathematical model that is difficult to derive. And fuzzy logic allows decision making with estimated values under incomplete or uncertain information.
- Most of the time the drawback of the fuzzy systems are not take experience from the previous data and If the input parameters to be controlled increases, fuzzy logic controller will not be useful as effective rules cannot be determined.

Artificial Neural Network

Artificial neural networks are one of machine learning techniques which have been developed as generalizations of mathematical models of biological nervous systems. The learning capability of an artificial neuron is achieved by adjusting the weights in accordance to the chosen learning algorithm. The most widely-used neural network for prediction is the single hidden layer feed-forward network. The ANNs operate like a black-box model. It does not require detailed information about the system. They effectively learn the relationship between the input and the output variables by making use of trends in previously recorded data. Also ANNs have the ability to work with highly nonlinear relationships, can work with numerical or analogue data, are relatively robust in terms of finding best-fit solutions, and the user does not require sophisticated mathematical knowledge [22]. The non-linear variation of output voltage and current with solar radiation levels are mainly due to aging and load current. To predict this, artificial neural network using the back propagation theorem is trained. The relationship between input and output variables are studied from their previously recorded data. The ability to handle large and complex systems with many interrelated parameters is done using ANN. These trained data are used to approximate an arbitrary input-output mapping of the system. Since the solar insolation is varying, the corresponding reference voltage (Vref =Vmpp) for the feed forward loop also changes which is estimated. The main

problem in ANNs are it is difficult to get the trained data, in addition to that the ANN is not make decision

Hybrid Fuzzy-Neural Network

Instead of using the above intelligent controller individually, there is a way to form hybridization that the combination of neural network and fuzzy algorithms. This hybridization overcomes the weakness of individual controllers and cooprate the strongest. The parameters like change in error (ΔE) and error (E) with respect to time is fed into the fuzzy controller and it determines the suitable firing angle for the inverter which is used to supply voltage to suitable loads. Fuzzy logic system deals with explicit knowledge which is explainable and understandable, whereas neural networks deal with implicit knowledge which acquired only by learning. As discussed by Chin – Teng (2000), fuzzy logic has tolerance for imprecision of data and neural networks have tolerance for noisy data and neuro-fuzzy system is one of the most powerful data handling method for PV arrays. The following table compares the FL and NN and, used for Hyberdized the two by co-oprate the strongest and care thire weaknesses.

Table 2.2 comparison of fuzzy logic and neural network controls

Properties	FL	NN
Knowledge representation	Good	Bad
Imprecision tolerance	Good	Good
Adaptability	Good	Good
Learning ability	Bad	Good
Explanation ability	Good	Bad

In general, all the combinations of techniques based on neural networks and fuzzy logic can be called neuro-fuzzy systems. The different combinations of these techniques can be divided, in accordance with [24], in the following classes.

Cooperative Neuro-Fuzzy Systems: In this system the neural networks are only used in an initial phase. In this case, the neural network determines sub-blocks of the fuzzy system using training data, after this, the neural networks are removed and only the fuzzy system is executed. In the cooperative neuro-fuzzy systems, the structure is not totaling interpretable what can be considered as disadvantage.

Concurrent Neuro-Fuzzy Systems:A concurrent system is not a neuro-fuzzy system in the strict sense, because the neural network works together with the fuzzy system. This means that the inputs enters in the fuzzy system, are pre-processed and then the neural network processes the outputs of the concurrent system or in the reverse way. In the concurrent neuro-fuzzy systems, the results are not completely interpretable, this may consider as a drawback.

Hybrid Neuro-Fuzzy Systems: In Nauck [24] definition: "A hybrid neuro-fuzzy system is a fuzzy system that uses a learning algorithm based on gradients or inspired by the neural networks theory (heuristical learning strategies) to determine its parameters (fuzzy sets and fuzzy rules) through the patterns processing (input and output)". A neuro-fuzzy system can be interpreted as a set of fuzzy rules. This system can be total created from input output data or initialized with the *à priori* knowledge in the same way of fuzzy rules. The resultant system by fusing fuzzy systems and neural networks has as advantages of learning through patterns (parameters of the fuzzy sets, fuzzy rules and weights of the rules) and the easy interpretation of its functionality.

As a summary traditional or conventional MPPT controlling techniques are enclosed by many problems, and it requires additional controlling systems to eliminate this drawbacks, but the intelligent controlling techniques are good in many futures such as:

- Problems for which an exact mathematically precise description is lacking and clearly enables a human being to interface easier with an automated system
- They are often robust, in the sense that they are not very sensitive to changing environments and erroneous or forgotten rules.

So that in this thesis, The intelligent and hybrid MPPT controlling techniques are applied, those are Fuzzy logic, artificial neural network and the hybrid of the two and compare the performance of each controlling techniques using Mat Lab software.

2.6 Motor-Pump system for photovoltaic system

The motor–pump system includes the motor,the pump, and the couplings. Different types of coupling are used for water pumping purposes depending on the type of application and the water demand. Various types of pumps and motors are available for water pumping application depending on the daily water requirement, the pumping head, the suction head (for surface mounted units), and the water resource. The most common types of coupling used to pump water are belt and pulley, feed screw, direct coupling (rack and pinion or bolt and flange), and gear trans- mission. The efficiency of the driving mechanism depends on the coupling ratio, which is the ratio of the torque of the motor to the torque of the load. The

power transmission loss in cases of gear trans- mission, which depends on the gearbox design and gear ratio and the size of the engine in relation to the speed reduction, can be very high.[25]

The most common commercially available configurations of motor–pump subsystems are:

- Submerged motor–pump unit.This is often called a submersible centrifugal motor–pump. Because it is simple to install and safe, this is the most common and suitable type of pumping systemfor village water supplies.
- Submerged centrifugal pump with surface mounted motor.Although this type of subsystem is advantageous for maintenance of the motor, the power losses in the shaft bearings and its high cost make it unattractive.
- Floating motor–pump. This type of pumping unit is recommended for pumping surface water for irrigation and drainage. It is portable and the chance of dry running is minimal.
- Positive displacement pump (volumetric pump).This type of pump is driven by a shaft from a surface-mounted motor, and is suitable for high head and low flow rate applications.

Brushless DC motors are the most attractive for smaller pumping applications and AC motors (incorporated with inverters) are more attractive for medieam to larger installations.

2.6.1 Types of pumps

Volumetric (positive displacement) pumps

These pumps operate by mechanically advancing a sealed quantity of water by using several mechanisms such as pistons, cylinders, and elastic diaphragms. The flow rate or speed of a positive displacement pump is directly proportional to the motor speed and power output. At low power input a positive displacement pump will a quantity of water to the same vertical lift as high power input, except at slower rate. Because of this, positive displacement pumps have a high starting torque as they must always work against the full system pressure even at low speeds.

Commercially available positive displacement pumps are categorized into two types: sub-mersible (diaphragm) and nonsubmersible (jack, piston, and rotary vane). The most common is the Jack pump. At high speeds positive displacement pumps can be more efficient than centrifugal pumps.

Diaphragm pumps are sometimes called submersible positive displacement pumps and are often used for small applications, such as pumping small quantities of water from deeper

wells or water tanks where surface pumps are limited by their suction head. Its generally use DC motors.

Piston pumps are generally connected to a surface-mounted motor and used to pump water from shallow wells, surface water sources, and pressurized storage tanks, or through long pipes. The suction head is limited to 6 meters. They are not tolerant to silt, sand, or abrasive particles because the piston seals are easily damaged. Filters may be used to remove the dirty.

Rotary vane pumps(sometimes called helical rotor pumps) operate according to a displacement principle for lifting or moving water by using a rotating form of dispenser. They contain spinning rotors with vanes that seal against the casing walls. Such pumps are mostly surface-mounted because of suction head limitations. They produce a continuous or sometimes a slightly pulsed water output. The unique advantage of helical rotor pumps over centrifugal pumps is their ability to operate efficiently over a wide speed ranges and heads, whereas the efficiency of centrifugal pumps deteriorates from the rated speed [25].

Centrifugal (rotodynamic) pumps

These pumps are designed for a fixed head, meaning their efficiency decreases when the pumping head deviates from the design point. Unlike volumetric pumps, a significant decrease in a rotodynamic pump's power supply can cause it to fail at delivering water from a borehole because its vertical lifting capability is directly proportional to the power input. The best type of equipment for a particular pumping application depends on the daily water requirement, pumping head, suction head (for surface mounted pump-sets), and the water source. As a discusion among the pump type descused befor the volumetric pumping type is sutable for this work but the motor driving a volumetric pump requires a constant current for a given head, apart from the starting current, which tends to be higher. This condition does not match the PV characteristics where the current varies almost linearly with solar radiation. Therefore, maximum power point tracking (MPPT) controllers are used with volumetric pumps.

2.6.2 Motors

Motors are generally grouped into two types DC and AC. DC motors are divided into permanent magnet (brushed and brushless) and wound-field DC motors. In a permanent magnet DC motor, the permanent magnet is used to produce the magnetic field so no power is consumed in the field windings, which leads to higher efficiencies. This makes this type of motor more attractive for smaller PV applications.

The simplest and cheapest type of AC motor is the squirrel-cage induction motor. Its low cost and rugged construction make it the most commonly used motor for wind/PV applications. Induction motors are classified as squirrel-cage (asynchronous) motors and wound-rotor motors. Wound-rotor motors are generally used for industrial applications.

DC-motors

A DC power supply has two wires one positive and the other negative. When they are connected to the DC motor, the shaft rotates as a result of the field flux supplied either by the permanent magnet or the field winding, by creating two or more poles in the armature and passing magnetic flux through it. This magnetic flux causes the current-carrying armature conductors to create torque on the shaft and rotates the load (pump). Permanent magnet DC motors are limited toratings of a few horsepower and have a maximum speed limitation. DC systems also have high cable-power losses as the distance from the power source increases. These limitations make these types of motors applicable for small water pumping applications.

AC Motors

An induction motor is simply an electric transformer whose magnetic circuit is separated by an air gap into two relatively movable portions, one carrying the primary winding and the other carrying the secondary winding. The essential feature that distinguishes the induction machine from other types of electric motors is that the secondary currents are created solely by induction, as in a transformer, instead of being supplied by a DC exciter or other external power source, as in synchronous and DC machines. The secondary windings on the rotor of squirrel-cage motors are assembled from conductor bars short-circuited by end rings or are cast in place from a conductive alloy. There is no electrical connection to the rotating squirrel cage, so there are no brushes or slip rings to wear or need adjustment [25].

AC motors are generally used for medium- to high-power demand applications. Induction motors with squirrel-cage rotors are available in either single phase or three phase. An induction motor operates at nearly constant speed. However, the speed of an induction motor can be varied with electronic converters (inverters). Using inverters to control induction motor speeds is highly efficient over wide speed and load ranges.Due to such reason Induction Motors are the sellected components for this research.

CHAPTER THREE

MODELLING AND DESIGN OF STANDALONE PV WATER PUMPING SYSTEM

3.1 Water pumping System design for Dolo-Ado Woreda

Dolo is a town in southeastern Ethiopia, within 30 kilometers of the Ethiopia-Somalia border. Located in the Liben Zone of the Somali Region, this town has a latitude and longitude of 04°10′N 42°04′E. Based on figures from the Central Statistical Agency in 2005, this town has an estimated total population of 30,970, and the 1997 census reported this town had a total population of 20,762. It is the largest settlement in Dolo Ado woreda [26]. This thesis tried to solve the water problems of 6000 residential house in Dolo Ado woreda, The Water-level data were compiled from UNESCO and IRC. The ground water lies at a depth of 50 to 700 m below land surface. [26]

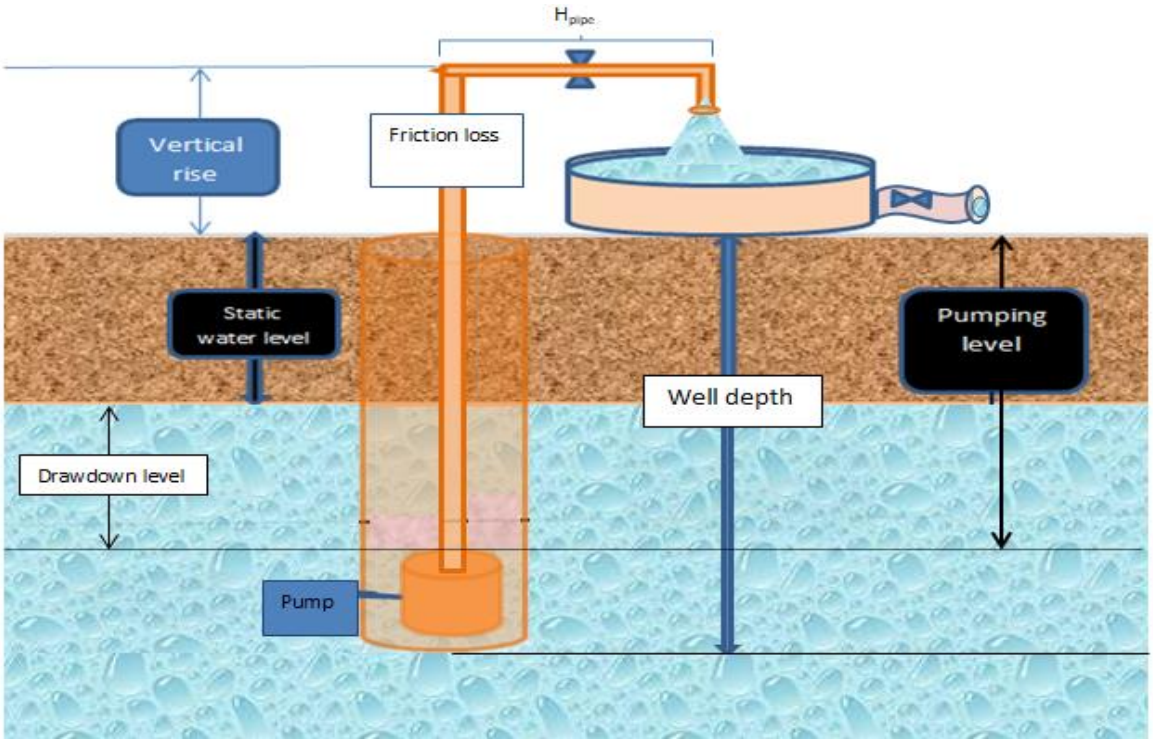

Fig. 3.1 General Diagram of Solar power utilization for water pumping system

If the 6000 residential houses have the average four members in a family are live in Dolo Ado Woreda and to satisfy the minimum water needs of the people from the ground water will be determine by using the following input data. The selected well depth is 150m, static

water level is 50m, drawdown is 20m and safe yield in that area is (19L/s) then recommended pump position will depend on the above data.

Table 3.1 Minimum Water requirement assumptions in a day per person in a family

Activities	Drinking	Cooking	Personal washing	Cleaning home	Average no of family members	Total
Water used L/day	3	3	10	5	4	84

$$\text{Then total water need}(Q_{day}) = (\text{No of residential house}) * (\text{their needs of water})$$
$$= 6{,}000 * 84 = 504{,}000\text{L/day}$$

3.1.1 Total System dynamic head (T_h)

In solar pumping system, the total lifting height (T_h) is the main parameter to determine the necessary power to move the water from the well depth level to the required place.

$$T_h = P_h + VR_h + f_h + V_h + D_h + H_{pipe} \quad (3.1)$$

Where: $VR_h \rightarrow$ vertical rise head

$P_h \rightarrow$ pump level head

$f_h \rightarrow$ A head due to friction loss

$V_h \rightarrow$ A velocity head

$D_h \rightarrow$ Dynamic head loss

$T_h \rightarrow$ Total system dynamic head

$H_{pipe} \rightarrow$ horizontal length of the pipe

Determination of head due to friction (fh)

To calculate f_h apply Darcy-Weisbach formula

$$f_h = \frac{4f\,L}{d}\frac{c2}{2g} \quad (3.2)$$

where; f = friction factor

l = length of pipe

d = pipe diameter

c = mean velocity of fluid

But determine the friction factor, f' is more problematic, for smooth flow and smooth pipes, Blasius equation is applicable

$$f = \frac{0.079}{Re^{1.4}} \quad (3.3)$$

Most simplify form of Blasius equation is

$$f = \frac{64}{Re} \tag{3.4}$$

where Re is Reynolds number ($Re = \frac{\rho v d}{\mu}$) and If $R_e > 400$

$$f = \frac{1.325}{[ln(\frac{e}{3.7d} + \frac{5.74}{Re^{0.9}})]^2} \tag{3.5}$$

ρ=density of water

μ= dynamic viscosity ($1.14x10^{-3}$Ns/m)

e= the roughness of the pipe take PVC (0.009)

$Re = \frac{\rho v d}{\mu}$ $\rho =$ 1000Kg /m^3, $\mu = 1.14x10^{-3}$Ns/m and d=0.2m

$$Re = \frac{1000kg/m3 * 0.372m/s * 0.2m}{1.14 * 10^{-3}\ N/m} = 6.526x10^4$$

Since Re > 400 I used equation (4.5)

$$f = \frac{1.325}{[ln(\frac{e}{3.7d} + \frac{5.74}{Re^{0.9}})]^2} = \underline{0.783}$$

$f_h = \frac{4 * 0.783 * 86}{0.2} x \frac{(0.354)2}{2 * 9.81}$; where $L = P_h + VR_h + H_{pipe} = 70+6+10 = 86m$

$= \underline{8.60m}$

Determination of velocity head (V_h)

$$V_h = \frac{c^2}{2g} \tag{3.6}$$

Where water velocity(c) $= \frac{Q_{pump}}{A}$ but cross section area (CSA) $= \frac{\pi}{4} d^2$ If the pump works 12 hours per day and also peak sunshine hours (*psh*) are 6h. (Assume d=200mm)

$$A = \frac{\pi}{4} 0.2^2 = \underline{0.0314 m^2}$$

But Pump capacity or flow rate can be calculated as;

Q_{day}= 504,000L/day (water required per day)

$$Q_{pump} = \frac{h_w}{psh} Q_{day}$$

$$Q_{pump} = \frac{12}{psh} Q_{day} \tag{3.7}$$

$Q_{pump} = \frac{504,000L}{day} * \frac{12h}{6h}$=1,008,000L/day =1,008,000L/day= $\frac{960,000L}{86400s}$= <u>11.67L/s</u>

$Q_{pump} = 0.01167 m^3/s = 43 m^3/h$

Then water velocity (c) $=\frac{0.01167m^3/s}{0.0314m^2}$=0.372m/s

Then velocity head loss will be

$$V_h = \frac{c^2}{2g} = \frac{0.372^2}{2*9.81} = \underline{0.007m}$$

Determination of dynamic head loss(D_h)

Using Darcy Weisbach equation given by:

$$D_h = \frac{k\,c^2}{2g}, \quad \text{where, } k = K_{pipe} + K_{fitting}$$

K_{pipe} is associated with the straight length of pipe used in the system and defends as

$$K_{pipe} = \frac{fL}{d} = 336.69$$

$K_{fitting}$ is associated with the fittings used in the pipe work's of the system to pump the water from ground to the receiving tank. Values can be obtained from standard tables and a total $K_{fitting}$ values can be calculated by adding all the $K_{fitting}$ values for each individual fitting within the system. The following table shows the calculation of $K_{fitting}$ for the system under consideration.

Table 3.2 K fitting factor consideration

Fitting items	N^o of items	$K_{fitting}$ value	Total items
No return valves	1	1	1
90^o bend	2	0.75	1.5
Valves (fully open)	1	0.3	0.3
Total $K_{fitting}$			**2.8**

$$D_h = \frac{319.915*(0.354)2}{2*9.81} = \underline{2.168m}$$

$$T_h = P_h + VR_h + H_{pipe} + f_h + V_h + D_h$$

$$=70m + 6m + 10m + 8.60 + 0.007m + 2.168m$$

$$T_h = \underline{96.78m}$$

3.1.2 Determination of power requirements

This step is an important step to estimate what amount of power is required to take the ground water to the surface.

$$E=\frac{mg(Th)}{\eta} \quad (3.8)$$

But $m=\rho V$

$$E=\rho V g\frac{Th}{\eta} \quad (3.9)$$

Where:- m = the mass of the water needed (kg)

g = the acceleration due to gravity (m/s^2)

T_h = total system head (m)

η = Efficiency of the system

E= Energy required to move the water from level to head.

V= volume of the tanker in m^3

Then conversion of joule in to KWh (1J= 2.77778 $x10^{-7}$kWh), gravitational acceleration ($g=9.81m/s^2$) and density of water ($\rho=1000kg/m^{3)}$

$$E=1000x9.81x2.77778x10^{-7}x(\frac{VTDH)}{\eta})KWh$$

$$E=\frac{VTh}{367\eta}\ KWh \quad (3.10)$$

3.1.3 Pump power determination and selection

From the above equation determine the required pump power from the work done dividing by hour.

$$P\ (KW)=\frac{E}{h}=\frac{\frac{V}{h}}{367}T_h, \text{ but } \frac{V}{h}=Q_{ph} \text{ (flow rate in } m^3/h)$$

$$P\ (KW)=\frac{Qph}{367\eta}T_h \quad (3.11)$$

Where, if it isn't know the efficiency of the system the recommended value is between 65 to 70 percent ($assume\ \eta = 0.66$)

P (KW) =<u>17.18kW</u>

The pump should satisfy the required flow rate and move waters in to the total dynamic head of the system to fill the desired liters of water. That is to lift $504m^3$ water at the head of 96.78m in the flow rate of $43m^3/h$ with the 17.5kW motor standard. The motor for this thesis is an AC three phase induction motor.

3.1.4 PV panel power determination

The size of PV array has also have a relationship to the pump requirements. This is the required hydraulic power to be generated by PV panel.

$$P\ (array) = \frac{P(KW)}{\delta} \tag{3.12}$$

$$P\ (array) = \underline{29.05kW}$$

29.05KW is the hydraulic power required. Where δ is mismatch factor, and the recommended standard mismatch factor is 60-70 percent, in this case 60% is sellected. Assume this mismatch factor includes the losses that occur during power conversions between the load and the PV panel.

3.2 Photovoltaic system design

The complete schematic diagram of the proposed system is depicted in Fig.3.2 It consists of the following main stages before getting the pure Ac powers for the purpose of PV panel based standalone water pumping system.

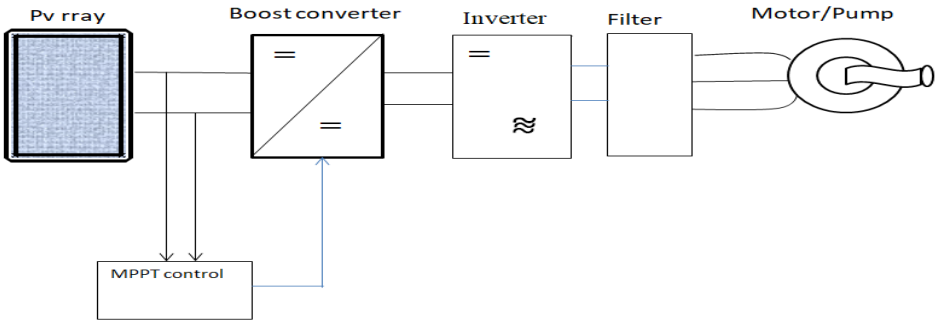

Fig. 3.2 schematic diagram of the proposed model

3.2.1 Photovoltaic cells

Photovoltaic cells are the basic components of photovoltaic panels. Most are made from silicon even though other materials are also used; Solar cells take advantage of the photoelectric effect: the ability of some semiconductors to convert electromagnetic radiation directly into electrical current. The charged particles generated by the incident radiation are separated conveniently to create an electrical current by an appropriate design of the structure of the solar cell. Polycrystalline silicon Consists solely of crystalline silicon grains, separated by grain boundaries, Main advantage over amorphous Si: mobility of the charge carriers can be orders of magnitude larger and Material shows greater stability under electric field and light-induced stress.

When placed in the dark, a photovoltaic cell behaves like a p-n junction diode under no voltage excitation. And when the structure of p-n is exposed to the sunlight, Photons with sufficient energy are absorbed by the semiconductor and form hole-electron pairs, if these mobile charge carriers reach the vicinity of the junction before they recombine, the electric field in the depletion region will push the holes into the p-side and push the electrons into the n-side. Hence, the p-side accumulates more holes and the n-side accumulates more electrons.

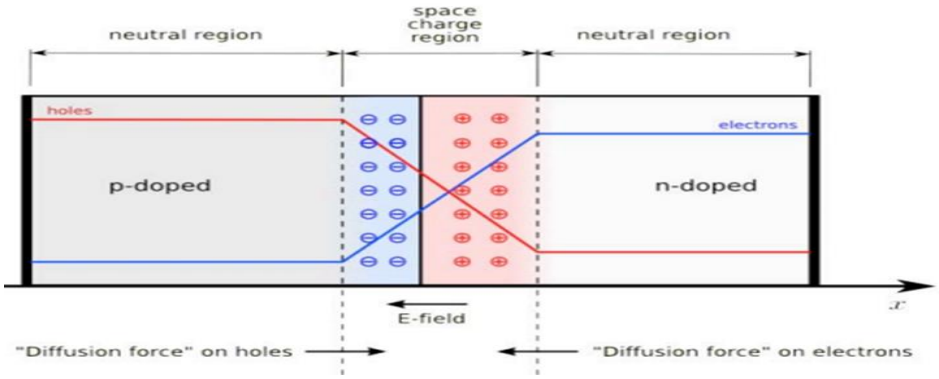

Fig. 3.3 Hole-electron pairs created by photons in p-n junction of PV cell

This separation of charge creates an electric field at the junction which is in opposition to that already existing at the junction, hence a weaker net electric field which increases the diffusion current. When the cell terminals are connected to an external circuit, the light-generated electrons are provided an external path, while the holes remain stuck in the p-type semiconductor. Herein, the electrons will flow out of the n-side through the connecting wire to the load, and then recombine with holes that are waiting on the p-side to complete the circuit.

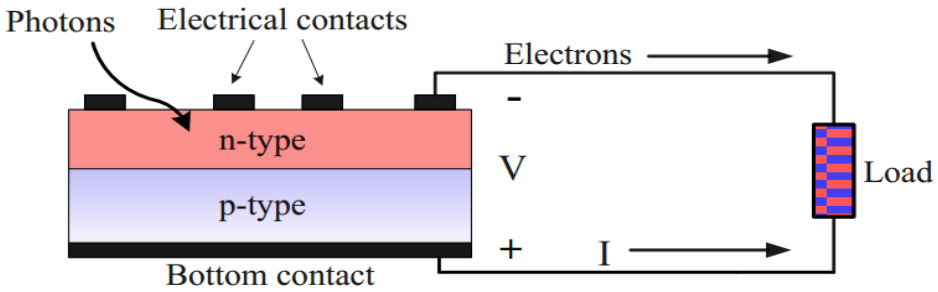

Fig. 3.4 connecting solar cells with a load and conducting current

This shows how the current in the external circuit is generated. Both sides of the junction are attached with metallic contact in order to collect the electrical current induced by the photons received on one side. The mono-crystalline and poly-crystalline silicon are the most common used material in PV cells.

Simple solar cell modeling

A simple solar cell model for a photovoltaic cell consists of a real diode in parallel with an ideal current source. The ideal current source delivers current in proportion to the solar flux to which it is exposed.

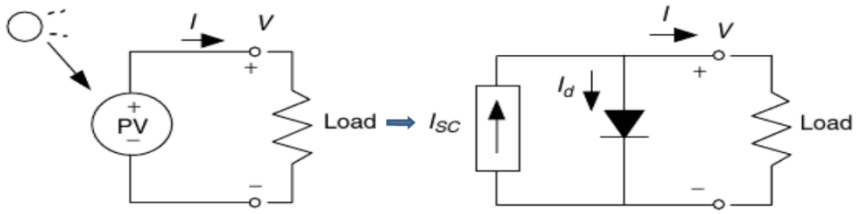

Fig. 3.5 simple equivalent circuit of PV cell

The short circuit current I_{sc} is defined as the current that flows when the terminals are shorted together. This is equal to the magnitude of the ideal current source and the open-circuit voltage V_{oc} is defined as the voltage across the terminals when the loads are left open

$$I = I_{sc} - I_d \tag{3.13}$$

Then applying Shockley diode equation

$$I = I_{sc} - I_s\left(e^{\left(\frac{qVd}{nKT}\right)} - 1\right) \tag{3.14}$$

Where q is the electron charge (1.602×10^{-19} C), k is Boltzmann's constant (1.381×10^{-23} J/K), and T is the junction temperature (K), n is ideality factor a common value for n is 1.2 for Silicon mono and 1.3 for Silicon poly, 1.3 for AsGa, and 1.5 for CdTe. (I) load current, (I_s) dark saturation current and (I_d) is diode current.

The open-circuit voltage can be found by setting the load current to zero:

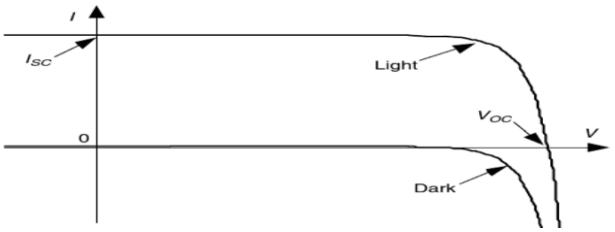

Fig. 3.6 open circuit and short circuit

If the light-generated carriers are prevented from leaving the solar cell, the forward bias of the junction increases to a point where the light-generated current is exactly balanced by the forward bias diffusion current, and the net current is zero. The resulting voltage at the cell terminals under this condition is called the open-circuit voltage (V_{oc}).

$$Voc = \frac{nKT}{q}\ln(\frac{Isc}{Is} + 1) \quad (3.15)$$

On other way open-circuit voltage is a measure of the amount of recombination in the device. Silicon solar cells on high quality single crystalline material have open-circuit voltages of up to 730 mV under the sun and AM 1.5 conditions, while commercial devices on multicrystalline silicon typically have open-circuit voltages around 600 mV. Thus V_{OC} can be determined from the carrier concentration.

$$V_{0c} = \frac{KT}{q}\ln\left[\frac{(N_A + \Delta n)\Delta n}{{n_i}^2}\right] \quad (3.16)$$

Where kT/q is the thermal voltage, N_A ($1.5x10^{16}cm^{-3}$) is the doping concentration, Δn ($1x10^{15}cm^{-3}$) is the excess carrier concentration and n_i ($8.6x10^{9}cm^{-3}$) is the intrinsic carrier concentration at standard temperature condition.

General solar cell Modeling

Addition of series resistance R_s and parallel resistance R_{sh}, the current –voltage equation becomes non-explicit but a general PV cell equation is drive. And used to control the parameters that makes difficult to produce the desired out puts.

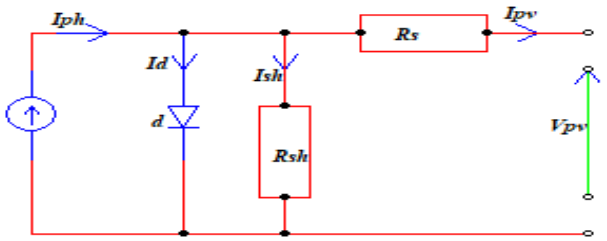

Fig. 3.7 Equivalent circuit of a general solar cell

Apply Kirchhoff law to the above equivalent circuit

$$I_{pv} = I_{ph} - I_d - I_{sh} \quad (3.17)$$

$$V_{pv} = V_d - I_{pv}R_s \quad (3.18)$$

$$I_{sh} = \frac{(Vpv + Ipv * Rs)}{Rsh} \quad (3.19)$$

$$I_d = I_s\left[\exp(\frac{q.Vpv}{n.K.T}) - 1\right] \quad (3.20)$$

The saturation current I_s also depends on the temperature according to the following expression:

$$I_s = I_{rs}.(\frac{T}{Tn})^3.\exp[\frac{q.Ego}{n.K}(\frac{1}{Tn} - \frac{1}{T})] \quad (3.21)$$

Where n is diode ideality factor, K is Boltzmann's constant, Tn is nominal temperature in kelvin (298.15K) and I_{rs} is the cell reverse saturation current in ampere at nominal temperature T_n and E_{go} is the band-gap energy of the semiconductor used in the cell. $E_{go} \cong 1.12$ for polycrystalline silicon panels [1] [23]. In eq. (3.21) saturation current is dependent on change of temperature.

$$I_{rs} = \frac{Isc}{[\exp\left(\frac{qVoc}{nNsKT}\right) - 1]} \tag{3.22}$$

The photovoltaic current is linearly dependent on the irradiance (G) and is also influenced by the temperature T according to the following equation

$$I_{ph} = [I_{ph'n} + K_i (T - T_n)] \frac{G}{Gn} \tag{3.23}$$

$I_{ph'n}$ is the photovoltaic current generated at nominal conditions (T = 298.15 K and G=1000 W/m²), and $K_{i,}$ coefficient of variation of current as a function of temperature.

$$\mathbf{I}ph, n = \frac{Rsh + Rs}{Rsh} x Isc, n \tag{3.24}$$

where $I_{sc,n}$ is the rated short-circuit current under nominal conditions of temperature and irradiation.

Then from the above equations Current Ipv generated by the panel is expressed as a function of Rs and Rp resistors, voltage and currents and as follows:

$$I_{pv} = I_{ph} - I_s\left[\exp\left(\frac{q(Vpv + Ipv.Rs)}{nKT}\right) - 1\right] - \left[\frac{(Vpv + Ipv * Rs)}{Rsh}\right] \tag{3.25}$$

Where I_{sc} is the short-circuit current and V_{oc} open circuit voltage at nominal temperature 25^{o} C and K_i is the temperature coefficient of short circuit current.

In practical applications the solar cells are connected in series strings which are then connected in parallel to produce the required voltage and current. Then finally practical pv panel models with parallel and series solar cells are:

$$Ipv = Np\left\{Iph - Is.\{\exp\left[\frac{(Vpv + Ipv.Rs).q}{n.K.T.Ns}\right] - 1\right\} - Ish\} \tag{3.26}$$

3.2.2 Photovoltaic module parameters determination in 240w module

The pv panel output current Ipv depends on many parameters such as the type of material that the pv panel is made (ideality factor n), shunt and series resistance, number of parallel and series solar cells (Ns & Np), temperature and irradiation variations are the main factors in Pv panel models to gate the required voltage, power or current.

Determination of number of cells

Starting from the above parameters and estimation I have to design a 240 watt of pv modules. A single cell produces only a voltage of 0.5-0.6V and few watts of power for little use. To produce a larger voltage, a number of pre-wired cells in series, all encased in tough, weather resistant package, to form a module. The combination of cells in series or parallel forms a module. A typical module may have 36, 54, 60, 72, or 96 cells in series as the required. When photovoltaic are wired in series, they all carry the same current, and their voltages add. The overall module voltage V_{module} is found by

$$\mathbf{V}module = \mathbf{N}s(\mathbf{V}d - \mathbf{IR}s) \quad (3.27)$$

Where; N_s is number of cells in series. Multiple modules can be wired in series to increase voltage and in parallel to increase current, in this case I want to achieve a power of 240 watt with 8.17 amps of current and determine the required cells and compare with the "Sharp ND-240QCJ Poly" data sheet values. From Mat lab Simulink I'd take the data of a solar cell.

Table 3.3 single solar cell data sheet

Open circuit voltage (Vd)	0.5-0.6	V
Irradiation (Ir)	1000	Watt/m^2
Quality factor	1.5	-
Saturation current (Is)	9.825*e-8	A
Series resistance Rs	0	Ω

Then V_{module}=240w/8.17A =29.38V
Ns=29.38/0.5 ≅ 60 cells in series where 8.17A is the required current to produce by the photon.

Determination of shunt and series resistors

The output of photovoltaic panel depends on the shunt and series resistance that the panels made off. The module voltage which the current begins to drop rapidly becomes progressively lower as series resistance (Rs) increases; this impact at low voltage is not significant for typical values of Rs. Since $Vd = V + IRs$ is still low. Similarly Shunt

resistor (R_{sh}) the low value of shunt resistance (Rsh) leading to higher power loss indicates processes defect or device degradation, this impact more sever at low irradiance. Unfortunately, not all the parameters are given in the data sheet. The values for Rs and Rsh are missing and have to be found in another way. When taking a look at the formula for the maximum power output, that makes the peak of the mathematical P–V curve coincide with the experimental peak power at the (Vmp, Imp) point. This requires several iterations until Pmax,m=Pmax,e. Each iteration updates Rs and Rsh toward the best model solution.

$$\text{Pmax, m} = \text{V}mp\left\{\text{I}ph + \text{I}s\left[\exp\left(\frac{q}{KT}\frac{\text{Vmp+RsImp}}{nNs}\right) - 1\right] - \frac{Vmp+\text{RsImp}}{Rsh}\right\} = Pmax, e \quad (3.28)$$

From equation (3.28) shunt resistance becomes;

$$Rsh = \frac{Vmp(Vmp+RsImp)}{\left\{VmpIph - VmpIsexp\left[\frac{Vmp+RsImp}{nNs}\frac{q}{KTn}\right] + VmpIs - Pmax,e\right\}} \quad (3.29)$$

I_{mp} and V_{mp} are respectively current and voltage of photovoltaic panel at maximum power point. $P_{max,m}$ is maximum power deduced via model identification procedure and $P_{max,e}$ is the experimental maximum power indicated by the panel manufacturer under nominal conditions. To find Rsh value, we have to find a value of Rs so that $P_{max,m}$ is equal to $P_{max,e.}$

($\varepsilon p_{max} = Pmax, m - Pmax, e \cong 0 < tol = 0.01$) This is possible with an iterative algorithm. To compute this algorithm, initial values for Rs and Rsh are needed. The value for initial Rs (Rs,ini) is fixed to zero and initial Rsh value (Rsh,ini) is found by substituting Rs by zero in the Rs equation above. For any value of Rs there will be a value of Rsh that makes the mathematical I–V curve cross the experimental (Vmp, Imp) point. The goal is to find the value of Rs (and hence, Rsh) that makes the peak of the mathematical P–V curve coincide with the experimental peak power at the (Vmp, Imp) point. This requires several iterations until Pmax,m=Pmax,e. Each iteration updates Rs and Rsh toward the best model solution.

The initial value of Rs may be zero and the initial value of Rsh may be given by

$$Rsh, min = \frac{Vmp}{Isc,n - Imp} - \frac{V0c,n - Vmp}{Imp} \quad (3.30)$$

Rsh,min which is the slope of the line segment between the short-circuit and the maximum power remarkable points. Although Rsh is still unknown, it surely is greater than Rsh,min and this is a good initial guess. According to the developed model and experimental data given by the datasheet exactly matched at the nominal remarkable points of I-V curve.

Table 3.4 Modeled and data sheet parameters comparison

Parameters	Modeling value	Datasheet value	Unit
Maximum power (Pmax)	240.0083	240	Watt
Open circuit voltage (Voc)	36	37.5	V
Short circuit current (Isc)	8.7	8.75	A
Maximum current (Imax)	8.17	8.19	A
Maximum voltage (Vmax)	29.38	29.3	V
Number of cells (Ns)	60	60	--
Series resistance (Rs)	0.08	_	Ω
Shunt resistance (Rsh)	337.31	_	Ω

3.2.3 Module I-V characterstics

The I-V Characteristic Curves show the current and voltage (I-V) characteristics of a particular photovoltaic PV cell, module or array giving a detailed description of its solar energy conversion ability and efficiency. Knowing the electrical I-V characteristics (more importantly P_{max}) of a solar cell, or panel is critical in determining the device's output performance and solar efficiency.

The main electrical characteristics of a PV cell or module are summarized in the relationship between the current and voltage produced on a typical solar cell I-V characteristics curve. The intensity of the solar radiation (insolation) that hits the cell controls the current (I), while the increases in the temperature of the solar cell reduces its voltage (V).

Solar cell I-V Characteristics Curves are basically a graphical representation of the operation of a solar cell or module summarizing the relationship between the current and voltage at the existing conditions of irradiance and temperature are shown in fig 3.8

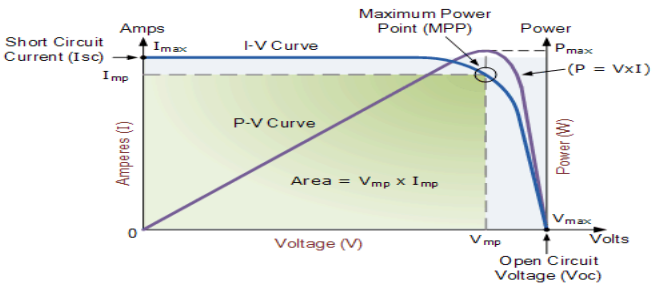

Fig. 3.8 solar cell I-V characteristics curve

The above graph shows the current-voltage (I-V) characteristics of a typical silicon PV cell operating under normal conditions. The power delivered by a solar cell is the product of current and voltage (I x V). If the multiplication is done, point for point, for all voltages from

short-circuit to open-circuit conditions, the power curve above is obtained for a given radiation level. Then the span of the solar cell I-V characteristics curve ranges from the short circuit current (Isc) at zero output volts, to zero current at the full open circuit voltage Voc . In other words, the maximum voltage available from a cell is at open circuit, and the maximum current at closed circuit. Of course, neither of these two conditions generates any electrical power, but there must be points somewhere in between were the solar cell generates maximum power. The MPP of a solar cell is positioned near the bend in the I-V characteristics curve.

3.2.4 Factors that affecting Solar PV System Performance

Understanding these factors will help us to make accurate predictions for controlling them and smart decisions on how to eliminate those problems as much as possible. There are many factors affect the photovoltaic systems

Irradiance

Irradiance is a measure of the amount of sunlight falling on a given surface. The higher the irradiance on a solar cell, the more energy a cell will produce. It is obvious that as the irradiation level increases the PV output voltage and current increases with it. In general, the increment in the irradiation level leads to a theoretical increment in the maximum power voltage when there is no change in the cell temperature. On the other hand, the short circuit current I_{SC} depends totally and linearly on the irradiance level therefore the maximum power current is changed as shown below. However, the total energy received by the system from the sun remains relatively constant from year to year. The angle of the sun, passing clouds, hazy weather, and air pollution can affect irradiance levels.

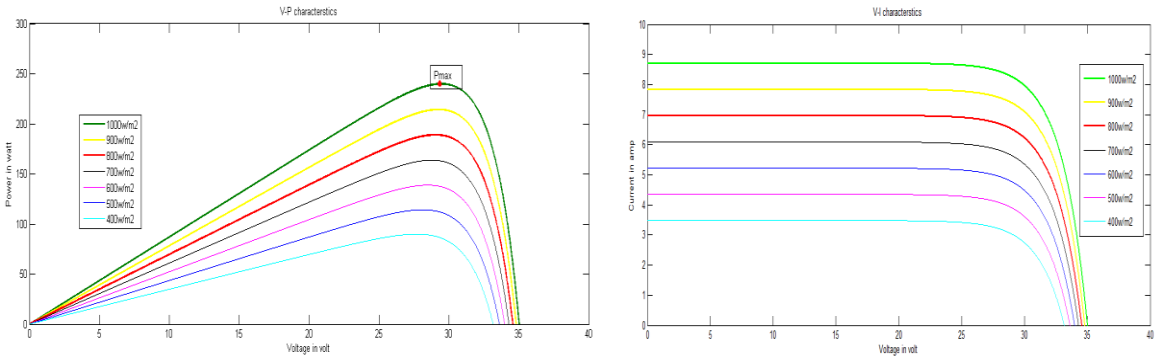

(a) (b)

Fig. 3.9 (a) V-P (b) V-C characteristics at constant ambient temperature (STD)

Temprature

As temperature increases, the band gap of the intrinsic semiconductor shrinks, and the open voltage (V_{oc}) decreases following the p-n junction voltage temperature dependency of seen in the diode factor circuit$\frac{q}{KT}$. Solar cells therefore have a negative temperature coefficient of V_{oc}.[15]

As temperature increases, again the band gap of the intrinsic semiconductor shrinks meaning more incident energy is absorbed because a greater percentage of the incident light has enough energy to raise charge carriers from the valence band to the conduction band. A larger photocurrent results; therefore, Isc increases for a given insolation, and solar cells have a positive temperature coefficient of I_{sc} [15].

In general as the temperature increases with a fixed irradiation level it results in a slight increase in the short circuit current I_{sc}, because the band gap energy decreases and more photons have enough energy to create electron-hole pairs. On the other hand, the increase of temperature have an obvious reduction in the PV panel output power due to the drop in the open circuit voltageV_{oc} and the fill factor; therefore the module efficiency is reduced [15].

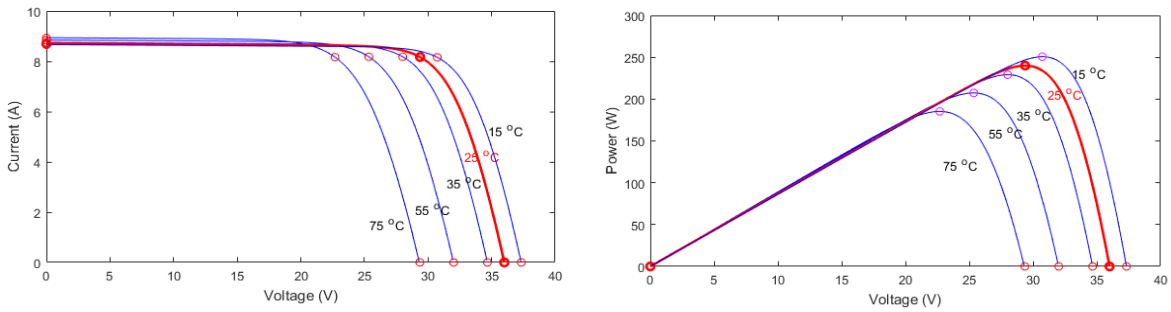

(a) (b)

Fig. 3.10 (a) V-I characteristics (b) V-P characteristics of PV module at fixed irradiance level

3.2.5 Photovoltaic arrays

In general a single solar cell generates very low output power. It is normally less than 2W at 0.6V. Therefore, the photovoltaic cells are connected in particular configurations so as to form an array which is called a photovoltaic module. The modules consist of group of cells connected in series and parallel to provide the desired output power and voltage In addition to that, for a photovoltaic system a group of several PV modules are connected in parallel and series in form of PV array to generate the required voltage and current values for the system. When two or more solar modules are wired in series, the same current flows through each

module and the output voltage is the sum of the voltages generated by each modules. the other hand when two or more solar modules connected in series the same voltage would have across each modules and the output current is the sum of each generated current. In addition to this to determine the construction of PV panel the following parameters are basic [27].

Maximum Dc voltage of PV systems

The maximum DC voltage commonly is a safety relevant limit for sizing a PV system. All components (modules, inverters, cables, connections, fuses, surge etc.) have a certain maximum voltage they can withstand or handle safely. If this voltage gets exceeded, damage or even worse harm can result. From an economic point of view, a high voltage makes sense, by causing lower investments (fewer strings) and higher earnings (lower losses and mostly higher efficiencies). So the challenge is to size a PV system with the highest possible and safe DC voltage. In this case the required voltage to generate frome the PV panel is 323.1volt.

Open Circuit Voltage of a PV module

On the datasheet of a PV module the open circuit voltage is specified most times at STC. (Standard Test Conditions) defining the irradiation at 1000W/m² and a cell temperature at 25°C) As the voltage correlates mainly with the cell temperature, also a temperature coefficient is specified, either in V/°C or %/°C. This is an inverse correlation, meaning the highest voltage occurs with the lowest cell temperature. Naturally also irradiation is necessary to produce voltage and power. So the voltage shows also a non-linear dependency from the irradiation, meaning at low irradiations also the voltages will be low. Modern PV Modules have an efficiency of 15% to 20% of the sun shine. While this percentage is converted into electricity the bigger “rest” (80% - 95%) of the irradiation is mostly converted into heat, meaning the PV cell (module) gets heated-up quite quickly. As a matter of fact, with irradiation (at daytime) the cell temperature always will be higher than the ambient temperature.

Defining the minimum cell temperature for calculating $V_{oc,max}$ With STC values

For the design of a photovoltaic system, the cell temperature limits established on the international market are minimum -10 °C and maximum +70 °C. Commonly these temperatures are used with the STC values of a module for the calculation of the extreme voltages.

As the voltage of a PV cell (module) has a high dependency on its temperature but also a dependency on the irradiation (especially at low irradiation levels) and further the cells own

temperature has a high dependency on the irradiation, the Minimum Cell Temperature can be chosen higher than the Minimum Ambient Temperature. Taking into account, that the lowest day temperatures are higher, modules are mounted on roofs where the surrounding air temperature is higher (heated up from the building, less dissipation of heat) and so on, even a higher difference (> +10°C) between the lowest Minimum Ambient Temperature and the lowest Minimum Cell Temperature can be assumed

Calculating the maximum arising open circuit voltage ($V_{oc,\ max}$)

The most established and easiest way to calculate the maximum dc voltage (maximum open circuit voltage) is to use the STC value from the datasheet with a certain estimated lowest occurring cell temperature.(from datasheet temperature Coefficient (Voc= -0.36%/°C) and Temperature Coefficient of (lsc= 0.53%/°C). As a matter of fact, STC (1000W/m²) doesn't take into account the influence from the irradiation. Lower voltage at lower irradiation.

$$\text{Voc, max} = (\text{Voc, stc [V]} + \text{Voc, stc [V]}\frac{(\text{Tcell,min [°C]} - \text{Tstc [°C]}) * \text{TC,Voc [\%/°C]}}{100} \quad (3.31)$$

Determine the size of module in the strings and number of strings

As described, calculating maximum DC Voltage with a lower ambient temperature enables sizing the strings and more flexibility, which reduces investment costs and leads to higher yields. When building a PV system with sizing strings often the number of strings can be reduced and therefor the costs for inverter, cabling, mounting and supporting systems, connections, fuses, and so on can be saved. With less cabling (and other current carrying components) also the energy losses are reduced.

$$\text{Maximum Modules/ String} = \text{rounded off}\left(\frac{\text{Maximum System Voltage}}{\text{Voc,max}}\right) \quad (3.32)$$

For the proposed system the maximum system voltage required to drive the Ac motor is 400volt, then the maximum module per string due to the above equations, it becomes 11 modules per string.

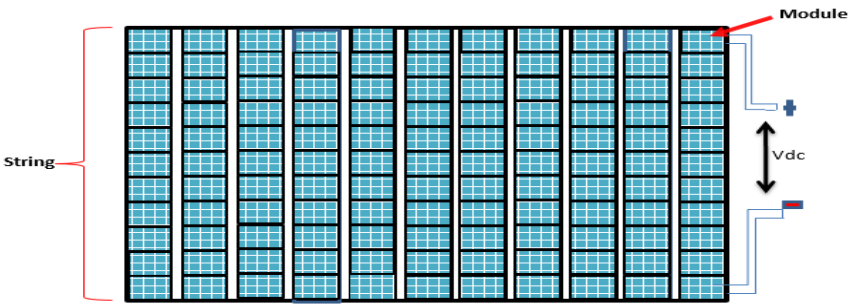

Fig. 3.11 The proposed real PV array series parallel structure

Now we can calculate the number of required strings for the system using the above equation and the desired output power. It requires eleven strings with eleven modules to generate the desired power which is 29.04kW. The proposed array has shown in the following figure and the calculated value of the array is listed in Table 3.5

Table 3.5 the proposed module and array value

Parameters	Modeled Module value	Proposed array Value	Unit
Maximum power (Pmax,)	0.24	29.04	kW
Open circuit voltage (Voc)	36	396	V
Short circuit current (Isc)	8.7	95.7	A
Maximum current (Imax)	8.17	89.87	A
Maximum voltage (Vmax)	29.38	323.1	V
Number of cells (Ns)	60	7260	-

3.3 Design of DC-DC boost converter

DC-DC converters are used to interface the photovoltaic module with the inverter, in order to ensure the photovoltaic module is always operating at the maximum power point. This is done by controlling the converter duty ratio (D) with maximum power point tracking algorithms (MPPT). When the converter is operating at steady-state condition, the duty ratio, D, can be expressed by equation 2.5.

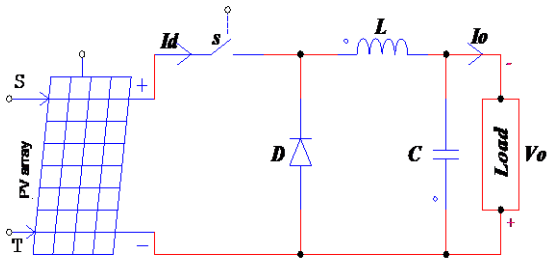

Fig. 3.12 Proposed Boost converter

The boost converter is used in this circuit which steps up the input voltage giving a steady output voltage but one which is always greater than the input voltage. The inductor, capacitor, load resistance & MOSFET values must be worked out for this circuit to be built. Determining a value for the output voltage is a key step in finding the value of components required and as shown the following table.

Table 3.6 boost converter parameters.

Power rating (P_{max})	29.04kW
Input voltage range (V_{in}=V_{pv})	(62-323) Volt.
Output voltage (V_{dc}=V_{out})	680Volt.
Max, input current (Ivp = P_{max}/V_{in})	89.87amp
Max. load current =P_{max}/V_{out}	40amp
Switching frequency (f_s)	5K Hz
V_{out} ripple (ΔV_{out})	1% -50%
I_{in} ripple (ΔI_{in})	20% -40%
Inductance (L)	≥292μH
Output capacitance (C)	≥660μF
Minimum Duty (D_{min}) $= 1 - \frac{Vin\_max}{Vout}\eta$	0.524
Maximum Duty (D_{max}) $= 1 - \frac{Vin\_min}{Vout}\eta$	0.853

3.3.1 DC Link Design

In many applications the solar converter is separated into two general components. The first component is the DC/DC converter which has the main task to ensure the required minimum DC input voltage of the second component, the DC/AC converter. The latter has to feed the power into the AC induction load which here is a three phase system. These two components are connected by a DC link capacitor to smooth the DC link voltage. An easy to use method to appreciate a minimal capacity of the capacitor bank is linked between the boost converter and the inverter [28]. This method of calculating a minimal capacity of the DC link capacitor depends on the expected maximum input power step and the definition of a limit of allowed voltage deviation. A widely-used limit is a deviation of ten percent of the DC link voltage at any step-on and step-off load response. The expected maximum input power step is equal to the solar panel power at the maximum power point (MPP). This method starts with the energy ΔW which is estimated as [29]:

$$\Delta W = \int_0^{Tr} \Delta Pmax.dt = \Delta Pmax.Tr \quad (3.32)$$

The stored energy of the capacitor can be written as follows:

$$W = \frac{1}{2} C_d {V_d}^2 \quad (3.33)$$

The variation of the stored energy in the capacitor also depends on the DC link voltage V_d, the DC link voltage deviation ΔV_d and the capacity $C_{d,min}$ can estimated as:

$$\Delta W = \frac{1}{2} C_d (V_d + \Delta V_d)^2 - \frac{1}{2} C_d {V_d}^2 \quad (3.34)$$

The combination of the equations (3.32) and (3.34) leads to the expression of the minimal capacity ($C_{d;min}$):

$$C_{d,min} = T_r . \frac{\Delta P_{max}}{V_d \Delta V_d + \frac{1}{2} {V_d}^2} \quad (3.35)$$

Another method to appreciate the minimal DC link capacity would be here, where the exchanged energy ΔW by the capacitor bank is estimated as follows:

$$\Delta W = \frac{T_r . \Delta P_{max}}{2} \quad (3.36)$$

The voltage deviation is given by:

$$\Delta V_d = \frac{\Delta W}{V_d V_d} \quad (3.37)$$

Finally this leads to another equation of the minimal capacity $C_{d,min}$:

$$C_{d,min} \geq T_r . \frac{\Delta P_{max}}{2.V_d \Delta V_d} \quad (3.38)$$

Assuming a DC link voltage deviation ΔV_d of commonly used ten percent and the control delay of the DC/DC (T_r) value of about five to ten modulation periods is a good choice.

3.4 Three phase full-bridge inverter design and interfaceing

The boost converter are step-up the photovoltaic output voltage of the PV array from 323.1volt (Natural) to 680volt (step up) DC outputs to feed the inverter, but the desired goal is to produce (400 ±5%)V AC in ordered to take waters from the ground.

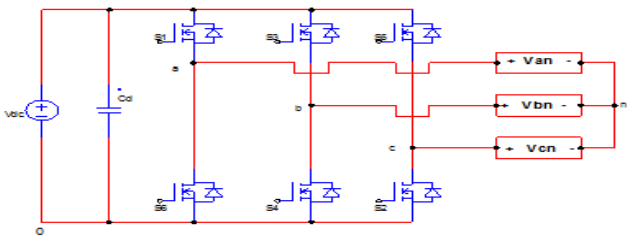

Fig. 3.13 the proposed three phase full bridge PWM inverter

The H-bridge inverter has been designed according to the specifications given in Table 3.7. The selection of its components must meet those specifications.

3.4.1 Photovoltaic Array – Inverter Interface

Totally 121 multi-crystalline silicon types, 60-cells PV modules series parallel combination is conducted in the previous topic to design 29.04kW power generator PV arrays.

Nominal power

The maximum power generated by the investigated PV array is 32.77kW at an irradiation of 1200 W/m^2, and an ambient temperature of 25°C. This operating point is however very seldom reached. The nominal power for the inverter is therefore selected to 32.77kW / 1.2 which is 27.31kW, with the capability of operating at 120% power during short time [30].

Starting power

The inverter should be able to invert even small amounts of DC power into AC power. In other words, the inverter must be able to operate at very low irradiation. The European efficiency is the weighted average of efficiencies down to 5%. Thus, the inverter should be able to operate at 5% or less of the nominal power, which is 1.37kW.

Open circuit voltage

The worst-case open-circuit voltage across the investigated PV array is estimated to 396V at 1000 W/m^2, and a cell temperature of 25 °C. Thus, the inverter must withstand at least 396V without being damaged, so that 500 V inverter is selected.

Maximum Short Circuit Current

The maximum short-circuit current generated by the investigated PV array is 95.7A. A maximum current of 100A is therefore chosen.

Over Voltage Protection

The inverter must be capable to withstand over-voltages caused by nearby lightning, etc. It is recommended to use a surge arrestor (Metal Oxide Varistor) with an inception voltage of 1.2 time nominal voltage [31]. The inception- and inclination-voltage should therefore be higher than 500V times 1.2 which is equal to 600V.

3.4.2 Inverter – load interface

This thesis aimed to enabled a three phase 400Volt by 39amp of induction AC motor to pumping ground water from the borehole to the system height (T_h =96.78m).

The Output Ac voltage (V_{rms}) is calculated as;

$$\text{VLL\_convr} = m\frac{VdC}{2}\sqrt{(\frac{3}{2})}$$

$$\text{VLL}_{\text{convr}} = 0.6124 * m * Vdc \quad (3.39)$$

where: - Vdc is output voltage of the boost converter, and 'm' is modulation index we had seen about modulation index in chapter two.

Table 3.7 specifications of three phase H-bridge inverter

Nominal Power rating	27.31kW
Input voltage, Vout of the boost converter(Vdc)	680volt
Modulation index(m)	0.96
Output Ac voltage(V_{rms})	(400±5%)volt
Output Ac current(Irms)	39amp
Frequency Ac out put	50Hz
PWM frequency	5kHz
DC link capacitor (C_{Dc_link})	200µF

3.5 LCL low pass filter design

Even if the LCL filter is selected, it is inherently unstable [32]. This is seen by the peak in the transfer-function around the resonant frequency, and some kind of damping must be added to make the filter more stable. This can be done in several ways either by introducing a damping resistor in series with the filter capacitor, or by adding a damping resistor in parallel with the load connected inductor or to include a damping circuit, made up around a resistor and a capacitor in series, in parallel with the filter capacitor. But in this thesis it chosen introducing a damping resistor in series with the filter capacitor due to its simplest.

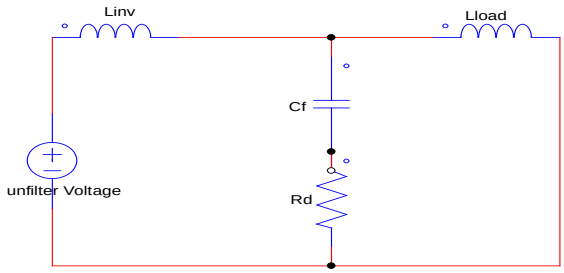

Fig. 3.14 LCL proposed Filter

The output ripple current (ΔIL) in the design of L_{inv} was assumed up to 10% of the rated output current of the inverter (I_{inv}).

$$\Delta IL=10\%I_{inv} \tag{3.40}$$

A simplified formula for the LCL filter parameters with damping resistance may have discussed and analysis through the following equations, to calculate the inverter side inductance (L_{inv}), load side inductance (L_{load}), filter capacitance (C_f) and the damping resistance (R_d).

First calculating filter parameters is founding L_{inv}, which is given as

$$Linv = \frac{V_{inv\_peak}}{16xfs\Delta IL} \tag{3.41}$$

Where $V_{inv\text{-}peak}$ is the peak output voltage of the inverter which is equal to the output of the boost converter input to the inverter. The output ripple current (ΔI_L) in the design of L_{inv} was assumed up to 15% of the rated output current of the inverter (I_{inv}). The load side inductance (L_{load}) is given by some Constance (r) multiply by the inverter side inductance

$$L_{load}= r * L_{inv} \tag{3.42}$$

The constant (r) is called relation factor which represents the ratio between L_{inv} and L_{load}. The voltage drop across the inductor filter (L_{inv}+L_{load}) must be less than 3% of the inverter output voltage (V_{inv}) [33].

$$I_{inv(max)} \times 2\pi \times f \times L < 0.03V_{inv} \tag{3.43}$$

Where, Iinv(max) is the max inverter current (rms), f is the output frequency(50 Hz) and ($L \approx L_{inv}+L_{load}$). The capacitance of the filter (Cf) is limited to less than 5% of the base capacitance (Cb) that is given by:

$$C_f= 5\%cb = 0.05\frac{Pinv}{2\pi f\ V_{inv}{}^2} \tag{3.44}$$

Whre P_{inv} is the rated output power of inverter.and the design of the filter capacitance adopts the fact that the max power factor variation acceptable by the grid in case of grid tied inverter should not exceed 5 % [34]. Then the value of the R_d ought to be one third of the impedance of the filter capacitor at the resonant frequency (f_0). The values of f_0 and R_d are given by:.

$$f_o = \frac{1}{2\pi}\sqrt{\frac{L_{inv}+L_{loa}}{L_{inv}*L_{load}*C_f}} \tag{3.45}$$

$$R_d = \frac{1}{3}\left(\frac{1}{2\pi f_o C_f}\right) \tag{3.46}$$

And assume the two inductor ratio is 0.8 which is constant r.and apply the given equations to calculate Table 3.8 parameters.

Table 3.8 LCL filter specification

Parameters	Specification
L_{inv}	4.2mH
L_{load}	3.3mH
C_f	52µF
R_d	0.2Ω

CHAPTER FOUR

DESIGN OF CONTROLLERS FOR PV WRATER PUMPING SYSTEM

4.1 Fuzzy logic controller

Fuzzy logic is work based on a mathematical model which deals with uncertainty and imprecise, ambiguous, noisy, or missing input information. It compares an analog input signal to a predetermined logic variable membership function or fuzzy sets that correspond to values in the range 0 and 1. It is implemented in a control system to emulate human-like decisions in control.

Essential characteristics of Fuzzy logics are listed below [35]:

- In fuzzy logic, exact reasoning is viewed as a limiting case of approximate reasoning.
- Knowledge is interpreted a collection of elastic or, equivalently, fuzzy constraint on a collection of variables and in FL everything is a matter of degree.
- Interface is viewed as a process of propagation of elastic constraints. And any logic system can be fuzzified.

The two main characteristics of fuzzy systems that I prefer to apply in my thesis are:

- Fuzzy systems are suitable for uncertain or approximate reasoning, especially for a system with a mathematical model that is difficult to derive.
- Fuzzy logic allows decision making with estimated values under incomplete or uncertain information.

4.1.1 Fuzzy logic controller structure

The fuzzy logic controller consists of four components: fuzzification interface, knowledge base, interface engine, and defuzzification interface.

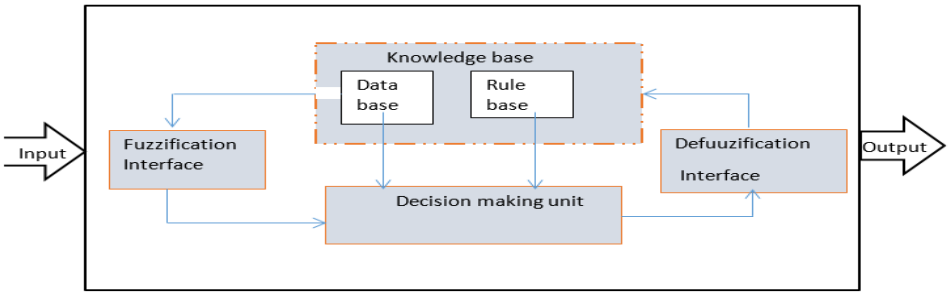

Fig. 4.1 General structure of fuzzy interface system.

The fuzzifier transforms crisp inputs into the fuzzy subsets to obtain degrees of memberships and represent them with linguistic variables, which in turn are used to activate rules. The fuzzy inference engine process those data to obtain the desired output. The defuzzifier converts those fuzzy outputs to crisp variables to complete the desired fuzzy logic control objectives. Every fuzzy set can be represented by its membership function. In practice the membership functions can have a number of different shapes depending on the designer interest. They can be triangular, trapezoidal, Gaussian, bell-shaped, sigmoidal or S-curve. Some of them are shown below. Trapezoidal or triangular membership functions are usually used in systems that require significant dynamic variation in a short period of time. A Gaussian or S -curve membership function is always selected if the system requires very high control accuracy [36].

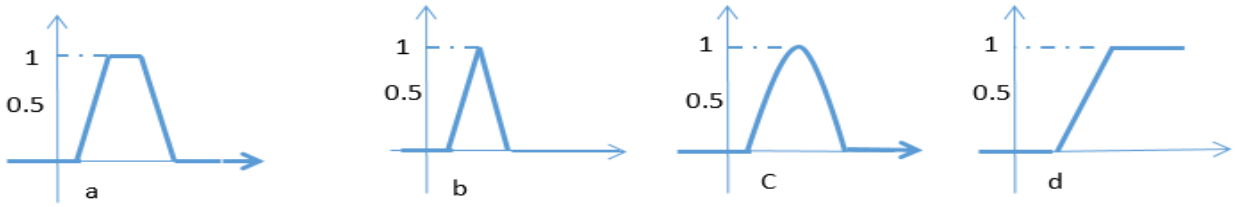

Fig. 4.2. Different types of membership function (a) Trapezoidal (b) triangular (C) Gaussian & (d) monotonic

4.1.2 Knowledge Base

It is the heart of the fuzzy control system. It is the inference basis for fuzzy control. The knowledge base defines all relevant language control rules and parameters.

The derivation of fuzzy control rules can be performed in not mutually exclusive, and it is necessary to combine them to obtain an effective system [37].

- Expert experience and control engineering knowledge: the fuzzy control rule is based on information obtained from the controlled system.
- Operators' control actions: observation of human controller's actions in terms of input-output operating data.
- Based on the fuzzy model of process: linguistic description of the dynamic characteristics of a process.

The number of base rules can be defined based on the number of membership in the fuzzy set and the inputs.

4.1.3 Fuzzy interface procedure

Among several techniques for performing the fuzzy interface process the Mamdani method and Takagi-Sugeno_Kang (TSK) method are the most commonly used methods in fuzzy controllers.

Mamdani method is usually more popular for most control engineering applications due to its computationally more efficient and has better interpolative properties than the other interface methods [38]. Mamdani fuzzy logic uses the linguistic variables to describe the process states and uses these variables as inputs to control rules. The terms of the linguistic variables are fuzzy sets with certain shape. Mamdani fuzzy logic usually uses the trapezoidal or triangular fuzzy set but other shapes are possible. The fuzzy interface process of the Mamdani method can be formed in four steps [39]: Fuzzification, rule evaluation, aggregation of the rule outputs and defuzzificatio.

Fuzzification; Fuzzification is the first step in fuzzy logic processing, in which the crisp quantities are converted to fuzzy inputs. The transformation process of fuzzy values is represented by the membership function. As an example if we have two inputs input 1 and input 2 firstly, take the crisp inputs, input 1 and input 2, and determine the degree to which these inputs belong to each of the appropriate fuzzy sets.

If μA1(x) = 0.5, μA2(x) = 0.2, μB1(y) = 0.1, μB1(y) = 0.

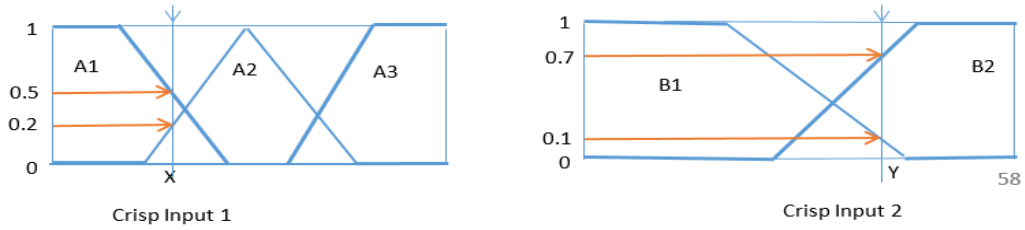

Fig. 4.3. Fizzification

Rule evaluation; in this step the fuzzified inputs are applied to the antecedents of the fuzzy rule, then applying the fuzzy operator to fuzzy rule that has multiple antecedents to resolve the antecedents to a single number between 0 and 1. The fuzzy operator (AND or OR) is used to obtain this signal number. If the OR fuzzy operation is used, thus the classical fuzzy operation union is used or Maximum is used.

$$\mu A \cup B(x) = \max [\mu A(x), \mu B(x)] \quad (4.1)$$

Similarly for AND fuzzy operation intersection is applied or minimum of the two is applied.

$$\mu A \cap B(x) = \min [\mu A(x), \mu B(x)] \quad (4.2)$$

From the above example we evaluate rule

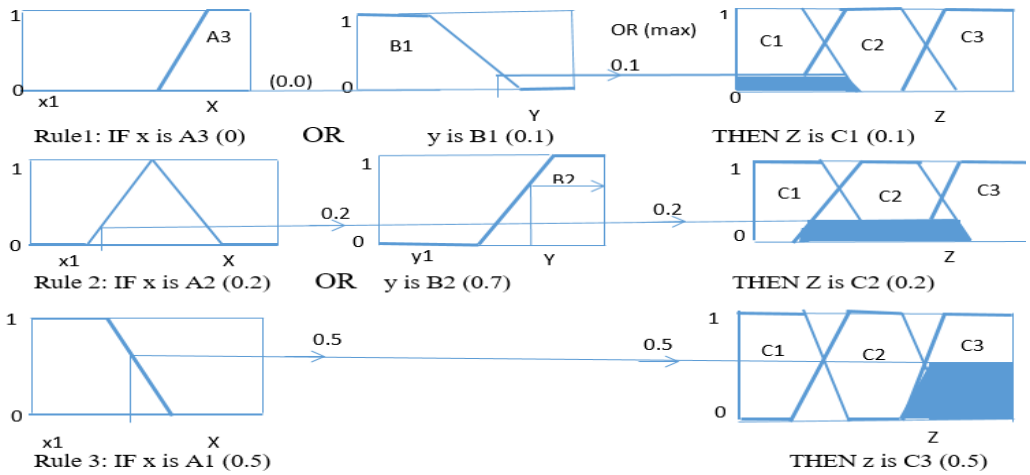

Fig. 4.4. Rule evaluation in Mamdani method

Aggregation of the rule outputs; after finding the output of each rule, the aggregation process is applied to unify all the rules outputs to become one output. The input to the aggregation process is the combination of scaled consequent membership function, and the output is the combined output fuzzy set.

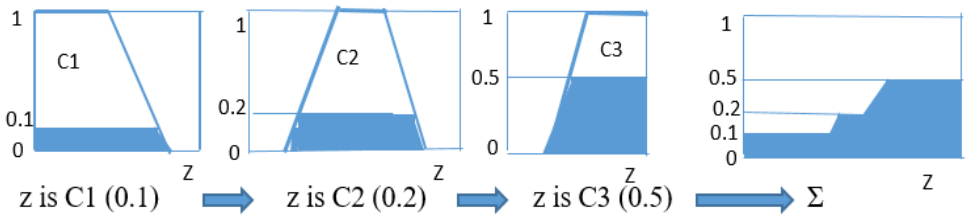

Fig. 4.5. Aggregation of the rule outputs

Defuzzification; The Defuzzification is the last step in the process of the fuzzy inference, and its reverse of the fuzzification process. The output of the fuzzy inference process result from the combination of the control inputs and it is still linguistic variable. However, the final output of the fuzzy control has to be a crisp number. Hence the defuzzification process is needed to convert the fuzzy output back to the crisp output to be available for real application controllers. Among several defuzzification techniques, Mean of maximum method (MOM), Height method (HM) and Centre of gravity method (COG) are the most common techniques

Mean of maximum method (MOM) The MOM defuzzification strategy computes the average value of all the control actions whose membership functions reach the maximum.

$$\text{MOM} = \sum_{i=1}^{l} \frac{\omega_j}{l} \tag{4.3}$$

Where; wj is the support value when the membership function reaches the maximum value

μz (wj), and *l* is the number of support values.

Height method (HM) is can only be applied when the output membership function is an aggregated union result of symmetrical functions [36].

$$Z = \frac{\sum_{j=1}^{n} wj.\mu(wj)}{\sum_{j=1}^{n} \mu(wj)} \tag{4.4}$$

Centre of gravity method (COG) is the most widely used defuzzification technique in real applications. The advantage of COG method is the defuzzified values tend to move smoothly around the output fuzzy region. The COG technique is a basic general defuzzification technique that computes the value of the abscissa of the center of gravity of the area below the membership functions.

$$Z = \frac{\sum_{j=1}^{n} wj.\mu_z(wj)}{\sum_{j=1}^{n} \mu_z(wj)} \tag{4.5}$$

where n is the number of quantization levels of the output.

4.1.4 Fuzzy logic controller for PV water pumping system

The variation of solar radiation and ambient temperature are the most important factor in the MPPT of PV system. It is changing periodically and nonlinearly, hence FLC based MPPT is proposed to solve the problem and to deliver the maximum available power of the PV array to the load. A schematic of the photovoltaic array and water pumping system used to investigate the fuzzy logic controller performance is shown in Fig 4.6.

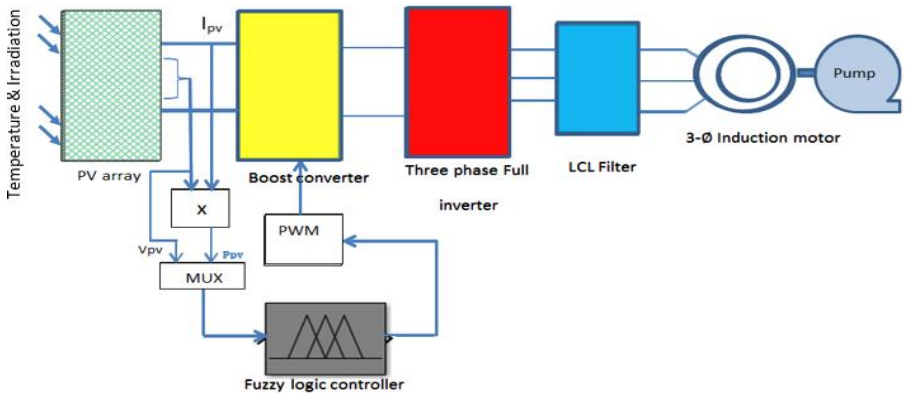

Fig. 4.6. Schematic diagram of the proposed FLC MPPT based water pumping system.

Operation of Fuzzy logic controller in the photovoltaic water pumping system

It is introducing to determine the operating point corresponding to maximum power for different insolation levels and temperature. A fuzzy logic controller has been proposed to adjust the boost converter duty ratio which adapts online the PV array output voltage to maximize the output power, which in turn increases the water discharge of the water pump.

In the fuzzification stage, numerical input variables are calculated or converted into linguistic variables based on subsets called membership function the proposed FLC has two input variables and one output variable as shown above. The input variables of the fuzzy logic controller are power variation (ΔPpv) and voltage variation (ΔVpv) at sampling instant k. The output variable is the duty ratio (D) of the boost converter. The input variables ΔP_{PV} and ΔV_{pv} are expressed by the following Equations

$$\Delta P_{pv}=G_p \{P_{pv}(k) - P_{pv}(k-1)\} \quad (4.6)$$

$$\Delta V_{pv}=G_V \{V_{pv}(k) - V_{pv}(k-1)\} \quad (4.7)$$

And the crisp value of the output variable ΔD (k) is computed by;

$$D (k) = D (k-1) + G_D \Delta D (k) \quad (4.8)$$

G_p, G_V and G_D are scaling factors used to normalize the ΔP_{pv} (k), ΔV_{pv} (k) and ΔD (k) respectively. The scaling factors play an important role in optimizing performance and can be chosen using trial and error. D (k) is the final output signal sent to the system.

The membership functions of the both inputs and output variables are represented by symmetric triangular functions and defined normalized range of (0, 100) for input 1, (0, 200) for input 2 and (0, 1) for output. The membership functions of the input variables ΔP_{PV} and

ΔV_{pv}, and the output variable sets which are assigned for fuzzy sets have the same shape. The membership function of both inputs and output variables are assigned seven sets, including big positive (BP), medium positive (MP), small positive (SP), zero (Z), big negative (SN), medium negative (MN) and small negative (NB) and the class range arrangement is listed in appendix (C).

The fuzzy control rules have been set up using a set of IF-THEN statements that contain all information for the controlled parameters. The fuzzy control rule includes 49 rules as described in Table (4.1). These rules are used for the control of the boost converter such that the maximum power is achieved at the output of the PV array.

The fuzzy rules are designed to incorporate the following considerations keeping in view the overall tracking performance.

- If a positive variation in the generated voltage is accompanied with a positive variation of PV array output power, then the duty cycle ratio should be increased. Otherwise if the variation of PV array output power is negative, then duty cycle ratio should be decreased.
- If the generated voltage variation is zero or sufficiently close to zero which means that its maximum is reached, then there should be no change in the duty cycle ratio.
- If a negative variation in the generated voltage is accompanied with a positive variation in PV array output power, then the duty cycle ratio should be decreased. Otherwise if the variation of PV array output power is positive, then duty cycle ratio should be increased.

Table 4.1 fuzzy rule base table

V_{pv}/P_{pv}	BN	MN	SN	Z	SP	MP	BP
BN	BP	BP	BP	BP	MP	SP	Z
MN	BP	BP	BP	MP	SP	Z	SN
SN	BP	BP	MP	SP	Z	SN	MN
Z	BP	MP	SP	Z	SN	MN	BN
SP	MP	SP	Z	SN	MN	BN	BN
MP	SP	Z	SN	MN	BN	BN	BN
BP	Z	SN	MN	BN	BN	BN	BN

In the defuzzification stage and inference mechanism the output of fuzzy logic control is converted from linguistic variables to numerical variables. The inference mechanism

determines the matching degree of the current fuzzy input with respect to each rule and the controller has to resolve the conflict between different rules being obeyed at the same time and decides which rules are to be obeyed according to the input field. Then the obeyed rules are combined to form the control actions. The method of dfuzzifcation used for this is called Centre of Gravity (COG) or centroid. The idea of (COG) is to find the variable value of the center of gravity of the composite membership function for the fuzzy value.

4.2 Artificial neural network controller

The concept of artificial neural network (ANN) analysis was developed by Warren McCulloch and Walter Pitts [40] However, applications software has only been developed in the last 30 years to handle practical problems. Artificial neural networks (ANNs) systems are computing systems vaguely inspired by the biological neural networks that mimics human biological neural network behavior. Such systems "learn" to perform tasks by considering examples, generally without being programmed with any task-specific rules. Artificial neural network (ANN) technology has been successfully applied to solve very complex problems. Recently, its application in various fields is increasing rapidly. The science of artificial neural network is based on the neuron, which loosely model the neurons in a biological brain. The ANNs operate like a black-box model. It does not require detailed information about the system. They effectively learn the relationship between the input and the output variables by making use of trends in previously recorded data. Also ANNs have the ability to work with highly nonlinear relationships, can work with numerical or analogue data, are relatively robust in terms of finding best-fit solutions, and the user does not require sophisticated mathematical knowledge

4.2.1 Artificial neuron model

The common building block, known as a neuron and the network interconnection structure is neural network models. The well-known and the most used example of the model of neuron, initially proposed by (McCulloh-Pitts 1949), is illustrated in Fig below.

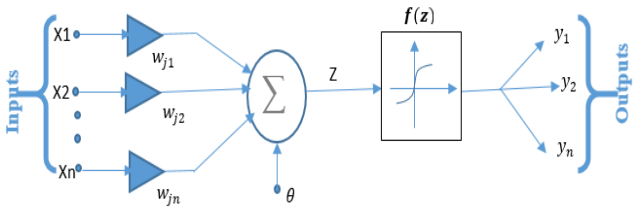

Fig. 4.7. Basic artificial neuron model

The net function determines how the network inputs ((*xnj*; $1 \leq j \leq N$)) are combined inside the neuron. In Fig.5.7 a weighted linear combination is described by

$$Z=f\left(\sum_{j=1}^{N} w_{nj}x_{nj}+\theta\right) \tag{4.9}$$

Where the parameters ((*wnj*; $1 \leq j \leq N$)) are known as synaptic weights and θ is called the bias, offset (or threshold) and is used to model the threshold. The output of the neuron denoted by y_n is computed through the activation function, which is *f*. The strength of the exiting signal are controlled by activation function. There are several types of transfer function that are used as activation functions, such as sigmoidal (or log-sigmoid), hyperbolic tan (or tan-sigmoid), linear (bipolar), threshold and Gaussian etc. in neural network design activation function selection plays an important role. However, the sigmoidal, hyperbolic and linear function activations are the most commonly used function among the others.

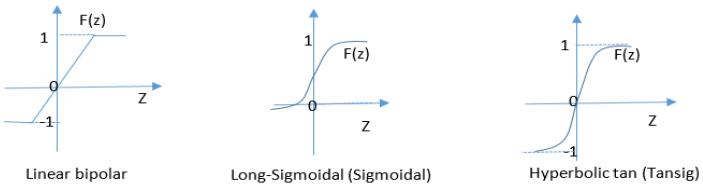

Fig. 4.8 different types of activation function graphs

The activation functions of the above transfer functions are described as follow.

Linear bipolar

$$y_n = f(Z) \tag{4.10}$$

Long-sigmoidal

$$f(Z) = \frac{1}{1+\exp(-Z)} \tag{4.11}$$

Hyperbolic tan (Tansig)

$$f(Z) = \frac{1}{1+\exp(-2Z)} - 1 \tag{4.12}$$

4.2.2 Artificial neural network architecture

Neural Networks are known to be universal function approximations, various architectures are available to approximate any nonlinear function and different architectures allow for generation of functions of different complexity and power. These are feedforward networks, feedback networks and lateral networks.

Feedforward Networks

In this type no feedback within the network and the coupling takes place from one layer to the next. The information flows, in general, in the forward direction.

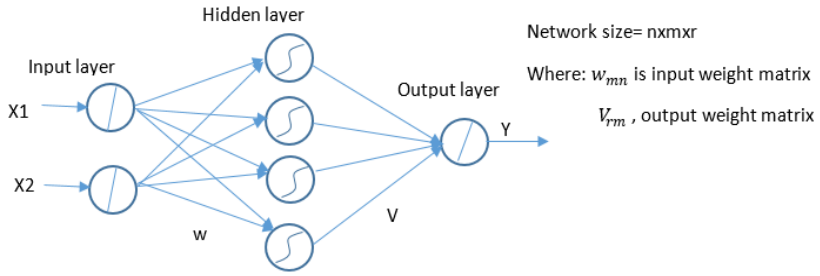

Fig. 4.9. Feedforward network structure

Input layer: Number of neurons in this layer corresponds to the number of inputs to the neuronal network. This layer consists of **passive nodes**, i.e., which do not take part in the actual signal modification, but only transmits the signal to the following layer.

Hidden layer: This layer has arbitrary number of layers with arbitrary number of neurons. The nodes in this layer take part in the signal modification, hence, they are **active**.

Output layer: The number of neurons in the output layer corresponds to the number of the output values of the neural network. The nodes in this layer are **active** ones.

FFNN can have more than one hidden layer. However, it has been proved that FFNNs with one hidden layer has enough to approximate any continuous function [Hornik 1989].

Feedback networks:

The output of a neuron is either directly or indirectly fed back to its input via other linked neurons, it used in complex pattern recognition tasks, e.g., speech recognition etc.

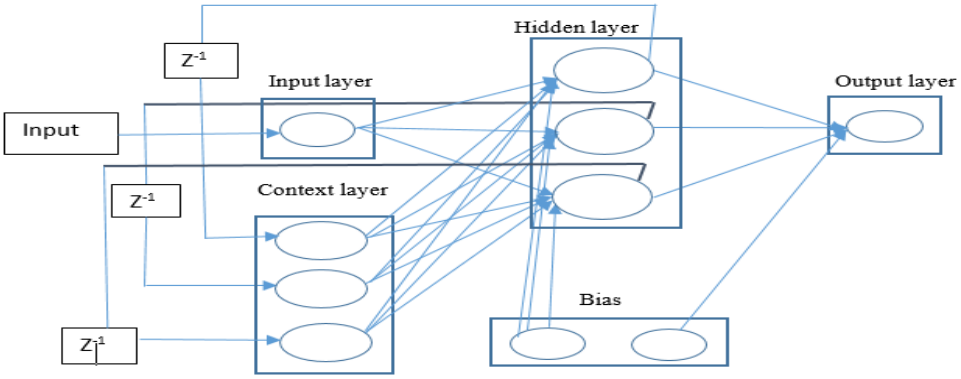

Fig. 4.10 Elman Recurrent Feedback networks

Lateral Networks

In this type of Networking there exist couplings of neurons within one layer and there is no essentially explicit feedback path amongst the different layers. This can be thought of as a compromise between the forward and feedback network.

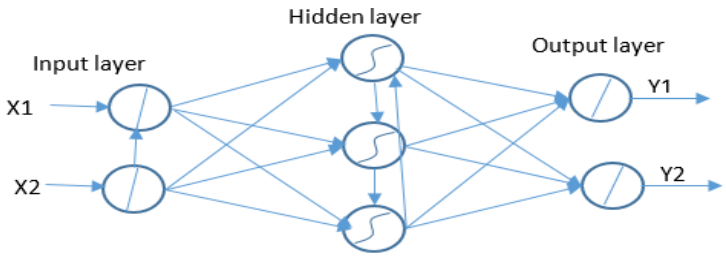

Fig. 4.11 Lateral network structure

4.2.3 Learning Methods

In all prediction methods a training dataset is used. The dataset comprises a sub-set of the data that we wish to model. In the learning process we try to teach the network how to produce the output when the corresponding input is presented. When learning is complete: the trained neural network, with the updated optimal weights, should be able to produce the output within desired accuracy corresponding to an input pattern. The learning or trained methods can be supervised learning, unsupervised learning or reinforced learning.

Supervised learning

In this method the training set contains the input features of the system and the output data which has been predetermined by another method such as human decisions or experimental measurement and the learning algorithm attempts to find a functional mapping between the inputs and outputs by using the training data to determine the parameters (weights and thresholds) of the prediction technique.

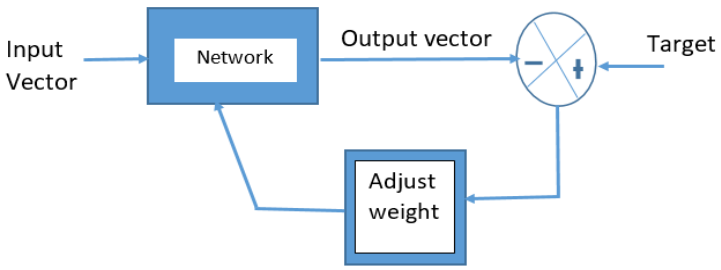

Fig. 4.12 Supervise training scheme.

The performance of the ANN model is monitored by the use of a “performance” or “error” functions during the training process. This function provides a comparison between the predictions of the ANN model and the actual output values. The training process performed by iteratively decreasing in the error function and continuously until a predetermined value is reached. After training, the trained ANN model is evaluated by application of a “test dataset”, containing new data to determine how well the model performs. A model which performs well when working on new data is said to have good generalization.

Unsupervised learning or self-organized learning

The objective of unsupervised learning is to discover patterns or features in the input data with no help from a teacher, basically performing a clustering of input space. unsupervised methods are often only the initial stage in a two (or more) stages training process, later stages involving supervised learning, the first training stage uses an unsupervised process to determine locations and sizes of the basic functions.

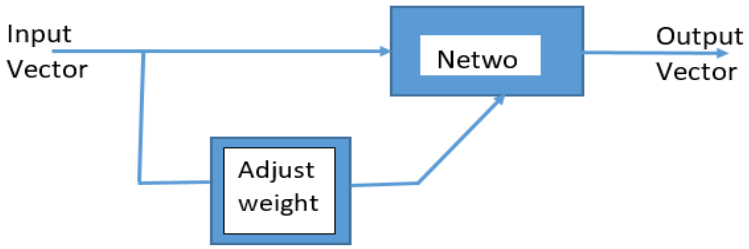

Fig. 4.13 Unsupervised training scheme.

The system learns about the pattern from the data itself without a priori knowledge. This is similar to our learning experience in adulthood.

Reinforced learning

In this type of train method a ‘teacher’ though available, does not present the expected answer but only indicates if the computed output is correct or incorrect and the information provided helps the network in its learning process. After trained a reward is given for a correct answer computed and a penalty for a wrong answer.

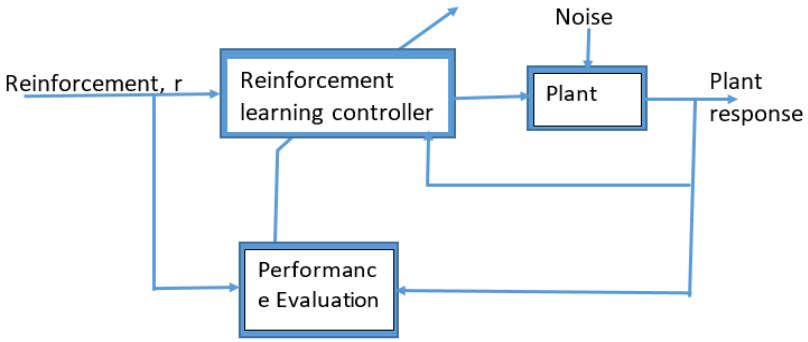

Fig. 4.14 Reinforce training scheme

There are several existing types of training algorithms such as back propagation algorithm, Delta-bar-Delta, Quasi-Newton algorithm, conjugate gradient algorithm, Kohonen training and Levenberg-Marquardt algorithm [41].

In this work the supervised training by feedforward network architecture is selected. For training the multilayer feedforward network, the Levenberg-Marquardt method is generally recommended due to its robustness, and it provides fast convergence and it is not necessary for the user to initialize any strange design parameters [41].

4.2.4 Artificial neural network controller for photovoltaic water pumping system

After designed the required components of PV water system, connect the whole components in a combined to artificial neural network controlling system. The inputs of the proposed ANN controller are the PV array output power P_{PV} and the output voltage V_{pv} from the PV array and the output of ANN controller is the boost converter control signal. To get the required maximum power of the PV array and to operate the pump load at different solar insolation levels and temperatures the duty ratio of the boost converter is adjusted accordingly by the ANN controller.

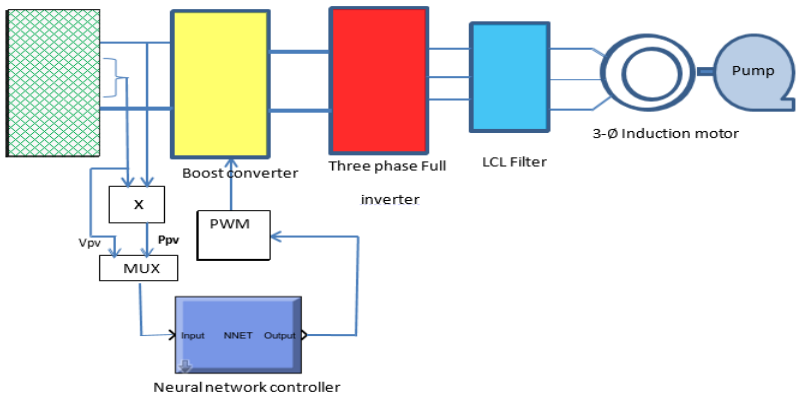

Fig. 4.15 Schematic diagram of the proposed neural network based PV water pumping system

Neural network controller architecture for photovoltaic water pumping system

The proposed ANN is a feed forward neural network comprising input layer, hidden layer and the output layer is considered for the online estimation of the duty ratio. The structure of multilayer feed forward networks are mostly determined by experience and according to the previous studies there is no a valid formula that is appropriate for different situations. ANN in the default setting has 10 neurons in the hidden layer. Increasing the number of neurons in the hidden layer increases the power of the network, but requires more commutation and is likely to produce over fitting. There are two categories from which to select the architecture of the ANN techniques as in [42, 43]. The first category start with a small network and gradually adding connections or nodes as needed. In the second category, a big network is selected, and then reduced by gradually eliminating the unnecessary connections or nodes. The first category was used in this study to map the relationship between the duty ratio and the PV power and the PV voltage. The input layer consists of a two dimensional vector, PV array output power and the PV array output voltage. The output layer of the proposed ANN comprises a one dimensional vector, which is the controlling signal of the boost converter duty cycle (D).

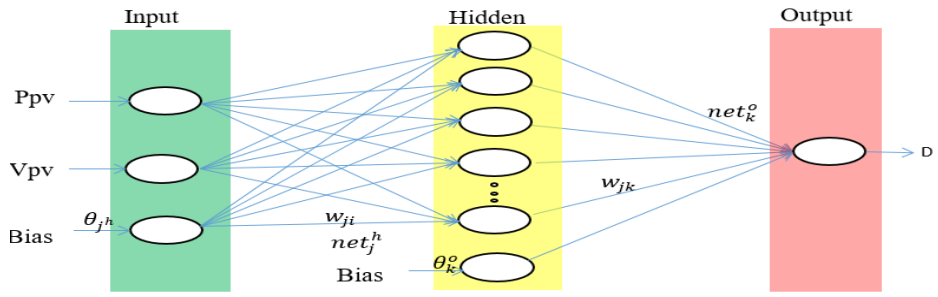

Fig. 4.16. The selected feedforward neural network architecture

The outputs of the input layer are weighted and summed together, and then a bias is added to the sum of the weighted inputs. The summation of the weighted inputs and the bias are passed through the transfer function f. A hyperbolic tangent sigmoid transfer function was used as an activation function to calculate the hidden layer output and linear transfer function was used to provide a wide range of output solutions.

The collected data for training should be first normalized before being applied to the input layer as the input vector.

$$x_n = (x_{n1}, x_{n2}, x_{n3}, \ldots\ldots x_{nn} x_n)^T \tag{4.13}$$

When the weight vectors of the input layer are multiplied to the hidden layer and added to the bias vector, the net input for the j^{th} hidden unit is

$$net_j^h = \sum_{i=1}^{n}(w_{nji}x_{ni} + \theta_j^h) \tag{4.14}$$

Where w_{nji} is the weight on the connection from the i[th] input unit to the j[th] hidden layer, and θ_j^h, is the bias for each joint from the input layer to the output layer, which is mainly used to improve the learning speed during network training process. Now the output value from the hidden layer is

$$y_n{}_j^h = f_1 \sum_{i=1}^{n}(w_{nji}x_{ni} + \theta_j^h) \tag{4.15}$$

The net input to the neurons in the output layer becomes

$$net_k^o = \sum_{j=1}^{N_h}(w_{nkj}y_j^h + \theta_k^o) \tag{4.16}$$

Where w_{nkj} is the output weight connecting the i[th] input unit to the k[th] output unit and θ_k^o is the threshold value for neuron in the output layer. The output of the neurons in the output layer is

$$y_n{}_k^o = f_2 \sum_{j=1}^{N_h}(w_{nkj}y_j^h + \theta_k^o) \tag{4.17}$$

Training the neural network for photovoltaic water pumping system

A set of input output pairs of the training patterns or training data are required to accomplish the training process. The set of input output training data is collected from the PV panel outputs and corresponding to the boost converter duty cycle, this are the PV panel maximum power and voltages are used as an input, whereas the output data set is the corresponding duty ratio D of the boost converter.

The backpropagation algorithm with the Levenberg-Marquardt optimization method is used in this work. This type of algorithm is one of the most widely used algorithms for training the feedforward ANN because of the ease of implementation, robustness and stability. The learning stage of the network is performed by updating the weights and biases using a backpropagation algorithm with the Levenberg-Marquardt optimization method in order to minimize a mean squared error performance index E

$$E_P = \frac{1}{2}\sum_j(t_{pj} - o_{pj})^2 \tag{4.18}$$

where $E_P$the index of the output neurons, O_{pj} is the measured output of the outputs and tpj is the desired output of the output neurons.

The overall performance of a multilayer perceptron (E) neural network measured as mean square error (MSE), can be the summation of each index of the output neurons (Ep) starts from 1 to m number of neurons.The smaller the mean square error is, the better the performance and accuracy the network will achieve in real life.

In this thesis, the connection weights are updated by

$$w_{nji}(n+1) = w_{nji}(n) - \sigma\left(\frac{\partial E_n}{\partial w_{nji}(n)}\right) + \gamma(w_{nji}(n) - w_{nji}(n-1)\Big) \quad (4.19)$$

$$w_{noi}(n+1) = w_{noi}(n) - \sigma\left(\frac{\partial E_n}{\partial w_{noi}(n)}\right) + \gamma(w_{noi}(n) - w_{noi}(n-1)\Big) \quad (4.20)$$

Where η is the learning rate, which is used to adjust the weights between layers and γ is the momentum factor, which is added to the last variation of weights on the variation of weights, in order to reduce the vibration and avoid the problem of slow convergence speed in the learning process of the weights [44].

Neural network model in MATLAB for the photovoltaic water pumping system

The neural network model shows multiple layers of neurons with nonlinear transfer functions to allow the network to learn nonlinear and linear relationships between the input and corresponding output values using the 2017a MATLAB software. This is a two layer feedforward configuration.

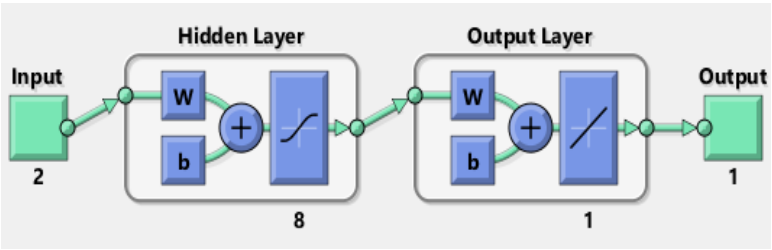

Fig. 4.17 Neural network mat lab model

The network weights and biases have been adjusted, the network is ready for training, and to accomplish the training process a set data is required. The training data in this work are the data which is recorded from the PV panel in different level of Irradiation of the sun and ambient temperatures, these inputs are in three classes the input train data used for training, the target data for validation, and sample data for testing. The weights and biases of the

network are iteratively adjusted during the training process to minimize the network output error. The average square error against different epoch for training process and the regression plot are shown below in Fig. (4.18) and (4.19) respectively.

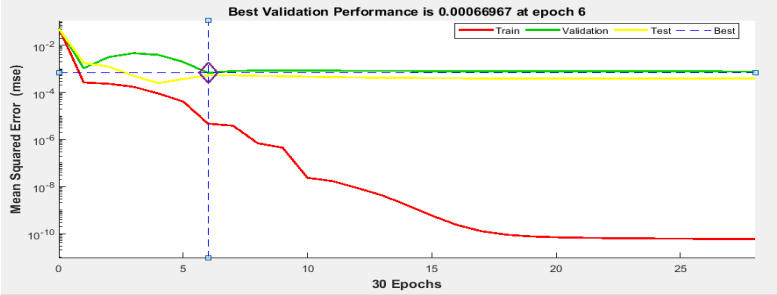

Fig. 4.18 Training result of ANN Mat lab block

To test the network response, the sampling test data sets are put through the network and will perform a linear regression between the network outputs and the corresponding targets. Then, a regression analysis is carried out between the network response and the corresponding targets. Next, the output (predicted duty ratio) and the corresponding targets (calculated duty ratio) of the network are passed to the linear regression analysis function.

Where the parameter R represents the correlation between the target output and the predicted output network. As shown in regression plot below all points are located on the line of best regression, which means the both networks predict the duty ratio for training data set very well. Finally, the selected neural network size is 2 input nodes, 8 hidden nodes and one node output layer gives the best precise prediction.

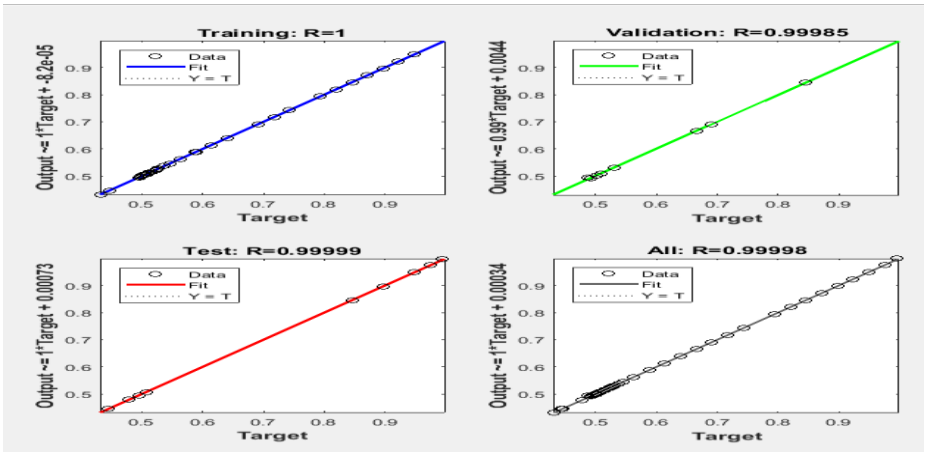

Fig. 4.19 The network performance analysis

4.3 Neuro-Fuzzy hybrid intelligent controller

A hybrid intelligent system is one that combines at least two intelligent technologies but in a time of combination selection of the right components for building a good hybrid system is basic. Hybridization improves the weakness and cooperate the strongest of each individual. Among many hybrid systems Neuro-Fuzzy hybrid system is applied for this work.

Neural networks and fuzzy systems can be combined to join its advantages and to cure its individual illness. Neural networks introduce its computational characteristics of learning in the fuzzy systems and receive from them the interpretation and clarity of systems representation. Thus, the disadvantages of the fuzzy systems are compensated by the capacities of the neural networks. In general integrated neuro-fuzzy systems can combine the parallel computation and learning abilities of neural networks with the human-like knowledge representation and explanation abilities of fuzzy systems. As a result, neural networks become more transparent, while fuzzy systems become capable of learning.

In this work the Adaptive Network based Fuzzy Inference System (ANFIS) is applied, since the hybrid neuro-fuzzy systems present an interpretable model and they have learning capacities in a supervised way.

4.3.1 Adaptive Network Based Fuzzy Inference System (ANFIS)

ANFIS implements a Takagi Sugeno fuzzy inference system and it has five layers as shown in figure 4.20. ANFIS is preferable for integrate the best features of Fuzzy Systems and Neural Networks. Note that neurons in ANFIS have different structures, thus are the Membership function defined by parameterized soft trapezoids (Generalized Bell Functions), the Rules which is Differentiable T-norm - usually product and methods of normalization is Sum and arithmetic division. And also the activation function is linear regressions and multiplication with normalized weights. Finally the output function is algebraic sum.

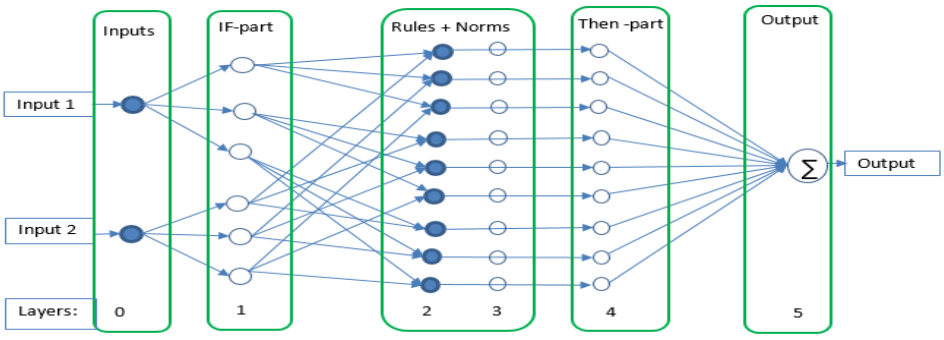

Fig. 4.20 ANFIS layer structure

Each layer in the neuro-fuzzy system is associated with a particular step in the fuzzy inference process.

Layer 1: The first hidden layer is responsible for the mapping of the input variable relatively to each membership functions and transmits external crisp signals directly to the next layer.

That is

$$y_i{}^{(1)} = x_i{}^{(1)} \tag{4.21}$$

Layer 2: The second hidden layer is the fuzzification layer which receives a crisp input and determines the degree to which this input belongs to the neuron's fuzzy set. And the operator T-norm is applied in this layer to calculate the antecedents of the rules.We use Gaussian sets, and therefore, the activation functions for the neurons in this layer is set to the triangular membership functions. A Gaussian membership function (MFs) can be specified by two parameters $\{a, b\}$ as follows:

$$\text{Gaussian}(\alpha, \text{b}) = e^{-\frac{1}{2}(\frac{x-a}{b})^2} \tag{4.22}$$

Layer 3: The third hidden layer is the fuzzy rule layer, a fuzzy rule neuron receives inputs from the fuzzification neurons that represent fuzzy sets in the rule antecedents. It normalizes the rules strengths followed by the fourth hidden layer where the consequents of the rules are determined. In a neuro-fuzzy system, intersection can be implemented by the product operator. Thus, the output of neuron *i* in Layer 3 is obtained as:

$$y_i{}^{(3)} = \prod_{j=1}^{k} x_{ji}{}^{(3)} \tag{4.23}$$

Layer 4: The forth layer is a normalization layer. Neuron in this layer represents fuzzy sets used in the consequent of fuzzy rules and calculates the normalised firing strength of a given rule. The normalised firing strength is the ratio of the firing strength of a given rule to the sum of firing strengths of all rules. An output membership neuron combines all its inputs by using the fuzzy operation union. This operation can be implemented by the probabilistic OR. That is,

$$y_i{}^{(4)} = \sum_{j=1}^{k} x_{ji}{}^{(4)} \tag{4.24}$$

Layer 5: This layer is the defuzzification layer. Each neuron in this layer represents a single output of the neuro-fuzzy system. It takes the output fuzzy sets clipped by the respective integrated firing strengths and combines them into a single fuzzy set. Neuro-fuzzy systems can apply standard defuzzification methods, including the centroid technique. This layer

calculates the global output as the summation of all the signals that arrive to this layer. We will use the sum-product composition method.

The sum-product composition calculates the crisp output as the weighted average of the centroids of all output membership functions. For example, the weighted average of the centroids of the clipped fuzzy sets *C*1 and *C*2 is calculated as,

$$y = \frac{\mu_{c1} \times a_{c1} \times b_{c1} + \mu_{c2} \times a_{c2} \times b_{c2}}{\mu_{c1} \times b_{c1} + \mu_{c2} \times b_{c2}} \quad (4.25)$$

Sugeno fuzzy model

The Sugeno fuzzy model was proposed for generating fuzzy rules from a given input-output data set. A typical Sugeno fuzzy rule is expressed in the following form;

IF x_1 is A_1 AND x_2 is A AND x_m is A_m THEN

$$y = f(x_1, x_2 \ldots x_m) \quad (4.26)$$

where $x_1, x_2 \ldots x_m$ are input variables; $A_1, A_2 \ldots$ are fuzzy sets.

When *y* is a constant, we obtain a zero-order Sugeno fuzzy model in which the consequent of a rule is specified by a singleton.

When *y* is a first-order polynomial, i.e.

$$y = k_0 + k_1 x_1 + k_2 x_2 + \ldots + k_m x_m \quad 4.27)$$

ANFIS learning methods

In general, ANFIS is used to predict the output data parameters from inputs. ANFIS uses training data to adapt the Sugeno-type model to perform a high accuracy in output data prediction.

The Sugeno-type model has two type of parameters:

- Nonlinear parameters or membership functions parameters (premise parameters)
- Linear parameters or rules parameters (consequent parameters).

The input output training data is used with different learning algorithm strategies to adapt the premise parameters and consequent parameters. The least-squares estimate (LSE) method and the backpropagation gradient descent method are used for training FIS membership functions parameters to estimate a given training data set [45]. LSE learning algorithm calculates the

square error between training data output and predicted output that is obtained from the Sugeno-type model. This error is utilized to adapt the consequence parameters of the Sugeno parameters

The backpropagation gradient descent method uses the error between output training data and predicted output in backward pass to calculate the error in different nodes. Accordingly, the learning rate is calculated to adapt the Sugeno parameters. There are four methods are used to update the parameters. These methods are listed below according to their computational complexities [45]:

- Gradient descent only: all parameters are updated by the gradient descent.
- Gradient descent and one pass of LSE: the LSE is applied only once at the very beginning to get the initial values of the consequent parameters and then the gradient descent takes over to update all parameters.
- Gradient descent and LSE: this is the proposed hybrid learning rule.
- Sequential approximate LSE only. The selection of above methods should be based on the trade-off between computation complexity and resulting performance. Jang in [36] used the third method, which achieves a high performance.

In hybrid learning rule algorithm, ANFIS uses a two pass learning algorithm:

- Forward pass: here consequent parameters are computed using a LSE algorithm and premise parameters are unmodified (Off-line Learning).
- Backward pass: here premise parameters are computed using a gradient descent algorithm and consequent parameters are unmodified (usually uses Back-propagation).

4.3.2 Neuro-fuzzy controller for photovoltaic water pumping system

Similar to the ANNC and FLC ANFIS has two inputs and one output, which are the voltage and power generated by a PV panel as inputs in different level environmental changing periodically and nonlinearly and duty cycle ration D as output.

This database is created from an experimental data acquisition, hence ANFIS based MPPT is proposed to solve the problem and to deliver the maximum available power of the PV array to the ac load. Schematic diagram is shown in fig 4.21.

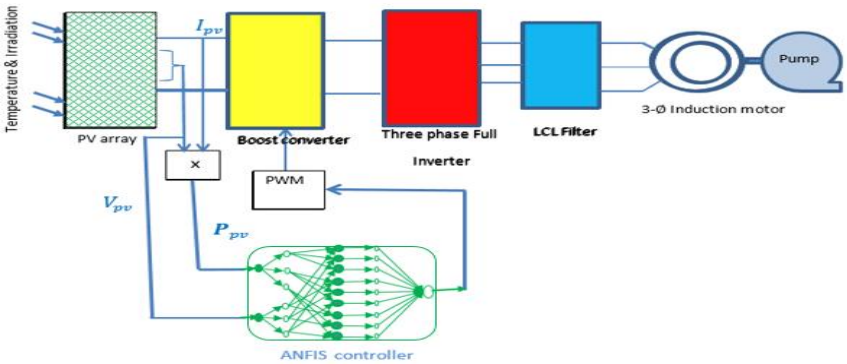

Fig. 4.21 schematic diagram of ANFIS controller based MPPT of PV water pumping system

The proposed ANFIS controller Mat lab model

The proposed ANFIS controller had two inputs and one output and applies 5x5 Gaussians MFs to gate Maximum powers, even if the surrounding condition is vary. The number of generated rules can be computed from all possible connectives between MFs of inputs. Therefore, the number of rules equal the number of MFs of input one times the number of MFs of input two.

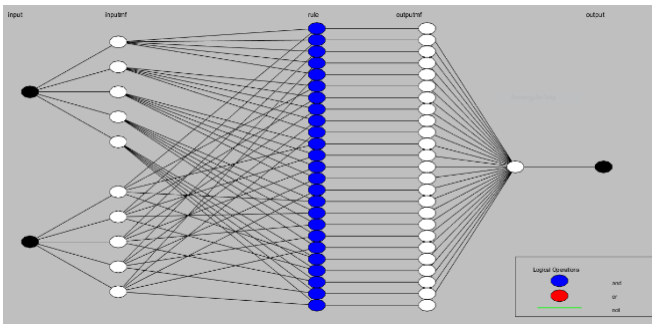

Fig. 4.22 ANFIS Mat lab mode structure

All actual data is used as a learning data to train the ANFIS model. Also, this data is used as a test data to find the individual errors between actual data and predicted data. From the PV power and voltages inputs and the Gaussian MFs the designed controller had 5x5 membership functions at two inputs and 25 rules.

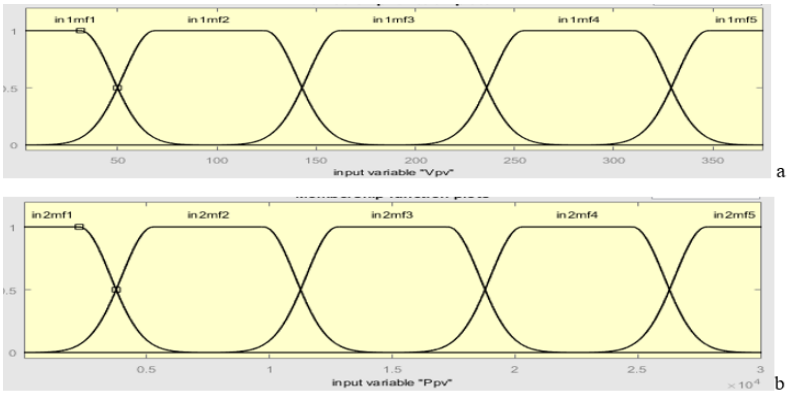

Fig. 4.23 ANFIS Generated membership functions

Learning an ANFIS with Five membership functions assigned to each input

The ANFIS training data includes 72 training samples. They are represented by a 72 × 3 matrix [V_{pv} P_{pv} D], where V_{pv} and P_{pv} are input vectors, and D is a desired output vector. By applying Sugeno model the least-squares estimate (LSE) method and the backpropagation gradient descent method are used for training FIS membership functions parameters to estimate a given training data set.

Fig. 4.24 the trained data LSE result in different epochs

CHAPTER FIVE

SIMULATION STUDIES AND ANALYSIS OF RESULTS

This chapter describes how the MATLAB/SIMULINK models of the proposed PV power systems are implemented to test and verify the functionality of the proposed MPPT controllers. PV system is simulated in MATLAB, with an AC water pump load (17.5kW) to demonstrate the feasibility and performance of the proposed artificial intelligence controller based on MPPT of water pumping system. Furthermore, a comparison has been carried out between each proposed controllers, those are Neural Network controller, Fuzzy Logic Controller and Neuro-Fuzzy controller.

5.1 Photovoltaic System modelling using simulink

The system design is modeled and simulate using MATLAB 2017a /SIMULINK. The modelled system consists mainly of PV array model, DC/DC boost converter model used to interface PV output to the inverter to track the maximum power of the PV array, DC/AC three phase PWM inverter model used to interface with the AC load, LCL low pass filter to supply a pure sinusoidal output voltage to the load.

The PV model simulator was implemented in MATLAB/SIMULINK as shown in the appendix (A).

The PV array used in the simulation is a 29.04kW power that eleven strings with eleven modules of 240W power. Or 11x11 elements are combined to generate the desired power at standard conditions specified at irradiation of (G = 1000kW/m2) and temperature of (T =25^{o}C).

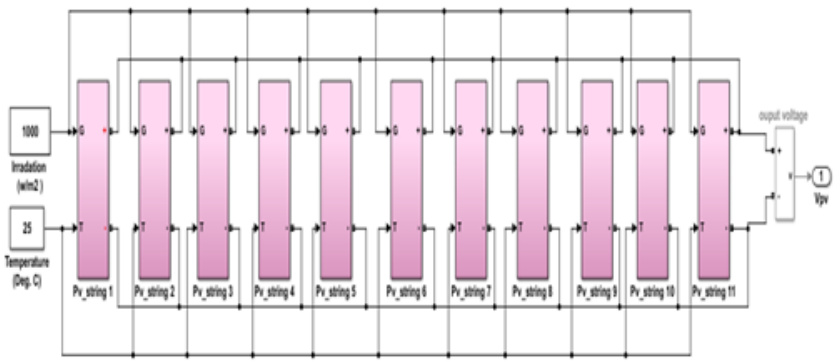

Fig. 5.1 Connection of Eleven PV strings in parallel

In fig 5.1 series parallel connections are applied, first a 240W PV module are designed to build a strings which consists eleven series modules, then constrict the PV array or PV panel by connecting 11 PV strings in parallel as the designed calculated values.

Totally one hundred and twenty one modules are implemented to get the PV power that used to generate 29.04kW for the required purpose.

The PV panel Simulink block has been masked in the embedded form as follow. The temperature T and isolation G are fed to the Embedded MATLAB Function and the outputs are the current and voltage produced by the panel**.**

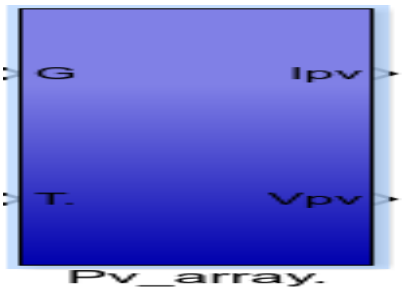

Fig. 5.2 Embedded PV Array or PV panel SIMULINK model.

Table 5.1The proposed module and array value

Parameters	Modeled Module value	Proposed array Value	Unit
Maximum power (Pmax,)	0.24	29.04	kW
Open circuit voltage (Voc)	36	396	V
Short circuit current (Isc)	8.7	95.7	A
Maximum current (Imax)	8.17	89.87	A
Maximum voltage (Vmax)	29.38	323.1	V
Number of cells (Ns)	60	7260	-

The current to voltage, voltage to power and current to power relation curve of the simulated model is used to know the influence of temperature and irradiation change on the output characteristics of the PV panel.

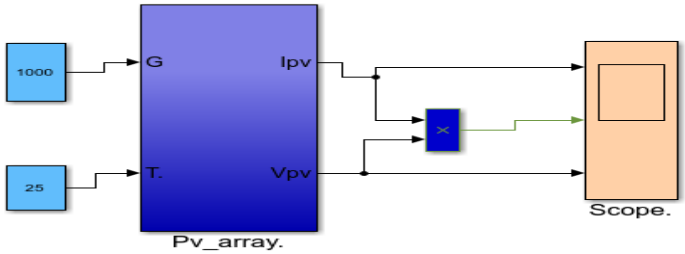

Fig. 5.3 Simulink model for data collecting system of PV array

The output of the PV array is recorded in different level of irradiation (1400, 1200, 1000, 800 & 600) w/m^2 at 25^0 C, as well as different environmental temperature (70, 45, 25, 15 & -10) at standard irradiation values or random value of temperature and irradiation level and the result of the characteristics curves are shown in figures below.

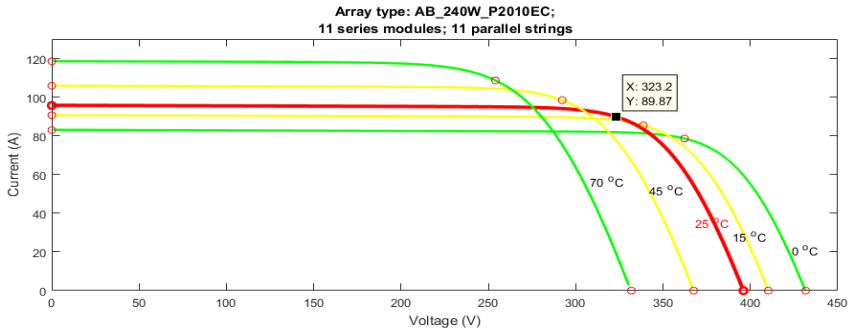

a) V-I characteristics

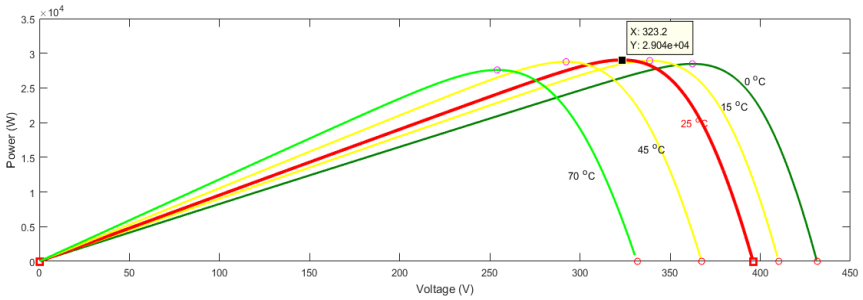

b) V-P characteristics

Fig. 5.4 V-I and V-P characteristics of the PV array at standard irradiation level.

In the fig.5.4 the effect of temperature clearly shown on current voltage and power, as temperature increased the voltage becomes less on the contemporary the generated current is increased. To get the maximum power the output current and voltage has been maximum, this phenomena occurs during the low value of temperatures.

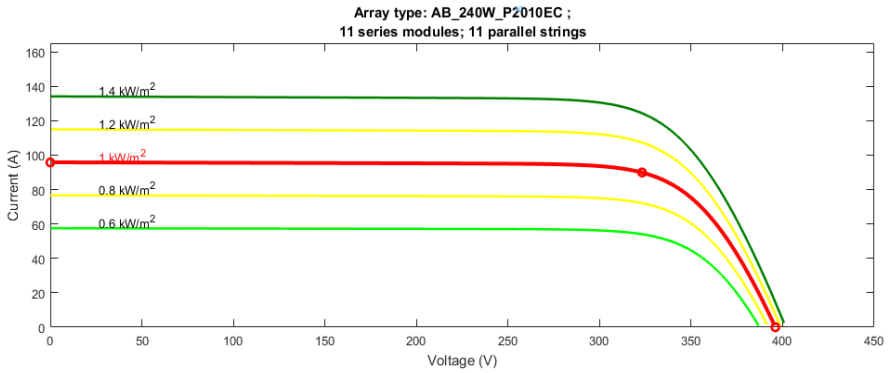

a) V-I characteristics

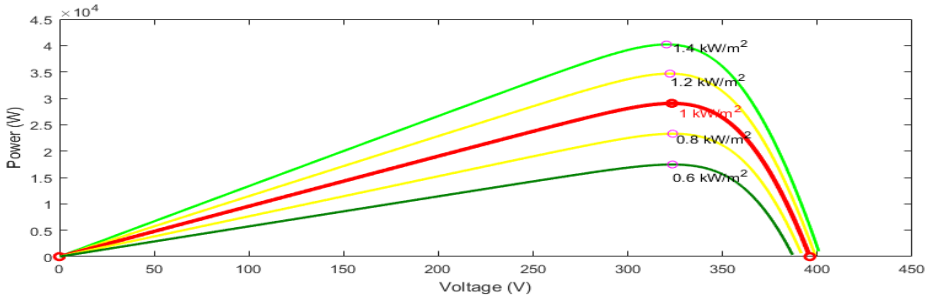

b) V-P characteristics

Fig. 5.5 V-I and V-P characteristics of PV array at standard temperature

In fig 5.5 the effect of irradiation at standard level of temperature is displayed. The irradiation had directly relationship with current and voltage, as the irradiation increased the current also increased and the voltage had slowly increased.

5.1.1 Boost converter modelling

The boost converter is conducted in MATLAB and simulated using SimPower Systems blocks and the circuit diagram is depicted in Fig. 5.6. The converter consists of IGBT switch and freewheeling diode. Additionally, input filter and output capacitor is included. The inductor is responsible for reducing the output current ripple; the larger the value of the inductor, the smaller the value of the ripple and the Capacitor responsible to minimize harmonic.

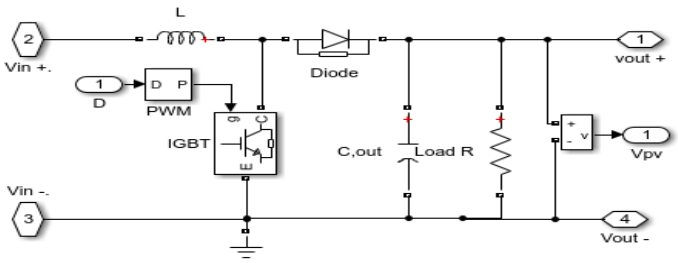

Fig. 5.6 simulation model of DC-DC Boost converter

The model can be masked by the SIMULINK and simplified into only one block

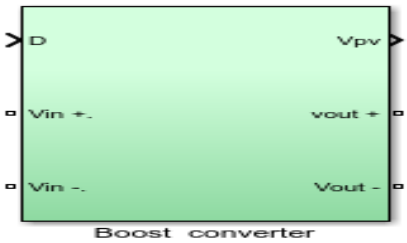

Fig. 5.7 Boost converter one block representation

There are three inputs and three outputs in the boost converter block, the inputs are the duty cycle(D) from the PWM block and Vin^- , Vin^+ are the input negative and positive voltage from the PV panel respectively. The outputs are $Vout^+$, $Vout^-$ the positive and negative output voltage and Vpv is the voltage to be generate from PV panel.

5.1.2 DC to AC converter modelling

In chapter two the inverter topology simulation result is mentioned detail, but in this circuit three phase full-bridge inverter takes the output of the boost converter as the input and the gate signal which is generated by two level PWM generator, finally it inverts the input DC voltage in to (400±5%) Ac voltage to drive the induction motor in ordered to capable of take waters to 96.78m height from the ground level to the surface.

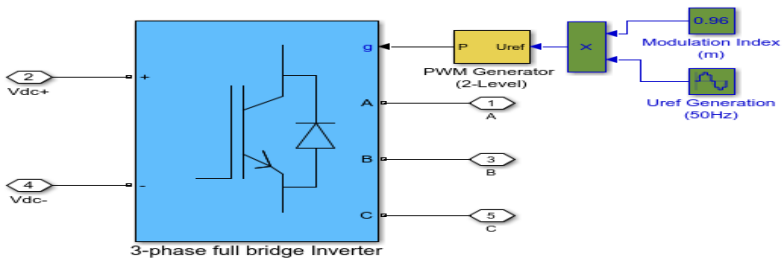

Fig. 5.8 Simulink models of three phase inverter

5.1.3 LCL Low pass filter modelling

The output of the full bridge inverter is not pure sinusoidal ac voltage this responsibility is taken to account for the low pass filter which is minimize the harmonic of the output voltage to supply a pure sinusoidal output voltage to the load. The inverter contains the input side and output side inductor, filter Capacitor and damping resistor with the appropriate scale.

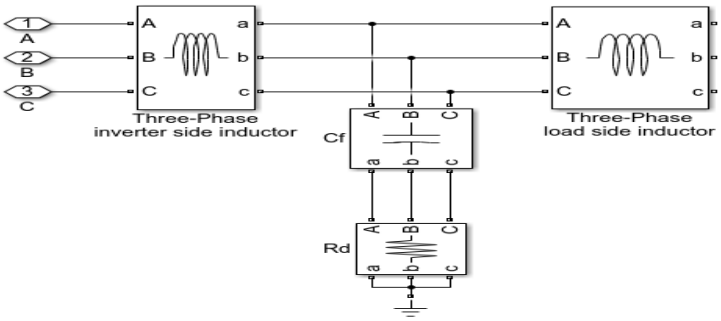

Fig. 5.9 Simulink model of LCL filter

5.1.4 Simulation test of the Ac output before and after output filter

To sow the validation of boost converter, three phase inverter and LCL filter, that are design above it ought to use the standard irradiation and temperature levels (T=25^{o} C and G=1000w/m^{2}) to the tested PV

In figures below tried to show the output result of the inverter line to line and line to neutral voltage before and after connected the design LCL filter, at the maximum power point, those phenomena used to test the performance of the designed inverter and the low pass filter that have seen in Fig 5.9, the output voltage is purify by the low pass LCL filter.

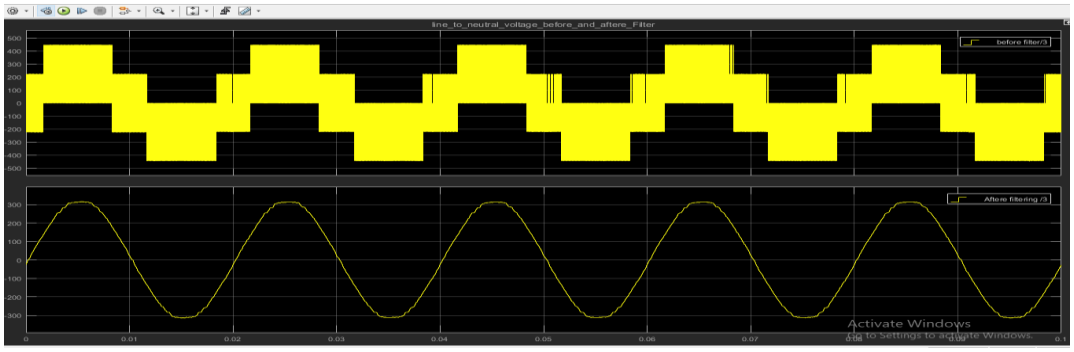

Fig. 5.10 line voltage before and after the low pass filter

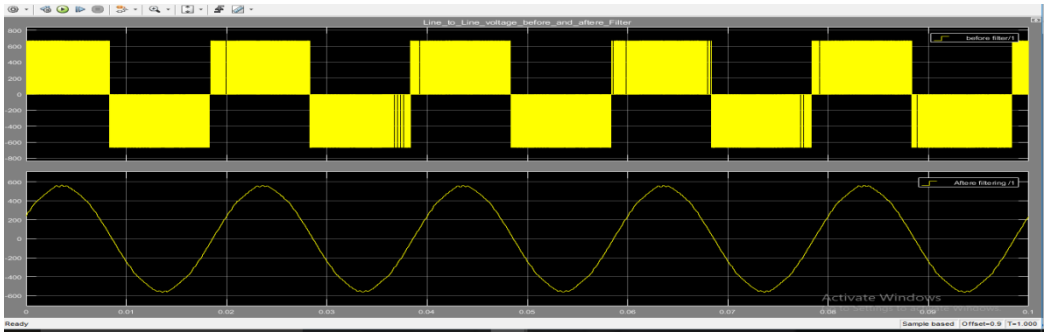

Fig. 5.11 phase voltage before and after the low filter

5.2 Simulink Model of controllers for PV water pumping system

In this thesis artificial intelligence and hybrid controlling method had been practice, those are fuzzy logic controller, neural network controller and ANFIS controller.

5.2.1 FL controller simulink model for PV water pumping system

The control model is shown in Fig. 5.12. The fuzzy control rule has been completed in MATLAB FIS as discussed in chapter five section two. The detailed design of the Fuzzy Interface system (FIS) editor, Membership Function Editor and Rule Editor are as shown in the Appendix (C). The FLC uses the PV array Power *Ppv* and the output voltage *Vpv* as input signals and produces duty cycle ratio *D* as a control signal for the boost converter.

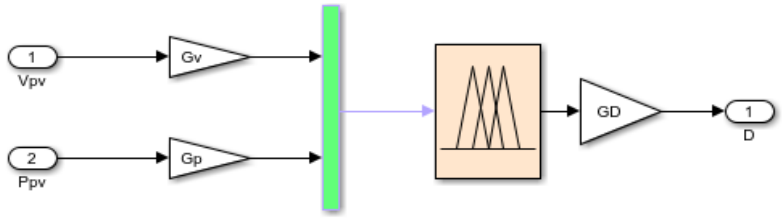

Fig. 5.12 SIMULINK block of fuzzy logic controller

Table 5.2 Fuzzy logic controller parameter

Fuzzy logic controller parameter	Scale
The scaling factor of the PV array output power variation (**Gp**)	0.003443
The scaling factor of the PV array output variation (**Gv**)	0.15475
The scaling factor the duty ratio variation (**GD**)	1.0

5.2.2 NNC Simulink model for PV water pumping system

The training and simulation model of the neural network has been carried out using MATLAB to identify the duty ratio of the boost chopper corresponding to the MPP from data of the PV array power and voltage see appendix (A). The MATLAB/SIMULINK model of the trained neural network is illustrated in fig. 5.13.

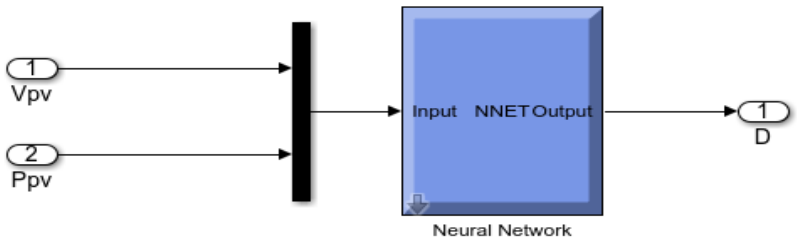

Fig. 5.13 Simulink block of designed neural network controller

The neural network block sizes are consists 2 input nodes, 8 hidden nodes and one node output layer. Each layer has a set of input and base. To calculate the output of the hidden layer, a tangent sigmoid transfer function was used as an activation function and a linear transfer function was used for the neurons of the output layer. The weights of each layer are multiplied with the input signals in each neuron. The MATLAB simulation of the ANN layers, weighted input and bias are represented in the Appendix (D).After trained the collected data, the NNC Simulink model is created and replaced on the place of FLC and simulate it. The system Simulink model is constructed using each components that are designed in the previous chapters and the parameters are matched and sized. The simulation result are shown below.

5.2.3 ANFIS controller Simulink model for PV water pumping system

The proposed ANFIS controller had two inputs and one output to achieve the goal. The designed controller had 5x5 Gaussian membership functions with 25 rules at two inputs (Voltage and Power) and one output which is fed to the boost converter to adjust the boost voltage.

The ANFIS training data includes 72 training samples from the PV panel output data by varing the irradiation and temperature level. They are represented by a 72×3 matrix [V_{pv} P_{pv} D], where V_{pv} and P_{pv} are input vectors, and D is a desired output vector. By applying Surgeon model the least-squares estimate (LSE) method and the back propagation gradient descent method are used for training FIS membership functions parameters to estimate a

given training data set, 70 percent of the sample data used as trained data and the remain 30 percent sample data was the checking and testing for the validation of the controller.

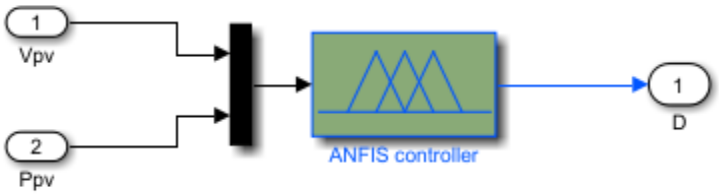

Fig. 5.14 Simulink block of designed ANFIS controller

5.3 Photovoltaic water pumping system with and without controllers

The MATLAB\SIMULINK software is used for simulation of the photovoltaic water pumping system. The system was simulated to verify the functionality and performance of the proposed ANN based MPPT, FLC based MPPT and ANFIS based MPPT algorithm, and to quantify how the proposed controllers contribute to an increase in the system efficiency compared with each algorithms to connect the PV array system to the 17.5kW AC load. The effectiveness of the three proposed methods to handle weather condition changes especially the change of solar irradiation and temperature change is evaluated through different levels of solar irradiation and temperature levels. The PV system implemented in this thesis is a stand-alone system where the load has insignificant variation, unlike in a grid-tied system. Therefore, the load variation has not been taken into account for testing the performance of the proposed three MPPT methods. The comparison has been carried out in the same PV water pumping system and under the same weather conditions to quantify how much each method contributes to improve the efficiency of the PV system. The total Simulink block of the system is shown in Fig 5.15.

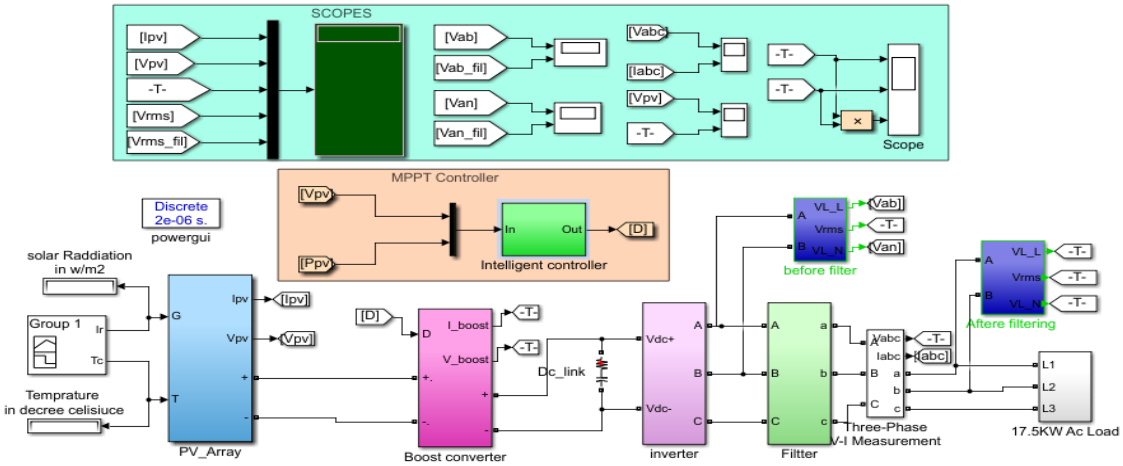

Fig. 5.15 General Simulink model of the PV systems

To test the performance and response of each controller for the PV system three conditions had applied.

First, slow and rapid changes in solar insolation using the three proposed MPPT controllers at standard temperature (25°c) and the insulation was started from 1000w/m^2 and then changed from 1000w/m^2 to 600 w/m^2 and 600 w/m^2 to 300W/m^2 at the time division of 0.2s, 0.4s 0.6s respectively.

The second division was both temperature and solar irradiation level is varied randomly, the insulation continues from 300W/m^2 raised to 800W/m^2 and then from 800W/m^2 to 1100W/m^2, from 1100W/m^2 to 700W/m^2 with the temperature (40°C, 50°C and 20°C) at the time division of 0.8s, 1s and 1.2s respectively.

The final division was slowly and rapid change in temperature at standard insulation (1000W/m^2) and the temperature changes starting from the previous division up to 35°C and then from 35°C to 45°C, finally tend to 25°C at a time of 1.4s, 1.6s and 1.8s respectively.

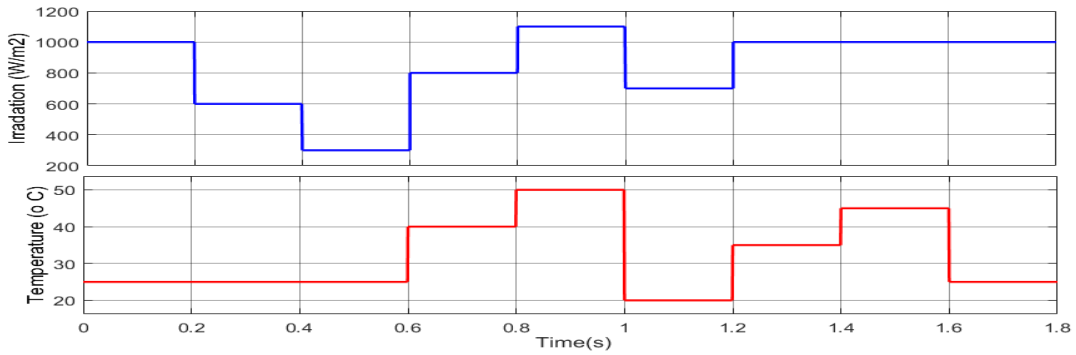

Fig. 5.16 Different level of solar irradiation and temperature values for testing system performance

5.3.1 PV water pumping system simulation without any controller

In this PV system, the PV array has been connected to the 17.5kW Ac load without controller at the MPP duty cycle (D_{mp}) to the boost converter using PWM generators. The system was

subjected to a sudden change in solar irradiation and temperature. The simulation results for these systems are shown in the following figures which are the PV array output current, voltage, power and the three phase ac voltage and current. The simulation waveforms show that connected system is operating far from the maximum power point at some irradiation and temperature levels. Fig. 5.17 and Fig. 5.18 illustrates that the PV array current and voltages are far from the optimum level. As a result of this, the system deviates from the maximum operating power all the time as shown in Fig. 5.19. The system is operating at a power point much less than the maximum power point and the three phase output voltage and current wasn't smooth and the optimum value is not achived. Therefore, some of the energy will be dissipated, this reduces the amount of water being discharged from the pump, hence, the systems is operating at a relatively poor efficiency or even not work, for various insolation and temperature levels.

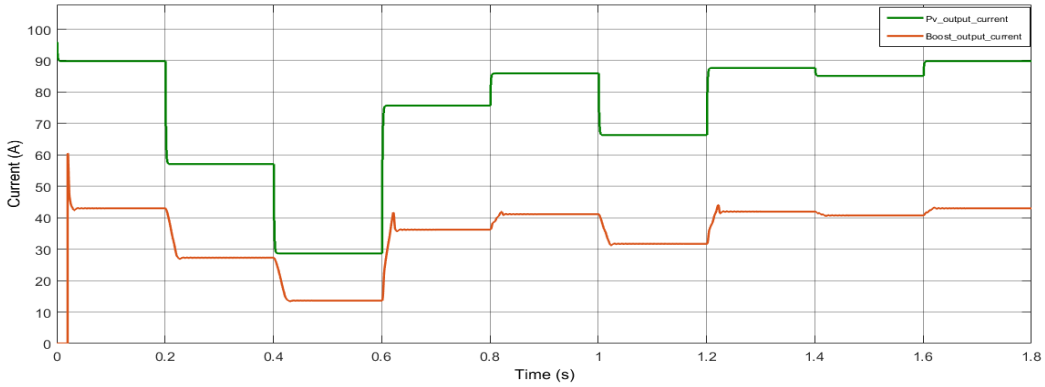

Fig. 5.17 PV array output current and boost output current at different environments

The generated 89.85A Ipv current is boosted to different level of amperes .The output boost current from zero to 0.2s and from 1.2s to 1.8s has been near to the optimum relative to other time intervals.

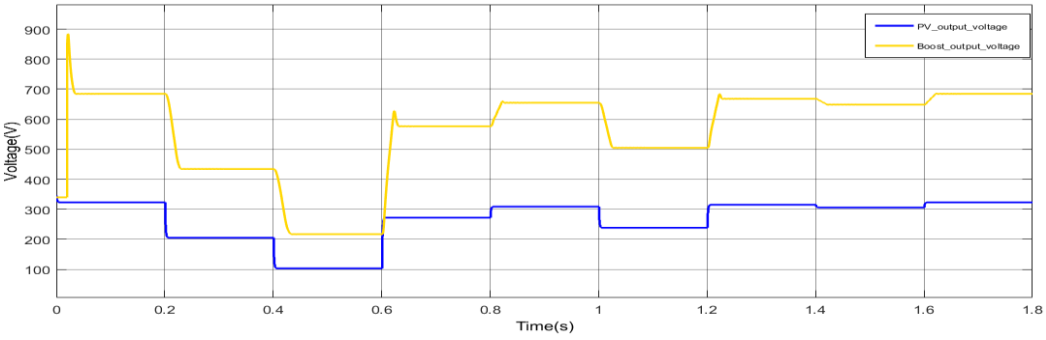

Fig. 5.18 PV array output voltage and boost output voltage at different condition.

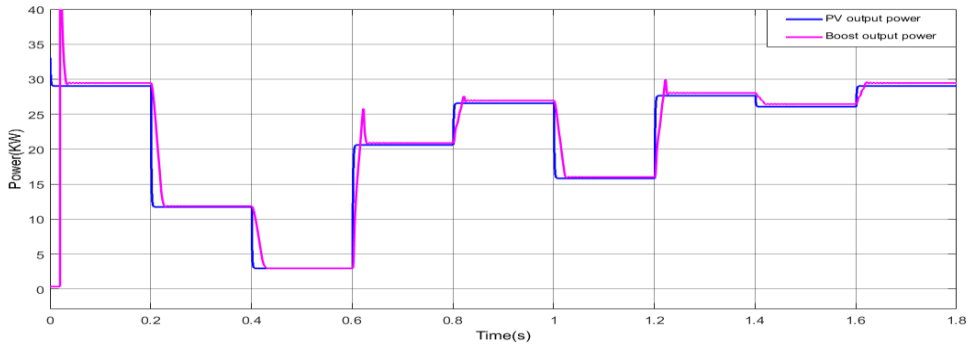

Fig. 5.19 The PV panel output power and Boost output power in direct connection systems

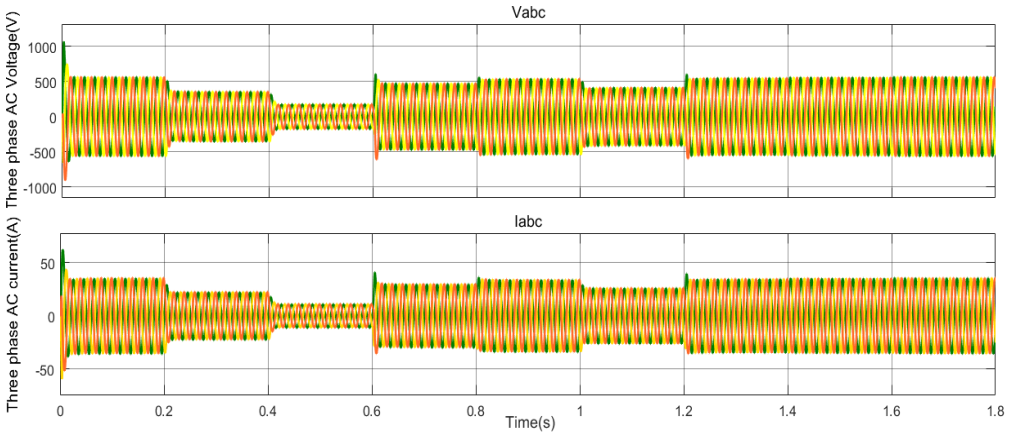

Fig. 5.20 The output three phase voltage and current of the PV system at different conditions

As we seen in figure 5.20 the three phase Ac output voltage is not good to use for the required purposes as well as any Ac equipment due to its harmonic output properties. In general the direct connected system is far from the MPP and poor performance.

5.3.2 PV water pumping system simulation using Fuzzy Logic controller

The seven class two input one output fuzzy logic system simulation results are listed below. In Fig.5.21 the fuzzy output signal is shown. When the Temperature and irradiation level is change to adjust the boost converter by sending optimum duty cycles. The fuzzy system is better than the direct connections but it requires expert designer to design the fuzzy class ranges as the system wants. In this section the simulation result shows Fuzzy logic controller comparing with the direct connection systems.

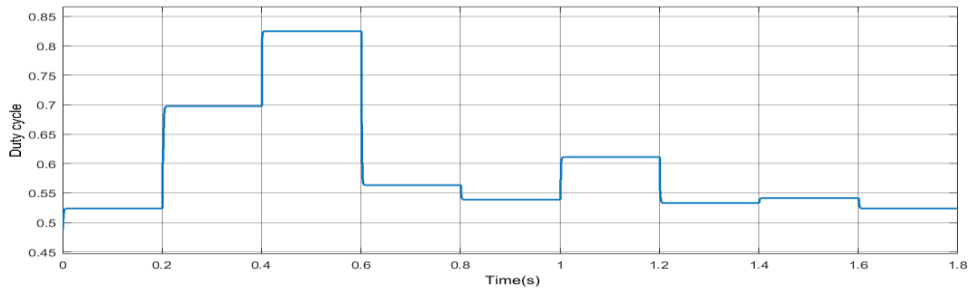

Fig. 6.21 Duty cycle signal output of FLC for different level of temperatures and irradiations

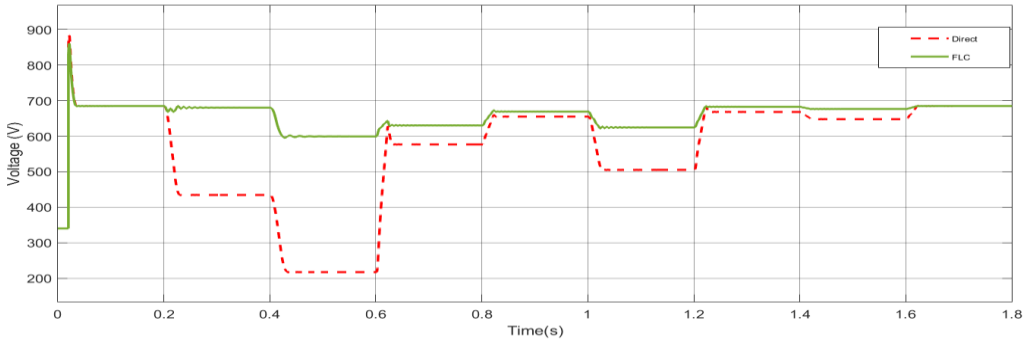

Fig. 5.22 Boost output voltage based on FLC and Direct connection PV systems.

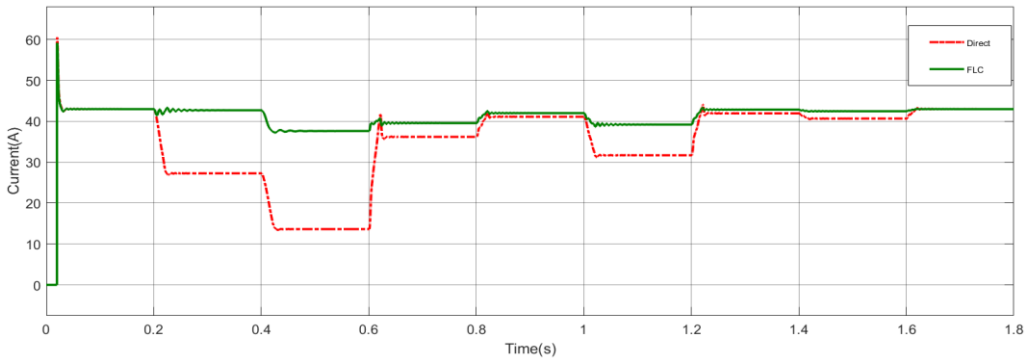

Fig. 5.23 Boost current based on FLC and Direct connection PV systems

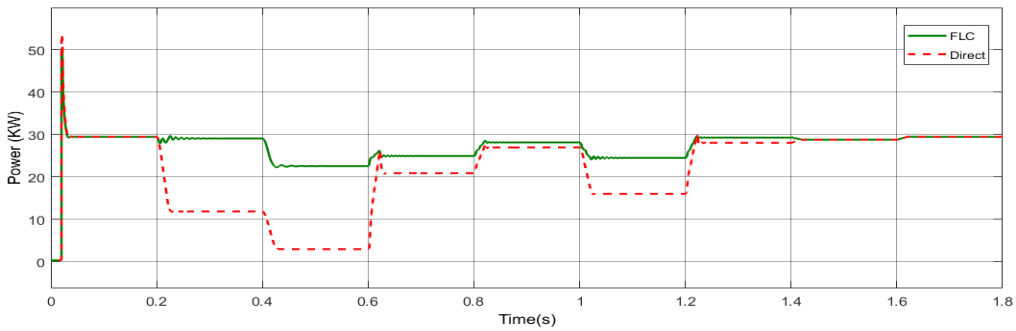

Fig. 5.24 Output power in KW based on FLC and direct connection PV systems

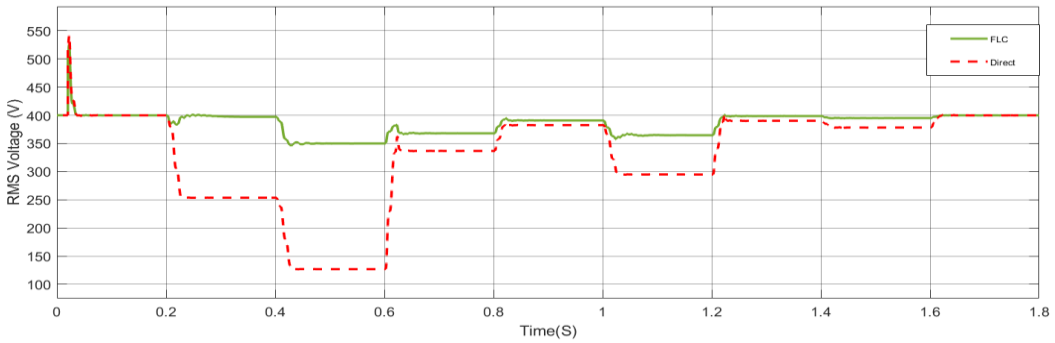

Fig. 5.25 RMS voltage value of the system based on FLC and direct connection PV systems

As shown in Fig. 5.25, even if Fuzzy logic is better than the direct connection PV system the three phase AC output voltage had some harmonic in a time of environmental changes occurred.

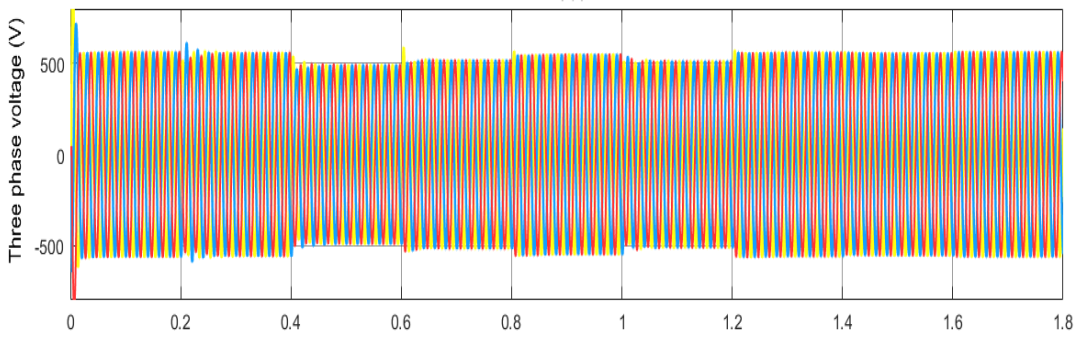

Fig. 5.26 Three phase output voltage based on FLC controller

5.3.3 PV water pumping system simulation using neural network controller

The ANN was trained with a set of input and target data until satisfactory results were gained as the systems required. Then a Simulink diagram was generated for the ANN and implemented into the PV water pumping system, to test the functionality and performance of the ANN controller in the PV system. It was exposed to sudden change in the irritation and temperature levels. The simulation results of the PV water pumping system with ANN MPPT controller compared with without controller system are shown in the following consecutive figures. The simulation results show the PV current, voltage, power Rms voltage and phase voltage is relatively near to the optimum in ANN controller at different levels of temperature and insulation. This gives an indication that, the direct connected system is operating far from the MPP all the time. Therefore, when the irradiation and temperature changes the ANN controller adjusts the duty ratio, as shown in Fig. 5.27, to decrease or increasing the PV output operating point until they reach the operating points that are corresponding to MPP and the three phase output voltage is smooth, sinusoid and the peak voltage is near to the

optimum point which is 562.7volt, but some harmonics is shown at a time of sudden environment changes.

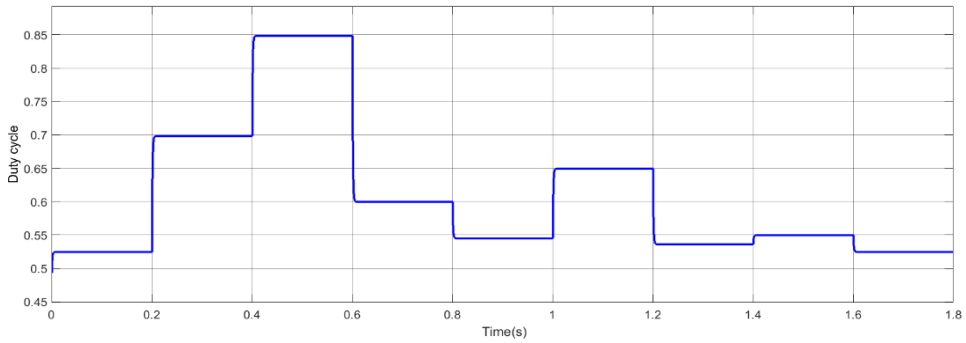

Fig. 5.27 Controller output signal of ANN at different temperature and insulation levels.

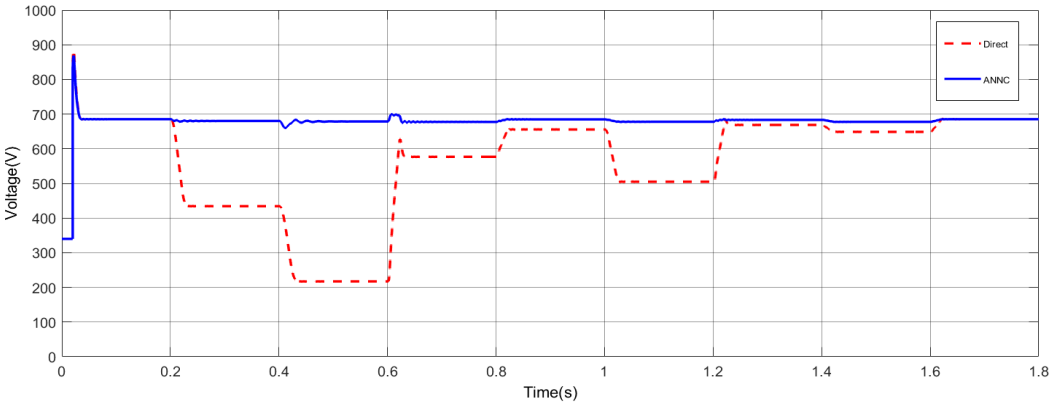

Fig. 5.28 Boost output voltage comparison between direct and ANNC at different condisions

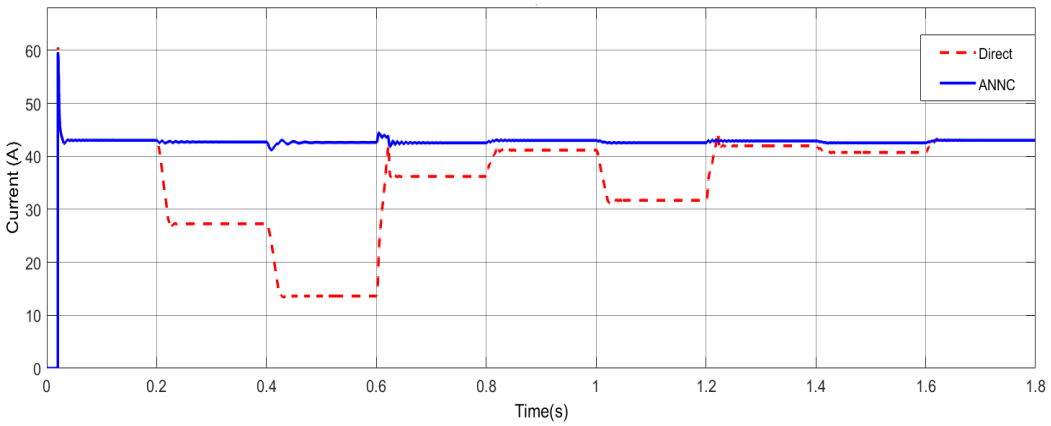

Fig. 5.29 Boost current comparison between direct and ANNC at different condisions.

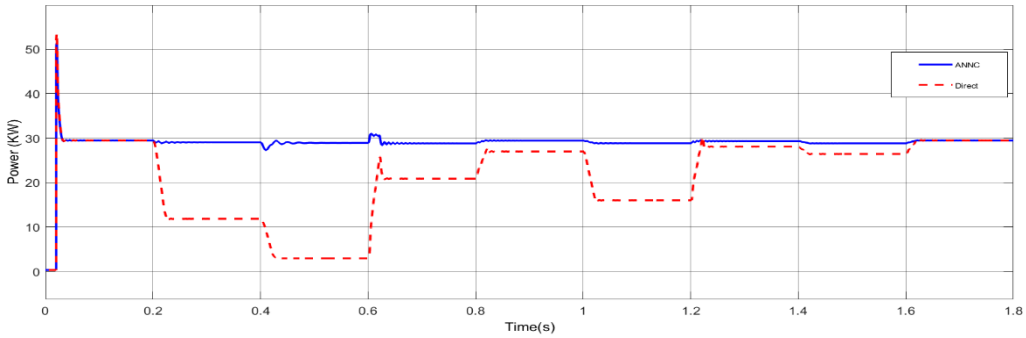

Fig. 5.30 Output power ccomparison between direct and ANNC at different condisions

In all the above figures show that the artificial neural network tried to maintain the optimum value near to the MPP, and the direct connection had been far from the MPP as the environment changed randomly.

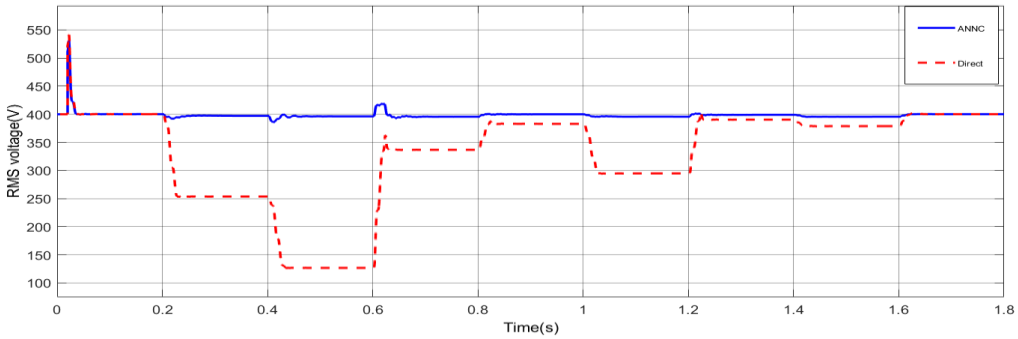

Fig. 5.31 RMS voltage of ANNC based and direct connection system at different condition

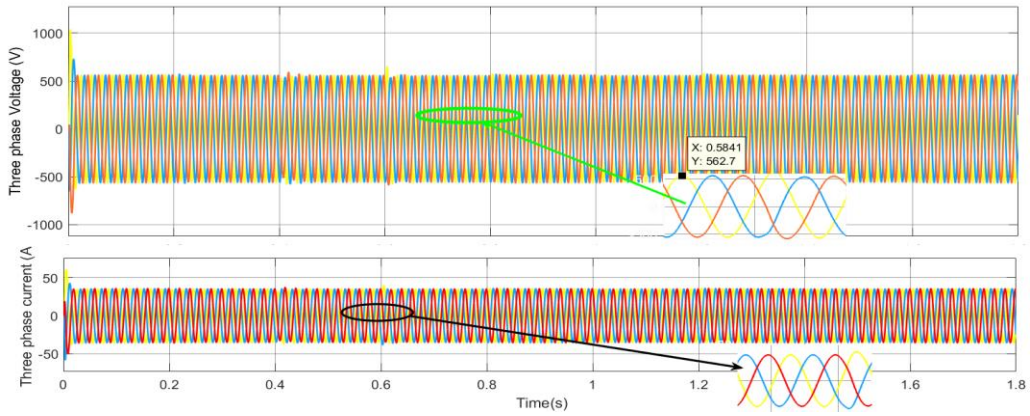

Fig. 5.32 the output three phase voltage and current value PV system based on ANNC

5.3.4 PV water pumping system simulation using ANFIS controller

The ANFIS was trained with 70 percens trained data and 30 percents checking and testing data from the PV panel output voltage, power and calculated Duty cycles. Then the ANFIS controller output signal is shown in fig. 5.33 to adjust the Boost output voltage and currents, which is nearest to the calculated values. In the remain consecutive figures the ANFIS shows

good performances in a time of environment changes and it operates nearest to the optimum maximum power point and the smooth AC three phase 566.1Volt peak voltage is generate which is the best output for a 400V AC load equipment.

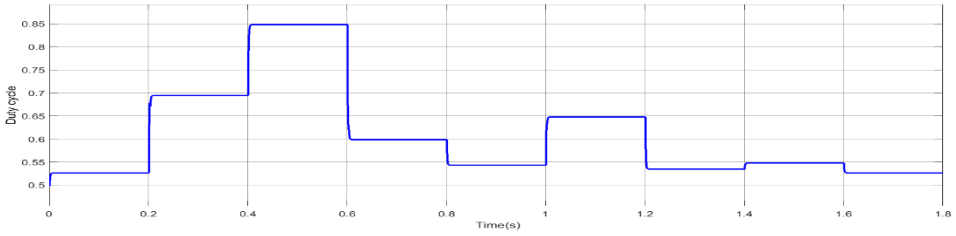

Fig. 5.33 Output signal of ANFIS controller at different level of temperature and irradiation

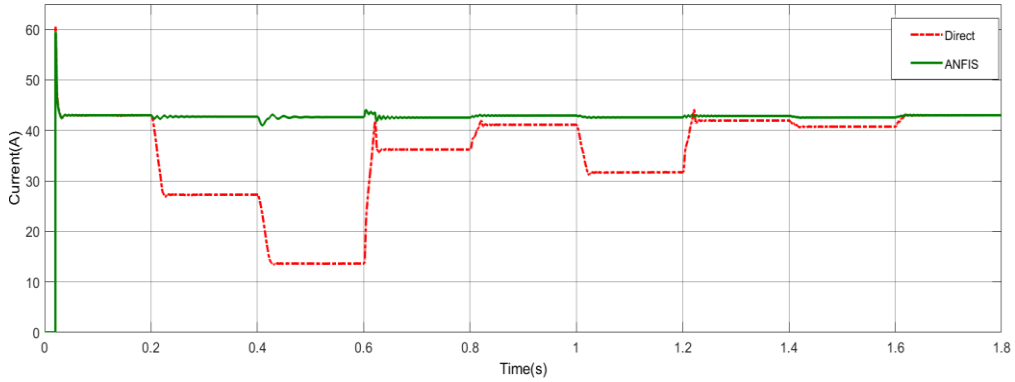

Fig. 5.34 Boost current due to direct and ANFIS controller at different condition

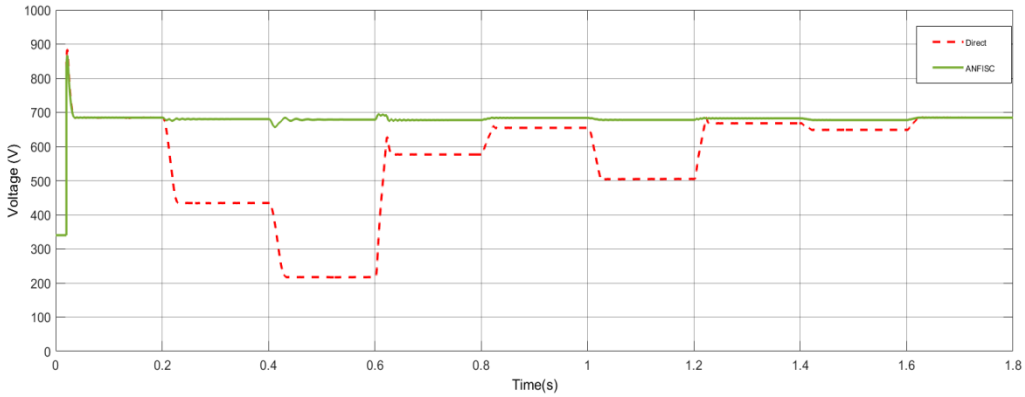

Fig. 5.35 Boost voltage due to ANFIS controller and direct connection at different condition

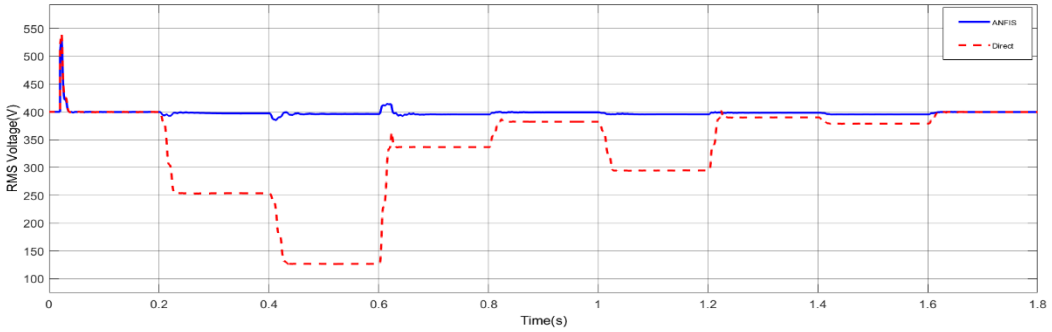

Fig. 5.36 RMS voltage of the PV system based on ANFIS controller at different level of temperature and irradiation

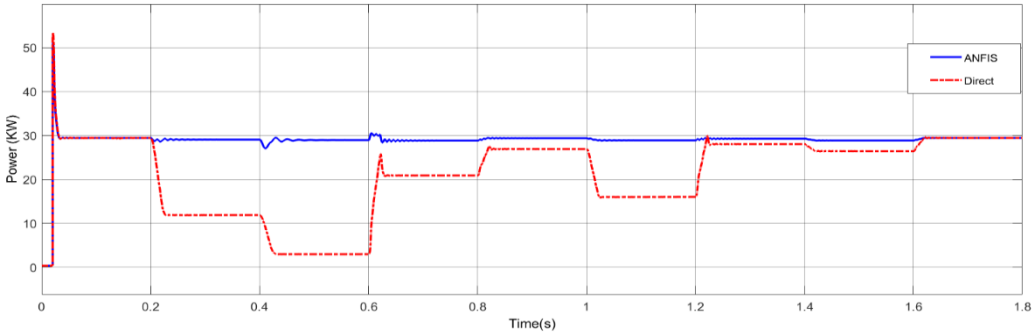

Fig. 5.37 Output Power based on ANFIS controller and direct connection at different condition

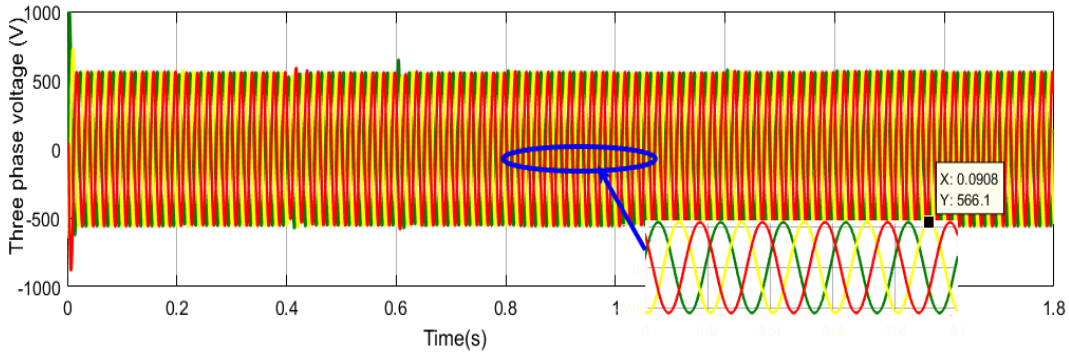

Fig. 5.38 Three phase output voltage due to ANFIS controller for different levels temperature and irradiation

As we have seen the simulation result ANFIS controller was much better than the direct connection PV systems and the output of the ANFIS controller is the nearest to the MPP and it respond the environment changes and tried to track the maximum pont.

5.4 Performance analysis of controllers

In this section, a comparative analysis between the three MPPT techniques are carried out to show the performance of each techniques in the same condition. In order to compare the performance of the three controllers in tracking the maximum power, the simulation power of

the boost converter RMS voltage value and the controllers' output signal are compared to for each controller for the same level of solar irradiation and temperature.

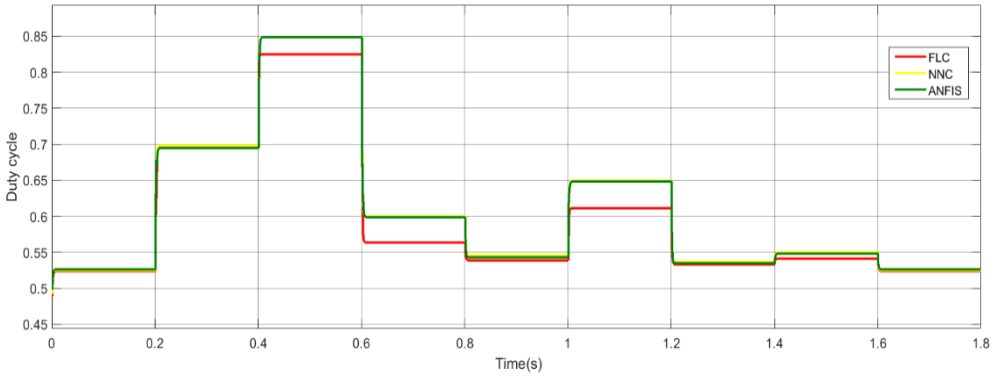

Fig. 5.39 Controllers' output signal at different level of temperature and insulation level

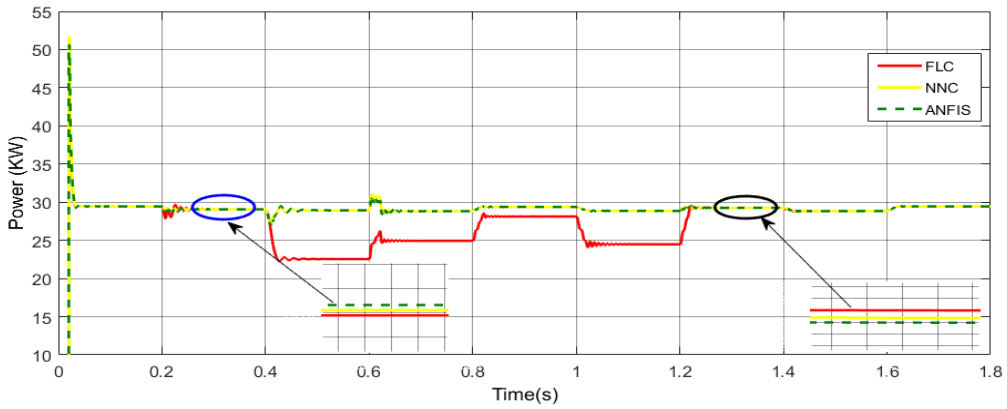

Fig. 5.40 comparision of output power based on FLC, ANN and ANFIS controller on PV systems

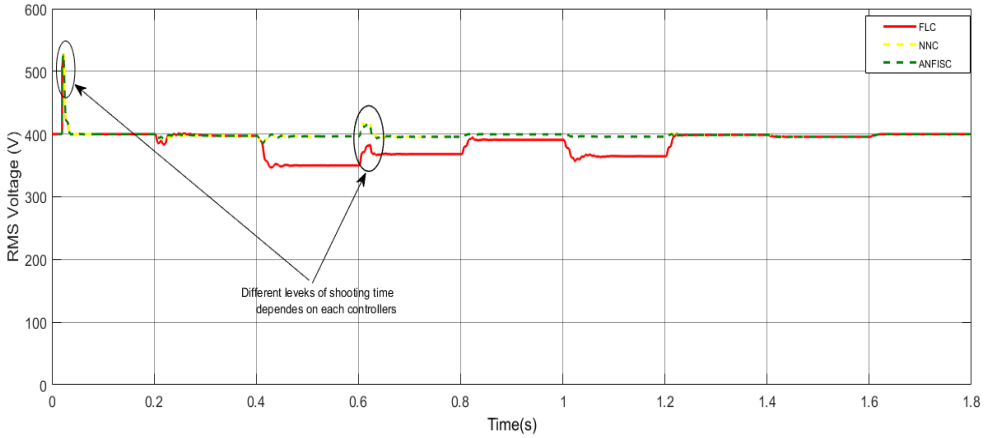

Fig. 5.41 RMS voltage value based on FLC, ANN and ANFIS Controllers at different condition.

As the simulation shown in Fig 5.39 the output signal of the ANFIS controller is much better than ANN and FLC controllers to adjust the duty cycles to feed the boost converters in a time of poor irradiation or shadow and high temperature is occurred.

If the PV panel generated power is above the rated power the ANFIS controller tried to track and send adjustable signals to make optimum outputs this conditions had shown at 1.2s to 1.4s.

At a time of 0.2s to 0.4s the irradiation level decreases from 1000W/m^2 to 700W/m^2 and becomes more shadow to 300W/m^2 at 0.6s to 0.8s, at this time we can compare the three proposed MPPT controller techniques. At tis condition the system requires higest value of duty cycle ratio that used to track the maximum points. As we show on the simulated result ANFIS had higher than ANN and ANN had higher than FL controller.

Generally the three controllers tried to track MPP,all controllers are better than direct connecting PV systems , but we have seen that the ANFIS controller is much effective and efficient than the other based on its performance, settling time. On the other hand the ANNC is also better than the fuzzy logic controller even beter than ANFIS because of it's minimum overshoots compaired to the the two controllers.

On the other hand we have to compared the proposed MMPT controller performances with the direct connected systems. The direct system onece connected with the best or the desired output signal at the MPPT which is ($\mathbf{D_{Mppt} = 0.524}$) and vary the environmental conditions and compared with other conttrollers as follow.

Table 5.3 The controller output at different level of environmental condition

Irradiation	G (W/m^2)	1000	800	300	1000	1100
Temperature	T(^{o}C)	25	25	22	40	35
Direct	Calculated(D)	0.524853	0.60177	0.84985	0.54294	0.499706
	Output signal	0.524	0.524	0.524	0.524	0.524
	Error e (%)	0.000753	0.07777	0.32585	0.01894	0.024294
	Efficiency η (%)	99.837478	87.0772	61.65794	96.51159	95.36374
FLC	Output signal	0.5241	0.5635	0.8248	0.5373	0.4943
	Error e (%)	0.000347	0.00357	0.00105	0.00564	0.0008
	Efficiency η (%)	99.856531	93.6412	97.052421	98.96121	98.91816
ANNC	Output signal	0.5252	0.5982	0.8488	0.5401	0.5006
	Error e (%)	0.00035	0.00357	0.00105	0.00284	0.00089
	Efficiency η (%)	99.433359	99.4076	98.57645	99.37692	99.82141
ANFISC	Output signal	0.5248	0.5996	0.8486	0.5429	0.4998
	Error e (%)	5.00E-05	0.00197	0.00125	4.00E-05	9.40E-05
	Efficiency η (%)	99.990473	99.6735	99.85292	99.99263	99.98119

The output signal from the controller fed to the boost controller is used to adjust the output voltage and current , and tried to maintain the output voltage to be 680volt Dc to fed the inverter.

Table 5.4 Performance compression of FLC, ANNC and ANFIS controller

Irradiance	G(W/m^2)	1000	800	300	1000	1100
Temperature	T(^{o}c)	25	25	22	40	35
Direct	Efficiency η (%)	99.83748	87.07718	61.65794	96.51159	95.36374
	Avarage Efficiency η (%)	88.08				
FLC	Efficiency η (%)	99.85653	93.64121	97.05242	98.96121	98.91816
	Avarage Efficiency η (%)	97.68				
	Avarage Efficiency improvement by FLC η (%)	9.59				
ANNC	Efficiency η (%)	99.43336	99.40758	98.57645	99.37692	99.82141
	Avarage Efficiency η (%)	99.32				
	Avarage Efficiency improvement by ANNC η (%)	11.23				
ANFISC	Efficiency η (%)	99.90473	99.67346	99.85292	99.99263	99.98119
	Avarage Efficiency η (%)	99.88				
	Avarage Efficiency improvement by ANNC η (%)	11.84				

Table 5.4 shows that the comparison result of the three controllers performance has been explained, 97.68% for FLC, 99.32% for ANNC and 99.88% for ANFIS controller are shown depending on the duty cycle ratio or sending signal efficiency. As shown in the concicative simulated result and the comparision table above at the first column the direct system seems good performance since the condition is at standard temperature and irradiation level and the desired signal applied to the system.

CHAPTER SIX

CONCLUSIONS, RECOMMENDATIONS AND FUTUIRE WORKS

6.1 Conclusions

In this work, a stand-alone matched photovoltaic water pumping system is presented to supply water in remote location especially in Dollo Ado wereda refugee camp with a clean and sustainable source of energy. The main focuses of this research was how to improve the total system efficiency by implementing an efficient MPPT techniques to transfer the maximum available power to the load especially under rapidly changing atmospheric conditions which was temperature and irradiation.

The thesis reviewed and discussed some existing MPPT controller methods and illustrated the advantages and disadvantages of each individual MPPT technique tracking performance and showed their ability to track the MPP under rapidly changing weather conditions.

The three more efficient MPPT controllers proposed were analyzed and developed in more depth using system simulations to clearly show improvements. For the system which operates with MPPT based FLC the time response for tracking the MPP is not faster compared to ANNC and ANFISC. For the MPPT based ANN and ANFIS techniques have fastest in time response for tracking the MPP and high efficiency for delivering maximum power to the load. Among the proposed techniques ANFIS controller improved the optimal Maximum powers and nearest to the MPP and improve the performance of the PV systems like smallest settling time than FLC and ANNC due to its good learning and generalization capabilities. The simulations were performed using MATLAB/SIMULINK.

The simulation results were divided into three parts for each controller algorithm to show the effect of environmental changes. In the first part the PV system is feeding a variable irradiation at standard temperature to test the performance of each controller in a time of shadow occurred. Second the PV system fed both temperature and irradiation are varied and test the performance and efficiency of each controller. And then make Irradiation constant and show the effect of temperature on PV output characteristics and test the effect of the controllers.

The results showed that the directly connected PV water pumping system without MPPT has poor efficiency due to the mismatching between the PV array and the Ac load. Whereas, the

system with the three proposed MPPT techniques utilizes the available PV array energy. The proposed MPPT techniques were able to track the MPP deliver maximum power to the load with high efficiency under the dynamic and steady-state conditions. Based on the simulated result the efficiency have been 97.68%, 99.32% and 99.88% for FLC, ANNC and ANFISC respectively, whereas the same without any controller is found to be 88.06. So that the results confirm that the proposed MPPT methods have the potential to significantly increase the total efficiency of the PV water. In the comparison of the table shown above and from the simulated result ANFIS controller had good efficiency than ANNC and ANNC also better than FLC but direct connection Pv system is poor and unsatisfactory due to its low performance and unable to track MPP.The simulation result clearly showed that the ANFIS controller method has the ability to improve both the steady-state and dynamic performance of tracking the MPP and thereby.

6.2 Recommendations

In this work, simulation models were developed and used to compare the performance of the MPPT techniques. However, practical hardware tests at a representative power level and under the typical climatic conditions of an application need to be conducted to verify the simulation results. The simulation results achieved in this work will hopefully incentivize future investigations involving building prototype models to test experimentally the developed MPPT techniques for the PV water pumping system, and among the three proposed controllers hybrid controller shows better peroformance than the intelligent controllers so it ought to apply this controllers in practical maners for PV water pumping systems.

6.3 Suggestions for future work

The ac load used in the current work is equal to the required calculated load from standard tables but for future improvement design and model an AC motor and pump with its sized parameters.

In the current PV system, the boost converter is used as an interface to enable the MPPT process. Future research could investigate some other converters such as buck-boost along with the proposed MPPT techniques to improve flexibility in the choice and configuration of PV array connection. And instead of two level inverter three level inverter will smooth the output three phase voltages.

REFERENCES

[1] Dr. A. Mousse , A. Saudi, A. Beta, and G.M. Asher , “Photovoltaic pumping systems Technologies Trends” , Lahr’s Journal, ISSN, pp. 127-150,June 2003.

[2] Mehmet Ababa, “Matching induction motors to PVG for maximum power transfer”, Elsevier –Desalination, pp.31-38, 2007.

[3] Yun Tiam Tan, Daniel S. Kirschen, and Nicholas Jenkins, “A Model based PV Generation suitable for stability analysis”, IEEE trans. on energy conv., vol.19, no.4, pp. 748-755, Dec 2004.

[4] E. Koutroulis E, K. Kalaitzakis, and NC. Voulgaris, “Development of a microcontroller based photovoltail maximum power point tracking control sytem”, IEEE trans. on Power Electronics, vol. 16, pp. 46-54, 2001.

[5] Abdulhadi Varnham, M. Abdulrahman, Al-Ibrahim, S. Gurvinder, Virk, and Djamel Azzi, “Soft computing model based controllers for increased photovoltaic plant efficiencies”, IEEE trans. on energy conv., vol. 22, no. 4, pp. 873-879, Dec. 2007.

[6] Weidong Xiao, Zeineldin, H.H., and Peng Zhang, "Statistic and Parallel Testing Procedure for Evaluating Maximum Power Point Tracking Algorithms of Photovoltaic Power Systems," Photovoltaics, IEEE Journal of , vol.3, no.3, pp.1062,1069, July 2013.

[7] X. Weidong and W. G. Dunford, "A modified adaptive hill climbing MPPT method for photovoltaic power systems," in Power Electronics Specialists Conference, PESC, /IEEE 35th Annual, 2004.

[8] T. Tafticht, et al., "A new MPPT method for photovoltaic systems used for hydrogen production," COMPEL: The International Journal for Computation and Mathematics in Electrical and Electronic Engineering, vol. 26, pp. 62-74, 2007.

[9] N. Mohan and T. M. Undeland, Power electronics: converters, applications, and design: Wiley-India, 2007.

[10] H. Sira-Ramirez and R. Silva-Ortigoza, Control Design Techniques in Power Electronics Devices, Power Systems Series: Springer-Verlag London, 2006.

[11] R. F. Coelho, et al., "A study of the basic DC-DC converters applied in maximum power point tracking," in Power Electronics Conference,. COBEP '09. Brazilian, 2009.

[12] J. M. Enrique, et al., "Theoretical assessment of the maximum power point tracking efficiency of photovoltaic facilities with different converter topologies," Solar Energy, vol. 81, pp. 31-38, 2007.

[13] E. Duran, et al., "Comparative analysis of buck-boost converters used to obtain I-V characteristic curves of photovoltaic modules," in Power Electronics Specialists Conference, PESC/IEEE, pp. 2036-2042, 2008.

[14] A. Oi, "Design and simulation of photovoltaic water pumping system,"Master Thesis, California ,2009.

[15] R. C. Neville, Solar energy conversion: the solar cell: Elsevier Science, 1995.

[16] O. Ojo, P. Kshirsagar, "Concise Modulation strategies for four leg voltage source inverter," Conference Records Power Electronics Specialists Conference, vol. 1, pp. 238-243, 2002.

[17] Kjær, S. B. . Design and Control of an Inverter for Photovoltaic Applications. Aalborg Universitet: Institut for Energiteknik, Aalborg Universitet, 2005.

[18] M. L. a. C. Greenwood, "Green investing: Towards a clean energy infrastructure," World Economic Forum USA Inc, Polytechnic State University, January 2009.

[19] V. Salas, et al., "Review of the maximum power point tracking algorithms stand-alone photovoltaic systems," Solar Energy Materials and Solar Cells, vol. 90, pp. 1555-1578, 2006.

[20] W. Xiao, "A modified adaptive hill climbing maximum power point tracking (MPPT) control method for photovoltaic power systems," Master Thesis The University of British Columbia, 2003.

[21] M. veerachary, et al., "Feedforward maximum power point tracking of PV systems using fuzzy controller," Aerospace and Electronic Systems, /IEEE Transactions on, vol. 38, pp. 969-981, 2002.

[22] Mohamed E. El Telbany, Ayman Youssef, Electronics Research Institution Computer and Systems Department, 4th International Conference on Artificial Intelligence with Applications in Engineering and Technology, 2014

[23] S. A. Kalogirou, "Artificial intelligence for the modeling and control of combustion processes: a review," Progress in Energy and Combustion Science, vol. 29, pp. 515-566, 2003.

[24] M. Figueiredo and F. Gomide; "Design of Fuzzy Systems Using Neuro-Fuzzy Networks", /IEEE Transactions on Neural Networks, Vol. 10, no. 4, pp.815-827, 1999.

[25] N. Argaw, R. Foster and A. Ellis Renewable Energy for Water Pumping Applications in Rural, National Renewable Energy Laboratory, Villages, pp.19-26, July 2003.

[26] "The UNISCO Report, 2014," www/en.wikipedia.org/wiki/Dolo, Ethiopia.

[27] H. Pollock and J. Flower, “New-method of power control for series-parallel load resonant converters maintaining zero-current switching and unity power factor,” /IEEE Transactions on Power Electronics, vol. 12, no.1, pp. 103-115, January 1997.

[28] Fathi A O Aashoor A thesis submitted for the degree of Doctor of Philosophy Department of Electronic and Electrical Engineering University of Bath, May 2015.

[29] B. Wittig, W.-T. Franke, F.W. Fuchs Institute of Power Electronics and Electrical Drives Christian-Albrechts-University of Kiel, D-24143 Kiel, Germany, 2007.

[30] Professor, Ph.D., Frede Blaabjerg (IET), Associate Professor John K. Pedersen (IET), Aalborg University Institute of Energy Technology, , pp.30, August 2005.

[31] Utility aspects of grid connected photovoltaic power systems, International energy agency – photovoltaic power systems programme, IEA PVPS T5-01, 1998,

[32] M. Liserre, F. Blaabjerg, S. Hansen, Design and control of an LCL-filter based three-phase active rectifier, /IEEE proc. of the 36th annual industry application conference vol. 1, pp. 299-307, 2001.

[33] H. Knopf, "Analysis, Simulation, and evaluation of maximum power point tracking (MPPT) methods for a solar powered vehicle," Master Thesis, Portland State University, 1999.

[34] Rashid, M. H. Pulse-Width-Modulation Inverters. Upper Saddle River, NJ: Prentice-Hall, pp. 237–248, 2004.

[35] R. J. Machado and A. Freitas da Rocha, "A hybrid architecture for fuzzy connectionist expert systems," in Hybrid architectures for intelligent systems, 1992.

[36] Y. Bai, et al., Advanced fuzzy logic technologies in industrial applications: Springer, 2007.

[37] M. Mobaied, "Fuzzy Logic Speed Controllers Using FPGA Technique for Three-Phase Induction Motor Drives," Master Thesis, The Islamic University– Gaza, 2008.

[38] N. S. D'Souza, "Variable perturbation size maximum power point tracking algorithms for photovoltaic systems," Master Thesis, Concordia University, 2006.

[39] I. Iancu, "A Mamdani type fuzzy logic controller," Fuzzy Logic: Controls, Concepts, Theories and Applications, InTech Croatia, Rijeka, pp. 55-54, 2012.

[40] McCulloch, Warren; Walter Pitts . "A Logical Calculus of Ideas Immanent in Nervous Activity". Bulletin of Mathematical Biophysics, 1943.

[41] F. d. O. Resende, "Contributions for microgrids dynamic modelling and operation," PhD Thesis, Porto University,2003.

[42] E. Karatepe, et al., "Neural network based solar cell model," Energy conversion and management, vol. 47, pp. 1159-1178, 2006.

[43] R. Reed, "Pruning algorithms-a survey," Neural Networks, IEEE Transactions on, vol. 4, pp. 740-747, 1993.

[44] Z. Yong, et al., "The MPPT Control Method by Using BP Neural Networks in PV Generating System," in Industrial Control and Electronics Engineering (ICICEE), 2012 International Conference on, pp. 1639-1642 , 2012.

[45] Abdulaziz M. S. Aldobhani and Robert John, "A novel ANFIS Model and Fuzzy Logic Controller for Maximum Power Point Tracking of PV Systems, American Institute of Physics for the IMECS, IAENG Transactions on Engineering Technologies, 2008.

APPENDIX A

A.1 MATLAB functions and scripts of PV panel

A.1.1 MATLAB Function of the module specifications and calculating Rsh and Rs

```
Iscn=8.7;              % a short ckt current
Vocn=36;               % short ckt voltage
Imp=8.17;
Vmp=29.38;             % current at mximum
Pmax_e=Vmp*Imp;
Kv=-0.36;              % Temperature coefficient of Voc
Ki=0.53;               % temperature coefficient of Iscn
Ns=60;                 % No of cells
K=1.3806503e-23;       % Boltzmann constant
q=1.60217646e-19;      % charge of electron
n=1.3;                 % Ideality factor
Gn=1000;               % Irradiation in w/m2
T=25+273.15;           % adjusting mechanism
G=1000;
Vtn=K*Tn/q;
Vt=K*T/q;
Isn=Iscn/(exp(Vocn/n/Ns/Vtn)-1);%saturation current
Is=Isn;
%reverence value of Rs and Rsh
Rs_max=(Vocn-Vmp)/Imp;
Rsh_min=Vmp/(Iscn-Imp)-Rs_max;
% initial guesses
Rsh=Rsh_min;
Rs=0;
tol=0.001;%power mismach tolerance
P=(0);
error=Inf;%dummy value
%itration processes
while(error>tol)
dT=T-Tn;
Ipvn=(Rs+Rsh)/Rsh*Iscn;
Iph=(Ipvn+Ki*dT)*G/Gn;% photon current
Isc=(Iscn+Ki*dT)*G/Gn;%actual short ckt current
%increments Rs
Rs=Rs+0.01;
%shunt resistance evaluation
Rsh=Vmp*(Vmp+Imp*Rs)/(Vmp*Iph-Vmp*Is*exp((Vmp+Imp*Rs)/Vt/Ns/n)+Vmp*Is-
Pmax_e);
%I-V equation pairs
clear V
clear I
V=0:1:50;
I=zeros(1:size(V,1));
```

```
for i=1:size(V,1);
%newton raphson equation
g(i)=Iph-Is*(exp((V(i)+I(i)*Rs)/Vt/Ns/n)-1)-(V(i)+I(i)*Rs)/Rsh-I(i);
while(abs(g(i))>0.001)
g(i)=Iph-Is*(exp((V(i)+I(i)*Rs)/Vt/Ns/n)-1)-(V(i)+I(i)*Rs)/Rsh-I(i);
glin(i)=-Is*Rs/Vt/Ns/n*exp((V(i)+I(i)*Rs)/Vt/Ns/n)-Rs/Rsh-1;
I_(i)=I(i)-g(i)/glin(i);
I(i)=I_(i);
end
end %for i=1:size(V,1)
% calculate power using I- v equation
P=(Iph-Is*(exp((V+I.*Rs)/Vt/Ns/n)-1)-(V+I.*Rs)/Rsh).*V;
Pmax_m=max(P)
error=(Pmax_m-Pmax_e);
end
fprintf('model info:\n');
fprintf('Rsh_min=%f',Rsh_min);
fprintf('\n Rsh=%f',Rsh);
fprintf('\n Rs_max=%f',Rs_max);
fprintf('\n Rs=%f',Rs);
fprintf('\n Pmax_m=%f(model)',Pmax_m);
fprintf('\n Pmax_e=%f(expermental)',Pmax_e);
fprintf('\n Iph=%f',Iph);
fprintf('\n tot=%f',tol);
fprintf('\n Isc=%f',Isc);
fprintf('\n Imp=%f',Imp);
fprintf('\n Vmp=%f',Vmp);
```

A.1.2 Script of the components of PV water pumping systems parameter.

```
%PV panel parameters
Voc=36;
Isc=8.7;
Vmp=29.38; % maximum voltage of a module at MPPT
Imp=8.17;  % maximum current of a module at MPPT
Ki=0.053;
Kv=-0.36;
q=1.6e-19;
K=1.3805e-23;
n=1.3;
Rs=0.08;
Rsh=337.31;
Gn=1000;              % nominal irradation at STD
Tn=298.15;            % nominal temperature
Cs=60;              % no of series cells in a module
Cp=1;               % parallel cells in a module
Ns=11;              %no of series module in a strings
Np=11;               %n no of parallel strings in an array
Rl=3.596,           % load resistance in a module
Ts=1e-06;           %setling time
Vmpv=Vmp*Ns; % maximum voltage of the PV panel at MPPT
Impv=Imp*Np;  % maximum current ofthe PV panel at MPPT
```

```
P_max_panel=Vmpv*Impv;

% Boost converter parameters
Sfb=5000;          % swiching frequence of the PWM generator
V_boost_out=680;       % required boost converter output voltage
I_boost_out=P_max_panel/V_boost_out;    % expected output current of the boost cnvertor
Vin_max=323.1; % maximum output voltage of the PV array Vinmax =Vpv at STD
Vin_min=100; % expected minimum PV output voltage
out_rI=0.4*I_boost_out*(V_boost_out/Vin_max);    % output repple current
d=1-(Vin_max/V_boost_out)*n;% duty cycle ration t STU
Lb=(Vin_min*d)/(out_rI*Sfb);    %boost converter inductor value
Cb=(I_boost_out*d)/(out_rV*Sfb);    % boost converter capasitor value
RLd=V_boost_out/I_boost_out;  %load resistor
%Invertor parameters
I_inv=41;            % invertor current
V_inv=500;
fn=50;               % signale generated index frequency
fs=50*33;            % swiching frequence of the 2 leve PWM generator
M=0.96;              % modulation index
inv_out_rI=0.15*I_inv; %inverter output repple current is up to 15% of the invertor rated
current
P_inv=500*41;                %invertor rated power
% LCL Filter parameters
r=0.8;                %ratio of invertor side and load side inductors
L_inv=V_boost_out/(16*fs*inv_out_rI);   % inverter side three phase inductor
L_Lo=r*L_inv;              % load side three phase inductor
Pi=3.14;
cb=P_inv/(2*pi*fn*V_inv^2);   % base capactor
Cf=0.2*cb;                %filter capacitor
fo=(1/2*pi)*sqrt((L_inv+L_Lo)/(L_Lo*L_inv*Cf)); % resonant freqeuncy
Rd= 1/(3*2*pi*fo*Cf);      %Damping resistance
% FLC parameters
Gp=0.0034435;          % power scalling factor
Gv=0.15475;           % Voltage scalling factor
GD=1;            % duity ratio scalling factor
%Output
fprintf('Output of the required parameteres:\n');
fprintf('\nBoost converter Modele parameters:');
fprintf('\n   d=%f(at STD)',d);
fprintf('\n   Lb=%f',Lb);
fprintf('\n   Cb=%f',Cb);
fprintf('\n   RLd=%f\n',RLd);
fprintf('\nInvertor Modele parameters:');
fprintf('\n   P_inv=%f(Invertor rated power)',P_inv');
fprintf('\n   f=%f(Hz)',fn);
fprintf('\n   fs=%f(swiching frequincy)\n',fs);
fprintf('\nLCL Filter Modele parameters:');
fprintf('\n   L_inv=%f(invertor side inductor)',L_inv);
fprintf('\n   L_Lo=%f(load side invertor)',L_Lo);
fprintf('\n   Rd=%f(damping resistance)',Rd);
fprintf('\n   Cf=%f \n',Cf);
```

APPENDIX B

B.1 Artificial Network Trained Data From Pv Panel.

Table B.0.1 The data set collected for training the ANN

Ambient Temperature (C)	Solar Insulation (W/m2)	PV array Current (A)	PV array Voltage (V)	PV array Power (W)	Duty Ratio (D)
5	50	4.744	17.06	80.93264	0.974912
10	100	9.507	34.19	325.0443	0.949721
15	150	14.29	51.38	734.2202	0.924441
20	200	19.09	68.64	1310.338	0.899059
21	250	23.85	85.78	2045.853	0.873853
22	300	28.62	102.9	2944.998	0.848676
23	350	33.38	120	4005.6	0.823529
24	400	38.15	137.2	5234.18	0.798235
25	300	28.67	103.1	2955.877	0.848382
25	400	38.17	137.2	5236.924	0.798235
25	500	47.64	171.3	8160.732	0.748088
25	600	57.08	205.3	11718.52	0.698088
25	700	66.48	239.1	15895.37	0.648382
25	800	75.72	272.3	20618.56	0.599559
25	900	84.04	302.2	25396.89	0.555588
25	1000	89.85	323.1	29030.54	0.524853
25	1050	91.78	330	30287.4	0.514706
25	1100	93.28	335.4	31286.11	0.506765
25	1150	94.47	339.7	32091.46	0.500441
25	1200	95.46	343.3	32771.42	0.495147
26	1200	95.15	342.2	32560.33	0.496765
27	1150	93.88	337.6	31693.89	0.503529
28	1100	92.45	332.5	30739.63	0.511029
29	1050	90.79	326.5	29642.94	0.519853
30	1000	88.81	319.4	28365.91	0.530294
31	1000	88.59	318.6	28224.77	0.531471
32	1000	88.37	317.8	28083.99	0.532647
33	1000	88.14	316.9	27931.57	0.533971
34	1000	87.9	316.1	27785.19	0.535147
35	1050	89.22	320.8	28621.78	0.528235
40	1100	88.99	320	28476.8	0.529412
45	1150	88.37	319.5	28234.22	0.530147
50	1200	87.52	314.7	27542.54	0.537206
40	1150	89.94	323.4	29086.6	0.524412

Table B.0.2 The data set collected for training the ANN.

Ambient Temperature (Co)	Solar Insulation (W/m2)	PV array Current (A)	PV array Voltage (V)	PV array Power (W)	Duty Ratio (D)
35	1100	90.46	325.3	29426.6	0.522
30	1050	90.53	325.6	29476.6	0.521
24	1000	90.04	323.8	29155	0.524
23	1000	90.22	324.4	29267.4	0.523
22	1000	90.4	325.1	29389	0.522
21	1000	90.58	325.7	29501.9	0.521
20	1000	90.75	328.8	29838.6	0.516
17	1000	91.22	328	29920.2	0.518
14	1000	91.62	329.5	30188.8	0.515
11	1000	91.97	330.7	30414.5	0.514
10	950	88.48	318.2	28154.3	0.532
9	900	84.31	303.2	25562.8	0.554
8	850	79.79	286.9	22891.8	0.578
7	800	75.15	270.3	20313	0.603
7	750	70.52	253.6	17883.9	0.627
7	700	65.87	236.9	15604.6	0.652
7	650	61.21	220.1	13472.3	0.676
7	600	56.54	203.3	11494.6	0.701
7	500	47.19	169.7	8008.14	0.75
6	400	37.78	135.9	5134.3	0.8
5	300	28.36	102	2892.72	0.85
4	200	18.93	68.06	1288.38	0.9
3	100	9.471	34.06	322.582	0.95
0	10	0.9468	3.405	3.22385	0.995
-1	100	9.451	33.99	321.239	0.95
-2	200	18.86	67.84	1279.46	0.9
0	300	28.29	101.7	2877.09	0.85
0	400	37.66	135.4	5099.16	0.801
5	500	47.13	169.5	7988.54	0.751
5	600	56.48	203.1	11471.1	0.701
20	300	28.59	102.8	2939.05	0.849
15	650	61.47	221	13584.9	0.675
40	1050	87.84	315.9	27748.7	0.535
30	200	19.19	69	1324.11	0.899
14	550	52.06	187.2	9745.63	0.725
34	450	43.11	155	6682.05	0.772
21	750	71.02	255.4	18138.5	0.624

APPENDIX C

C.1 Artificial Intelligent MPPT Controllers MATLAB Simulation

C.1.1 FIS of FLC based MPPT of PV water pumping system MATLAB SIMULINK

Fig. C.1 FIS editor

Fig. C.2 Membership function r input variable (dVpv).

Fig. C.3 Membership function editor input variable (dPpv)

Fig.C.4 Membership function editor output variable (D)

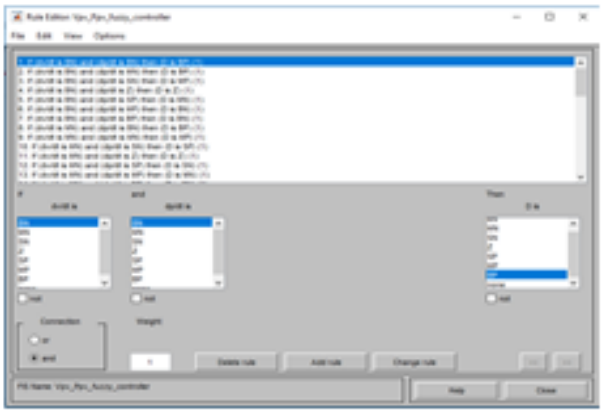

Fig. C.5 Rule-base editor

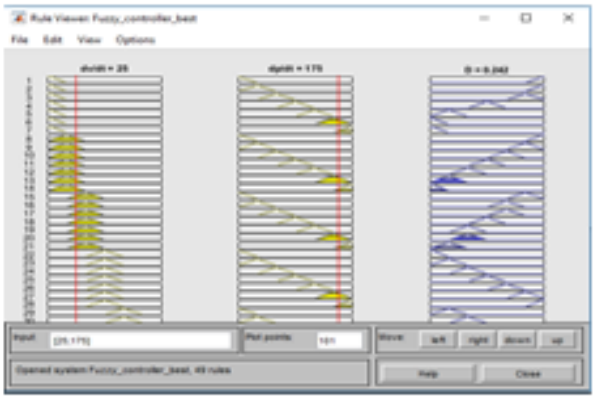

Fig. C.6 Rule viewer

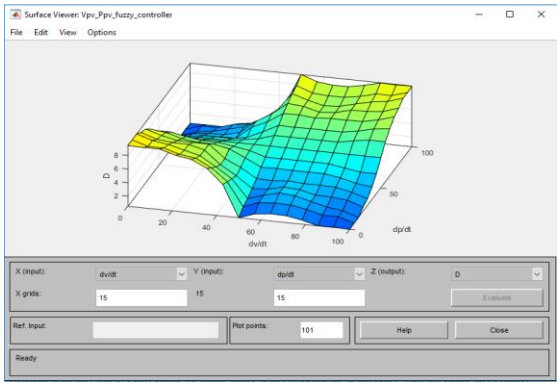

Fig. C.7 3D surface viewer

C.1.2 ANN based MPPT of PV water pumping system MATLAB SIMULINK

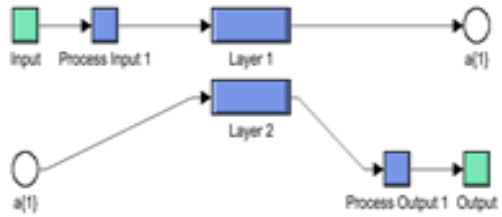

Fig. C.8 Layers of Neural Network Controller Layer

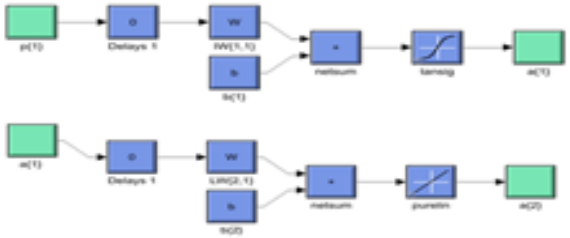

Fig.C.9 Structure of Neural Network

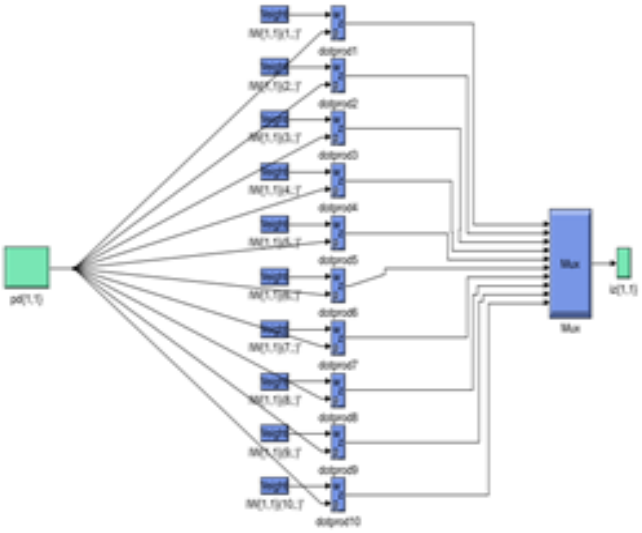

Fig. C.10 Structure of Hidden Layer Neuron Neuron

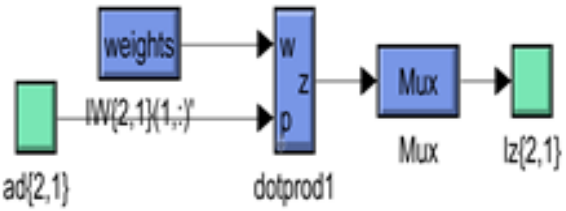

Fig. C. 11 Structure of Output Layer

Fig. C.8 Layers of Neural Network Controller

Fig. C.10 Structure of Hidden Layer Output Layer Neuron

Fig. C. 11 Structure of output layer

Fig.C.9 Structure of Neural Network Layer

C.1.3 ANFIS based MPPT of PV water pumping system MATLAB SIMULINK

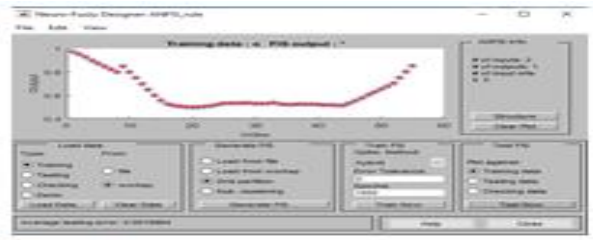

Fig. C.12 Trained data and its FIS output

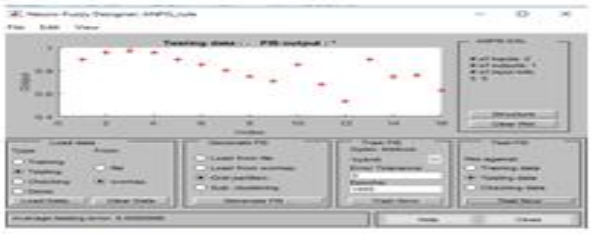

Fig. C.13 Testing data with FIS output

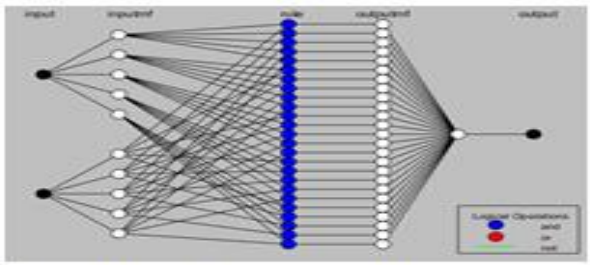

Fig. C.14 ANFIS trained backbrobagation structure

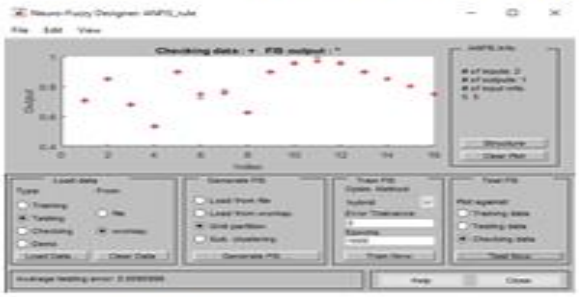

Fig C.15 ANFIS checking data

Fig. C.16 ANFIS rules

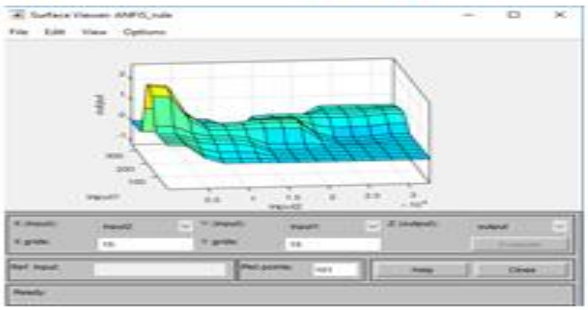

Fig. C.17 ANFIS 3D surface

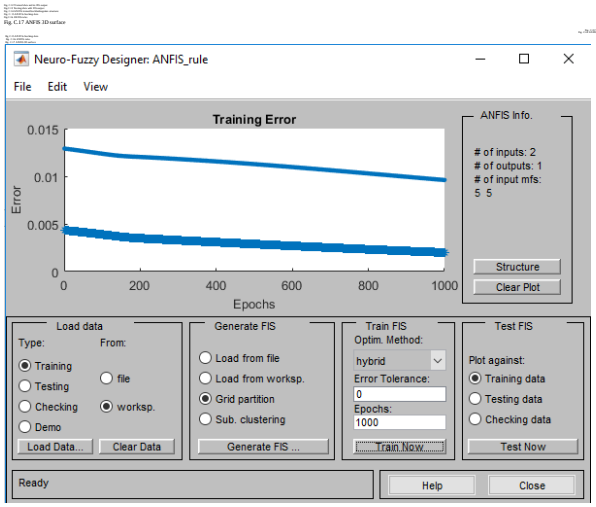

Fig. C.18 ANFIS training error